



University
of Glasgow

White, Marc A. (2012) *A dynamic light scattering study of small organic molecule and ionic salt solutions through cooling crystallisation.*

MRes thesis

<http://theses.gla.ac.uk/3780/>

Copyright and moral rights for this thesis are retained by the author

A copy can be downloaded for personal non-commercial research or study, without prior permission or charge

This thesis cannot be reproduced or quoted extensively from without first obtaining permission in writing from the Author

The content must not be changed in any way or sold commercially in any format or medium without the formal permission of the Author

When referring to this work, full bibliographic details including the author, title, awarding institution and date of the thesis must be given



University
of Glasgow

A dynamic light scattering study of small organic molecule and ionic salt solutions through cooling crystallisation

Masters in Research Thesis

University of Glasgow
College of science and Engineering
School of Chemistry
June 2012

Postgraduate Student: Marc A. White

First Supervisor: Prof. Klaas Wynne¹

Secondary Supervisors: Dr Jan Sefcik² and Prof. Lee Cronin

¹ University of Glasgow, ² University of Strathclyde

List of Abbreviations

- ΔG – Gibbs free energy (J/mol)
- k_B – Boltzman coefficient (1.3805×10^{-23} J/K)
- $\Delta\mu$ – Chemical Potential (J/mol)
- S – Supersaturation
- R – Universal Gas Constant (8.3144 J/molK)
- J – Rate of Nucleation (number of nuclei formed per unit time per unit volume)
- D – Diffusion Coefficient (m^2/s)
- AFM – Atomic Force Microscopy
- CNT – Classical Nucleation Theory
- MSZW – Metastable Zone Width
- SAXS – Small Angle X-ray Scattering
- WAXD – Wide Angle X-ray Diffraction
- SANS – Small Angle Neutron Scattering
- HPLC – High Performance Liquid Chromatography
- DLS – Dynamic Light Scattering
- SLS – Static Light Scattering
- PTFE – Polytetrafluoroethylene
- λ – Wavelength (nm)
- c – Speed of Light (300,000 km/s)
- n_0 – Refractive Index
- η – Viscosity (Pa.s)
- R_H – Hydrodynamic Radius (nm)
- γ – Interfacial Tension

Abstract

This project was concerned with observing the process of nucleation of crystalline species during the cooling crystallisation of supersaturated solutions prepared from both ionic salt and small organic solutes. Cooling crystallisation induces a steady temperature-dependant destabilisation of the supersaturated liquid phase where the chemical potential of the liquid state increases and so becomes less thermodynamically stable. This decrease in stability triggers the onset formation of the corresponding solid state, which has a lower chemical potential. This driving force permits the spontaneous formation of critical nuclei and their subsequent growth into larger crystalline structures. Desire to understand the processes occurring at the earliest stages of crystal nucleation have attracted much interest over the years.

Dynamic light scattering experiments were employed to closely observe the precursors to crystal nucleation. More specifically the phenomenon of molecular clustering and their consequent dispersion to form solute-rich regions within solution, where the generation of viable critical nuclei would be most likely occur, according to current theory. The pre-nucleation mechanism for cooling crystallisation was observed to involve large nano-droplet sized molecules of non-specific composition, for solutions of urea and glycine and almost micron-sized droplets for solutions of sodium chloride and sodium nitrate. Interestingly, there was evidence that clustering of larger aggregates was a phenomenon not wholly restricted by supersaturation as they were found in undersaturated solutions of all prepared samples.

The relative size of particle radii formed in pre-crystalline solution tended to depend on the extent of the supersaturation *i.e.*, the concentration of the solute present within the solution. This is not true in all cases though as supersaturated glucose indicated. This may suggest an alternate pathway in the route of nucleation of crystals than was previously assumed. The theory of a metastable phase forming within the bulk solution, where critical nuclei are thermodynamically more stable and hence are able to grow once formed might not hold true for all crystallising solutions or another factor may need to be better understood and manipulated in order to claim more control over the desired process. Further understanding of this could give an increased degree of control over yield and quality of products in pharmaceuticals and other material producing industries.

Contents

1	Introduction	10
2	Theory	142
2.1	Supersaturated Solutions.....	12
2.2	Nucleation.....	14
2.3	Thermodynamic Theory of Nucleation.....	16
2.4	Classical Nucleation Theory.....	17
2.5	Classical Nucleation Rate Theory.....	19
2.6	Inconsistency of Classical Nucleation.....	21
2.7	Two-Step Nucleation	22
2.8	Metastable zone	25
2.9	Liquid-Liquid Separation.....	27
3	Experimental Methods	30
3.1	Chemicals and Solvents.....	30
3.2	Concentrated Aqueous Solutions.....	30
3.3	Solubility measurements	31
3.3.1	Filtration	31
3.3.2	Dissolution of crystals	31
3.4	Preparation of Supersaturated Solutions.....	32
3.5	Cooling Crystallisation	32
4	Light Scattering.....	33
4.1	Dynamic Light Scattering.....	34
5	Data Acquisition.....	36
5.1	Latex Sphere	39
6	Dynamic Light Scattering	41
6.1	Summary.....	41
6.2	Deionised water background signal.....	41
6.3	Undersaturated Solutions.....	42
6.3.1	Urea.....	42
6.3.2	Glucose.....	44
6.3.3	Glycine.....	45
6.3.4	Sodium Chloride.....	46

6.3.5	Potassium Chloride.....	47
6.3.6	Sodium Nitrate.....	48
6.4	Supersaturated Solution.....	50
6.4.1	Urea.....	51
6.4.2	Glucose.....	53
6.4.3	Glycine.....	56
6.4.4	Sodium Chloride.....	57
6.4.5	Potassium Chloride.....	58
6.4.6	Sodium Nitrate.....	60
6.5	Multi-Angle Scattering.....	61
6.5.1	Urea.....	62
6.5.2	Glucose.....	65
6.5.3	Glycine.....	67
6.5.4	Sodium Chloride.....	69
6.5.5	Potassium Chloride.....	71
7	Conclusion.....	74
8	Appendix.....	77
8.1	Solubility.....	78
8.2	Viscosity.....	79
8.3	Background Signal.....	79
8.4	Collected Data.....	80
9	References.....	83

List of Figures

Fig. 1 Solubility Curve: Diagram shows concentration of a solution changing as a function of temperature. As the temperature decreases a barrier is crossed and a solution becomes supersaturated. The metastable zone represents a region of high solute concentration within the solution.	13
Fig. 2 Microscopic images of crystalline supersaturated urea.	14
Fig. 3 Particles in solution undergoing random Brownian motion (left), Diffusion of a two-component system (right)	15
Fig. 4 Free energy diagram for classical nucleation: Shows the free energy change of an embryonic cluster with respect to the nucleus size.....	17
Fig. 5 Comparison of the growth steps of two crystal nucleation theories	22
Fig. 6 Diagram of the two-step mechanism of nucleation. A clustered phase growing more ordered from left to right.	24
Fig. 7 Super-solubility curve diagram	25
Fig. 8 Composition diagram of a liquid-liquid separation region within the metastable zone	26
Fig. 9 Monomodal autocorrelation function of small particles (red) and large particles (blue).	37
Fig. 10 Bimodal decay autocorrelation function.....	37
Fig. 11 Polynomial fit of the function $\ln(g_1(\tau))$ vs t , 1 st order fit with polynomial $ax+b$	38
Fig. 12 Polynomial fit of the function $\ln(g_1(\tau))$ vs t using second order fit with polynomial ax^2+bx+c	38
Fig. 13 Autocorrelation function of mono-disperse aqueous diluted latex sphere solution	39
Fig. 14 Polynomial fit of the mono-dispersed latex sphere autocorrelation function $\ln(g_1(\tau))$ vs t , a) 1 st order fit with polynomial $ax+b$ and b) second order fit with polynomial ax^2+bx+c	39
Fig. 15 Autocorrelation function, $g_2(t)-1$, of water filtered through 0.2 μ m PTFE filter.....	41
Fig. 16. Autocorrelation functions of concentrated aqueous urea: a) 0.842 molar, b) 2.059 molar, c) 6.185 molar and d) 8.234 molar	42
Fig. 17 Autocorrelation functions of concentrated aqueous glucose: a) 0.5 molar, b) 2.5 molar, c) 4.5 molar	44
Fig. 18 Autocorrelation functions of concentrated aqueous glycine: a) 0.5 molar, b) 1.5 molar, c) 2.5 molar	45
Fig. 19 Autocorrelation functions of concentrated aqueous Sodium Chloride: a) 2 molar, b) 4 molar	46
Fig. 20. Autocorrelation functions of concentrated aqueous Potassium Chloride: a) 2 molar, b) 4.....	48
Fig. 21 Autocorrelation functions of concentrated aqueous Sodium Nitrate: a) 3 molar, b) 6 molar and c) 9 molar	49

Fig. 22. Autocorrelation function $g_2(t)-1$ of deionised water filtered through a $0.2\mu\text{m}$ PTFE filter, i) 45°C and ii) 25°C	50
Fig. 23. Light scattering autocorrelation function $g_2(t)-1$ of deionised water, cooling crystallisation	50
Fig. 24 Autocorrelation functions of supersaturated aqueous urea solutions cooling crystallised from 45 to 25°C : i) 45°C , ii) 40°C , iii) 35°C , iv) 30°C and v) 25°C	51
Fig. 25 Autocorrelation function of Supersaturated urea concentration 1.67g/ml at 40°C . Cooling crystallisation from 45 to 25°C	52
Fig. 26 Autocorrelation functions of supersaturated aqueous glucose solutions cooling crystallised from 45 to 25°C : i) 45°C , ii) 40°C , iii) 35°C , iv) 30°C and v) 25°C	54
Fig. 27 Autocorrelation function of Supersaturated glucose concentration 0.617g/ml at 40°C . Cooling crystallisation from 45 to 20°C	55
Fig. 28 Autocorrelation function of Supersaturated glycine concentration 0.317g/ml at 40°C . Cooling crystallisation from 45 to 25°C	56
Fig. 29 Autocorrelation function of Supersaturated sodium chloride solution, conc: 0.364g/ml at 40°C . Cooling crystallisation from 45 to 25°C	57
Fig. 30 Autocorrelation function of Supersaturated potassium chloride solution, conc: 0.390g/ml at 40°C . Cooling crystallisation from 45 to 20°C	59
Fig. 31 Autocorrelation function of Supersaturated sodium nitrate solution, conc: 1.040g/ml at 40°C . Cooling crystallisation from 45 to 25°C	60
Fig. 32 Multi-angle detection of urea solution, concentration 1.67g/ml . Autocorrelation function $g_2(t)-1$ at a) 45°C and b) room temperature	62
Fig. 33 Graphs of measured radii magnitude for supersaturated urea solution at varying angles of detection, a) 45°C b) room temperature	63
Fig. 34 Log-Log plot of the absolute scattering intensity, measured at 45°C (red) and at room temperature (blue), versus the wave vector, q . Urea solution concentration: 1.67g/ml	64
Fig. 35 . Multi-angle detection of glucose solution, concentration 0.617g/ml . Autocorrelation function $g_2(t)-1$ at a) 45°C and b) room temperature	65
Fig. 36. Graphs of measured radii magnitude for supersaturated glucose solution at varying angles of detection, a) 45°C b) room temperature	66
Fig. 37 Log-Log plot of the absolute scattering intensity, measured at 45°C (red) and at room temperature (blue), versus the wave vector, q . Glucose solution, concentration: 0.617g/ml	66
Fig. 38 Multi-angle detection of glycine solution, concentration 0.317g/ml . Autocorrelation function $g_2(t)-1$ at a) 45°C and b) room temperature	67
Fig. 39 Graphs of measured radii magnitude for supersaturated glycine solution at varying angles of detection, a) 45°C b) room temperature	68

Fig. 40 Log-Log plot of the absolute scattering intensity, measured at 45 °C (red) and at room temperature (blue), versus the wave vector, q . Glycine solution, concentration: 0.317g/ml..... 69

Fig. 41. Multi-angle detection of sodium chloride solution, concentration 0.364g/ml. Autocorrelation function $g_2(t)-1$ at a) 45 °C and b) room temperature..... 70

Fig. 42 Multi-angle detection of potassium chloride solution, concentration 0.390g/ml. Autocorrelation function $g_2(t)-1$ at a) 45 °C and b) room temperature..... 71

Fig. 43. Graphs of measured radii magnitude for supersaturated potassium chloride solution at varying angles of detection, a) 45 °C b) room temperature 72

Fig. 44. Log-Log plot of the absolute scattering intensity, measured at 45 °C (red) and at room temperature (blue), versus the wave vector, q . Potassium Chloride solution, concentration: 0.390g/ml 72

Fig. 45. Autocorrelation function of ethanol (reagent grade)..... 75

List of Tables

Table 1 Average hydrodynamic radii of mono-disperse latex sphere in aqueous solution	40
Table 2 Average hydrodynamic radii of concentrated aqueous urea solutions.	43
Table 3 Average hydrodynamic radii of concentrated aqueous glucose solutions.	44
Table 4 Average hydrodynamic radii of concentrated aqueous glycine solutions.	46
Table 5 Average hydrodynamic radii of concentrated aqueous NaCl solutions.	47
Table 6 Average hydrodynamic radii of concentrated aqueous KCl solutions	48
Table 7 Average hydrodynamic radii of concentrated aqueous NaNO ₃ solutions.	49
Table 8 Average hydrodynamic radii of cooling crystallised aqueous urea solutions.	53
Table 9 Average hydrodynamic radii of cooling crystallised aqueous glucose solutions.	55
Table 10 Average hydrodynamic radii of cooling crystallised aqueous glycine solutions.	57
Table 11 Average hydrodynamic radii of cooling crystallised aqueous sodium chloride solutions.	58
Table 12 Average hydrodynamic radii of cooling crystallised aqueous potassium chloride solutions.	59
Table 13 Average hydrodynamic radii of cooling crystallised aqueous sodium nitrate solutions.	61
Table 14 Solubility data of Urea.	77
Table 15 Solubility data of Glucose.	77
Table 16 Solubility data of Glycine.	78
Table 17 Solubility data of NaCl.	78
Table 18 Solubility data of KCl.	78
Table 19 Solubility data of NaNO ₃	78
Table 20 Viscosity of deionised water at specific temperatures.	79
Table 21 Measured and calculated data from Urea solution of composition 16.7 g/ml of water.	80
Table 22 Measured and calculated data from Glucose solution of composition 8.333 g/ml of water.	80
Table 23 Measured and calculated data from Glycine solution of composition 2.85 g/ml of water.	80
Table 24 Measured and calculated data from NaCl solution with composition 3.636 g/ml of water	81
Table 25 Measured and calculated data from KCl solution with composition 3.528 g/ml of water.	81
Table 26 Measured and calculated data from NaNO ₃ solution with composition 10.5 g/ml of water.	81
Table 27 Measured and calculated data from pure deionised water.	82

Chapter 1 - Introduction

The process of crystallisation via phase separation of a solute in a supersaturated solution is a vital principle for the production of crystalline compounds in industries such as pharmaceuticals, agriculture and the commercial foods trade. Study and research into control of the kinetics and thermodynamic aspects of crystal nucleation has been investigated since J. W. Gibbs theories on thermodynamics were accepted. The process is theorised to be split into two important steps: nucleation - birth of a stable critical nucleus followed by crystal growth - the rapid addition of more solute-building units to the growing nucleus. The problem that has fascinated previous researchers is exactly how nucleation occurs; the laws and pathways that must be obeyed to form crystal structures from solution. Does nucleation proceed first by generation of a more closely packed and more dense solute presences within solution, followed then by a careful and systematic alteration of molecular arrangement? Or do density and structure play a more combinatory role in nucleation, each one having integral influence on the process of the other? Before nucleation can be spontaneously achieved, does a molecularly specific critical size first have to be attained? Does the degree of supersaturation have any effect on the size or rate of generation of these critical nuclei?

In 1992 D. W. Oxtoby measured changes in nucleation rates within classical nucleation paths and had evidence that the nucleation rate could be manipulated by even delicate changes in factors such as temperature, pressure, and the extent of impurity and interaction potentials. P. G. Vekilov attempted to further the understanding of nucleation kinetics by observing crystal phase transitions from supersaturated solutions and found that classical nucleation theory was not sufficient in explaining kinetic data obtained. His research also showed that in protein solutions, an increase in extent of supersaturation had no effect on the rate of nucleation. And in 2007, Mendez-Villuendas *et al.* explored the limits of stability of gold nano-clusters in a supercooled liquid. They observed a local free energy minimum, which appeared at moderately supercooled temperatures. Nevertheless, the free energy becomes a monotonically decreasing function at lower temperatures. Therefore making it always thermodynamically more favourable to increase the size of the largest solid nuclei. This indicates that the liquid phase has become unstable.

By 2009, Erdemir, Lee and Myerson concluded that their own work in combination with previous work from Vekilov, indicated that nucleation of solids from a liquid state did not proceed via the classical methodology but instead by the alternative two-step model. Their work demonstrated that not only did the two-step nucleation method apply to macromolecules but also to small organic molecules. Whether or not this holds true for all liquid to solid phase transitions is uncertain.

Then, in 2010, Kawasaki and Tanaka found supercooled liquids to have hidden ordering, making their link with glass transitions fundamentally heterogeneous in nature and thus relating their positional ordering by critical fluctuations associated with bond-orientation ordering, originally proposed for protein solutions by Vekilov.

In the following work we will attempt to investigate whether or not the nucleation process for small organic solutions and ionic solutions conform to the classical or non-classical nucleation pathways, as discussed in related literature. To achieve this, one must first observe each selected solution in its undersaturated state before liquid instability begins to corrupt the dynamics of the solution. The average hydrodynamic radii will be measured and recorded over a range of solution concentrations using dynamic light scattering techniques.

Supersaturated aqueous solutions of the same molecular solutions will then be prepared and measured similarly to the undersaturated solutions. Analysis of critically sized nuclei within the solutions will be carried out using DLS and appropriate calculation of hydrodynamic radii. Cooling crystallisation on each solution will be employed to observe the relationship between the degree of supersaturation and both the average nuclei size and maximum (critical) nuclei size. We can then attempt to confirm whether or not a correlation exists between the mean hydrodynamic radii of undersaturated and supersaturated solutions.

A wide-angle range of measurements will then view the polydispersity of each solution to discern the existence of any hidden molecular species as larger particles will dominate the scattering signal at low angles and small particles will dominate at larger angles. This will give us a better understanding of the mean critical nuclei dispersed throughout the solution medium.

Once all data has been collected, an overall assessment can be carried out concerning the disparities and correspondences of small organic molecular and ionic salt solutions. General trends and patterns can be extracted and discussed using the relevant experimental data.

Chapter 2 - Theory

2.1 Supersaturation

For nucleation to occur the solution must be supersaturated. A supersaturated solution is one where the molarity of the solute species in its solution surpasses its thermodynamic solubility limits for a particular temperature and pressure.

The solubility of a compound substance in any solvent is the greatest concentration, which exists at equilibrium at a specific temperature and pressure. This maximum concentration often (but not always) increases with the solution temperature. Solubility therefore is defined by the extent that different compounds are dissolvable in one another. The component in largest excess in the solution is considered the solvent and the other component is therefore the solute. A saturated solution being one where equilibrium has been achieved and no more solute can dissolve.

A substance dissolves in a liquid if it has the capacity to disrupt the solvent-solvent interactions of the liquid and permits the bonding of solute-solvent molecules/ions.

The overall thermodynamic driving force for crystallisation is caused by the change in the chemical potential between two states. As chemical potential is difficult to quantify, it is more conveniently expressed by way of concentration of the solution: ¹

$$\Delta\mu = \ln(c/c^*) \cong c/c^* - 1 = \Delta c/c^* = S - 1 = \sigma,$$

where $\Delta\mu$ is the change in chemical potential, c is the standing concentration and c^* is the equilibrium saturation concentration, S is the supersaturation ratio and σ is the *relative* or *absolute* supersaturation. Supersaturation is often considered in terms of solute concentration in excess of solubility. In general, supersaturation is expressed in terms of concentration

$$\Delta c = c - c^*,$$

where c is concentration of the solution, c^* is the saturation concentration and Δc is known as the concentration driving force.

In general terms, a supersaturated solution, unlike a saturated solution, is not in phase equilibrium. The chemical potential for the solute in the solid phase is lower than that of the supersaturated solution. This causes the instability of the solution and will inevitably lead to nucleation and crystallisation of the more stable solid phase.

The solubility curve (Fig. 1) is divided into three distinct segments:

1. The undersaturated or stable segment. Here, no nucleation or crystal growth will take place. Any crystals present will dissolve into the solution
2. The supersaturated metastable region. In this region nucleation is under kinetic control and may not be possible near the solubility limit. Growth of existing crystals can still take place
3. The labile supersaturated segment, where nucleation and growth of crystals is rapidly spontaneous and favourable²

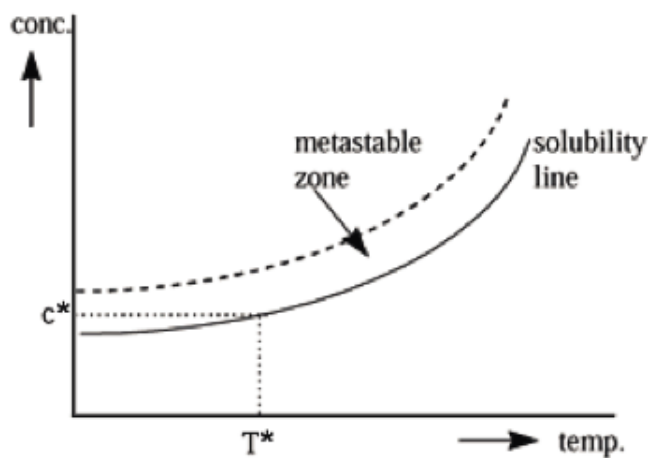


Fig 1. Solubility Curve³: Diagram shows concentration of a solution changing as a function of temperature. As the temperature decreases a barrier is crossed and a solution becomes supersaturated.

The metastable zone represents a region of high solute concentration within the solution. The metastable zone, shown in Fig 1, can be divided into two regions: a) very slow nucleation (below the super-solubility but above the solubility line) and b) significant nucleation (above the super-solubility line) but remains kinetically controlled. The super-solubility boundary is kinetically defined and is dependent on preparation of the sample and conditions of mixing. By altering a few key factors one can encourage a system to change from an undersaturated solution to a crystalline state.

- By reducing the temperature of the system we induce cooling crystallisation without the loss of solvent. Fig.2 (shown below) is an example of this method of crystallisation using urea as the crystallising solute.
- By altering the concentration of the solute within the system – evaporation of solvent at a constant temperature

- By altering the solvent composition - changing the solubility of the solute in the newly made solvent mixture⁴

Any significant change in one of these parameters would cause a change in the thermodynamic properties of the system. In general practice a combination of these techniques would be used.

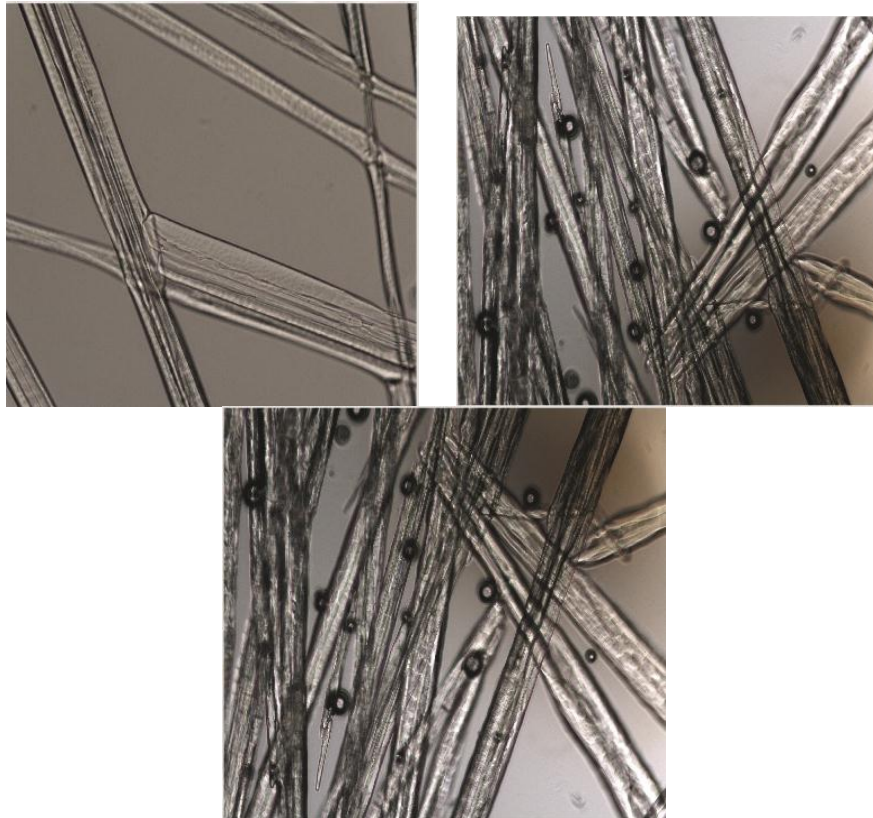


Fig. 2. Microscopic images of acquired from microscopic imaging of crystalline supersaturated urea performed using a cooling stage.

2.2 Nucleation

The first step in any crystal formation process is nucleation. It is commonly split into two distinct categories: primary – when dealing with a supersaturated solution free of any crystalline impurities and; secondary – when nuclei are formed due to influence from crystal fragments in the supersaturated solution.

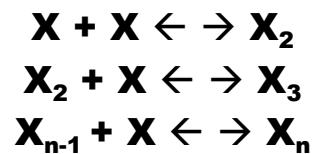
Primary nucleation is further subdivided into homogeneous nucleation and heterogeneous nucleation.⁵

- Homogeneous – spontaneous nucleation in clear, pure solutions, devoid of any solid matter and caused by phase transfer from least stable to most stable chemical state
- Heterogeneous – nucleation induced by interaction of solute molecules with foreign impurities in the bulk solution

The specifics for formation of a crystal nucleus within a homogeneous fluid are not explicitly known. In the supersaturated solution, constituent molecules or ions have to cluster together randomly in the medium

forming a new, denser phase. Not only must this new dense region of molecules resist the tendency to re-dissolve into the bulk medium again they must further re-order themselves to resemble the stable crystal lattice – this assumption was made for a condensation based nucleation and is not robust enough to be applicable for solution.⁶

In a standard undersaturated solution, Brownian motion governs the movement of solute particles; this is the randomised collision-based interaction of the solvent particles moving throughout the bulk solution (Fig.3). The phenomenon of fast-moving particles suspended in some fluid bombards any other molecule within the bulk and controls their diffusion throughout the system. The larger the molecular solute present, the slower it diffuses within the solution. A critical number of solute molecules need to gather together or, more precisely, a critical nucleus radii has to be reached before crystal stabilisation through growth can commence. It is not feasible to assert that a stable nucleus will be generated by the simultaneous collision of the exact number of molecules required to produce a critical nucleus. It is far more accurate to say that each critical cluster species is a consequence of many bimolecular collisions in a random ordered sequence.



Additional collisions preceding the formation of a critical nucleus will initiate nucleation and consequent growth of the nucleus.

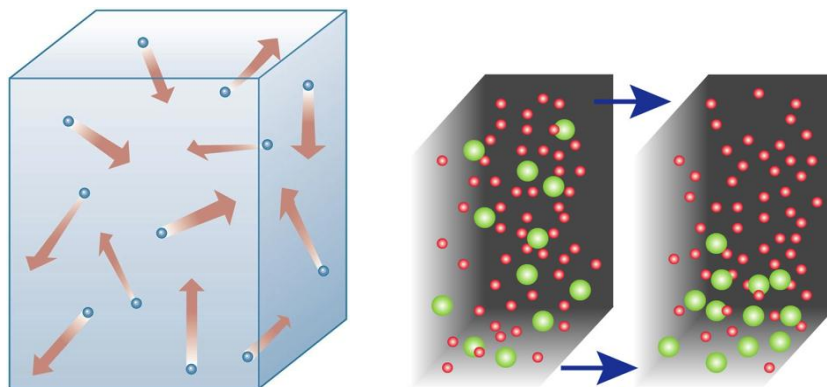


Fig. 3. *Particles in solution undergoing random Brownian motion⁷ (left), Diffusion of a two-component system (right)⁸.*

In heterogeneous nucleation, the process is stimulated by the presence of impurities such as particles, ions or foreign surfaces. Nuclei are normally formed on the sides of reaction vessels. These effects are

usually undesirable but the process of nucleation on foreign substrates is essential for epitaxial deposition of thin films.^{9, 10}

2.3 Thermodynamic Theory of Nucleation

Nucleation is typically considered under conditions of constant temperature and pressure. In this system the transfer of solute molecules from the solution to the crystal solid is driven by a change in the Gibbs free energy of crystallisation, $\Delta G^{\circ}_{\text{cryst}}$.¹¹ This change in energy of crystallisation is equal to the sum of contributions of enthalpy, $\Delta H^{\circ}_{\text{cryst}}$ and entropy, $\Delta S^{\circ}_{\text{cryst}}$:

$$\Delta G^{\circ}_{\text{cryst}} = \Delta H^{\circ}_{\text{cryst}} - T\Delta S^{\circ}_{\text{cryst}}$$

The associated crystallisation equilibrium constant:

$$K_{\text{cryst}} \equiv \exp(-\Delta G^{\circ}_{\text{cryst}} / RT), K_{\text{cryst}} = C_e^{-1}$$

Where C_e^{-1} is the solubility of the small organic molecule with respect to its crystalline form, R is the universal gas constant and T is the absolute temperature. Nucleation occurs within a supersaturated solution, where the concentration C of the solute is higher than the solubility at equilibrium, C_{eq} .

It was J. W. Gibbs who was first to recognise that there was a fundamental prerequisite required to form a new phase. That is, the appearance of small clusters of atoms, molecules or ions (the building units) within the volume of a supersaturated phase (fluid or melt).

The formation of ordered matter such as crystal solids is a first-order phase transition. As such, it is defined as having non-zero latent heat, $\Delta H^{\circ}_{\text{cryst}}$. More importantly, for the kinetics of phase transitions, is the second feature of first-order phase transitions, a discontinuity in concentration at the phase boundary. As a consequence of this discontinuity, the solution-crystal boundary and solution-dense liquid boundary have non-zero surface free energy. If a small fragment of a condensed phase forms in a supersaturated solution, the surface free energy of the emerging phase boundary makes this process unfavourable. Hence, a very limited number of embryos of the condensed phase appear as a result of the few fluctuations, which overcome the free energy barrier. The first step in the formation of a new phase in which, the kinetics of the phase transformation is determined by this barrier, is called nucleation.¹²

Gibbs theory was based on a simplistic thermodynamic approach, the classical nucleation theory. This theory, although oversimplified and flawed due to numerous assumptions, was a significant step forward in the understanding of the transitions between different states of aggregation.

2.4 Classical Nucleation Theory

In any thermodynamic system (stable or labile), there exists a trend for random, regional fluctuations of the medium's density. This tendency increases the thermodynamic potential of the system overall. When considering a homogeneous system (in a liquid or vapour phase) there are always small flux in density in the guise of small molecular aggregates, compatible with the bulk state of aggregation. The constant random motion of solvent molecules under Brownian diffusive control is the origin of these density fluctuations.¹³

If the initial phase is the stable phase then these “homophase” (named by Frenkel) fluctuations can be considered to have a negligible lifetime as they grow to insignificant size and decay without achieving unlimited growth. On the other hand, if the initial phase is unstable then the inclination to grow prevails once they have exceeded a certain critical size. It is these clusters of dense liquid that are known as the critical nuclei of the new phase. An energy barrier must be breached before such clusters can form, the height of which is given by the work of formation of the critical nuclei.

A general diagram of Gibbs free energy versus nucleus radii is given for a classical nucleation system (Fig. 4).

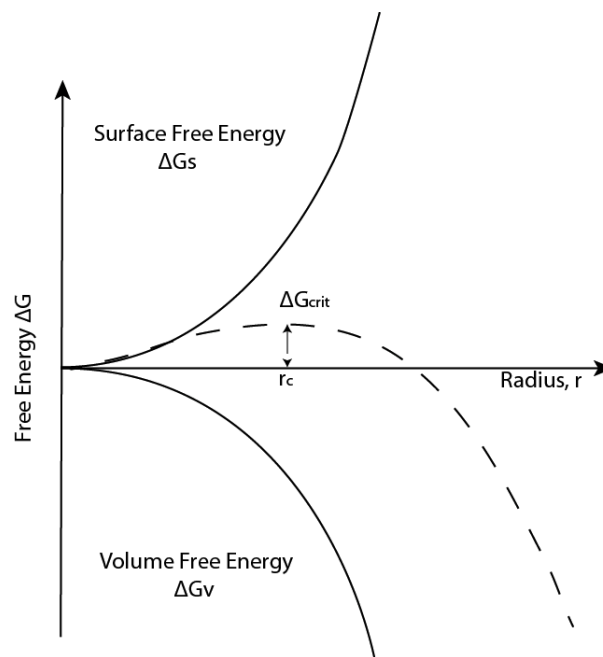


Fig. 4. Free energy diagram for classical nucleation: Shows the free energy change of an embryonic cluster with respect to the nucleus size.

$$\Delta G = \Delta G_s + \Delta G_v$$

The free energy change for a phase transformation, ΔG_v , is described as the spontaneous nature of a supersaturated solution to undergo deposition, which is fundamental in the generation of a new phase.¹⁴ As the solid form is more stable than the liquid (the chemical potential for an ordered solid is lower than that of an unordered liquid of equivalent chemical composition) ΔG_{vv} becomes negative and so decreases the Gibbs free energy of the system. Conversely, the introduction of a solid/liquid phase surface ΔG_s increases the free energy by a magnitude proportional to that of the clusters surface area. This results in the two factors competing in order to achieve a reserve of free energy and retain a stable chemical system. ΔG_s is positive and relates to the size of the nucleus by the expression:

$$\Delta G_s = 4\pi r^2 \gamma,$$

Where γ is the interfacial tension between the developing crystal phase and the supersaturated bulk phase and r is the nucleus radii. ΔG_v is a negative quantity related to the size of the nucleus via the expression:

$$\Delta G_{vv} = 4/3\pi r^3 \Delta G_v,$$

Where ΔG is the change in free energy of transformation per unit volume. So, the free energy needed for a phase transformation or the formation of a critical nucleus can be written in the form:

$$\Delta G = 4\pi r^2 \gamma + 4/3\pi r^3 \Delta G_v$$

In the case of a small sub-nucleus, the free energy ΔG increases with the size of the nuclei radius. The radius r increases until a limit in Gibbs free energy ΔG_{crit} has been attained. This signifies the generation of a critical nucleus. For a spherical cluster, this limiting free energy ΔG_{crit} is obtained by maximising the equation above,

$$\partial(\Delta G) / \partial(r) = 0.$$

Substituting ΔG gives:

$$\partial(4\pi r^2 \gamma + 4/3\pi r^3 \Delta G_v) / \partial(r) = 8\pi r \gamma + 4\pi r^2 \Delta G_v = 0$$

The critical size, which represents the minimum radial value for a stable nucleus can be acquired from rearranging the above equation gives:

$$r_c = -2\gamma / \Delta G_v,$$

Where ΔG_v is negative, therefore, the critical free energy of the system can be calculated from previous equations as:

$$\Delta G_{\text{crit}} = 4/3\pi \cdot \gamma \cdot r_c^2$$

Nuclei, which do not attain the critical radial size r_c will re-dissolve but aggregates which are larger than this value will continue growing in size, lowering their overall Gibbs free energy.^{15, 16}

The positive ΔG_s of surface energy dominate at smaller radii. This causes an increase in the total free energy. As a result, the smaller clusters within solution will tend to dissolve. As the cluster size increases, the total free energy will reach a maximum parabolic point at a critical size r_c . Above this point the free energy decreases continuously and the growth of the cluster becomes favourable and crystal nuclei are born.

2.5 Classical Nucleation Rate Theory

It was postulated by M. Volmer¹⁷ that the nucleation rate, J – the number of nuclei which, appear in a unit solution volume per unit of time – was analogous to the Arrhenius equation with expression:

$$J = J_0 \exp(-\Delta G^* / k_B T),$$

Where k_B is the Boltzmann constant.

The thermodynamics of classical nucleation theory were developed by J. W. Gibbs and his work was later modified by Vekilov (see ref. 4), to consider the free energy balance of a cluster containing n molecules of size a , instead of a cluster of radius r , as was presented in the Gibbs papers.

In a supersaturated solution, where the chemical potential of solution is greater than that of the chemical potential in the crystal phase, which has $\Delta\mu > 0$, the formation of dense solute regions causes a loss in free energy of $-n\Delta\mu$. Conversely, the generation of the phase boundary of area S and surface free energy α between the cluster and the solution leads to an energy gain of $S\alpha$. If we assume that the cluster is cubic then $S = 6a^2 n^{2/3}$. Thus giving,

$$\Delta G^* (n) = -n\Delta\mu + 6a^2 n^{2/3} \alpha$$

Where \mathbf{n} is the number of molecules in the crystal, $\Delta\mu$ is the degree of solution supersaturation, α is the surface free energy and $\Delta\mathbf{G}$ is the system free energy; (* notes critical cluster).

Differentiation of the above equation $\Delta\mathbf{G}^*(\mathbf{n})$, we find the cluster size \mathbf{n} for which $\Delta\mathbf{G}$ passes through a maximum. Factors such as pressure, temperature concentration and degree of supersaturation affect the rate of nucleation through $\Delta\mathbf{G}^*$ by:

$$\Delta\mathbf{G}^* = 32\Omega^2\alpha^3/\Delta\mu^2 \quad \text{and} \quad \mathbf{n}^* = 64\Omega^2\alpha^3/\Delta\mu^2,$$

where, $\Omega = \mathbf{a}^3$ is the volume occupied by a molecule in the crystal, $\Delta\mathbf{G}^*$ is the barrier that must be overcome to form a crystal from solute molecules. The growth of clusters smaller than \mathbf{n}^* is associated with an increase of free energy and is therefore unfavourable. Clusters may grow to such sizes as a result of fluctuations but since a driving force exists for the decay of these clusters, such events are rare. If a cluster reaches a size greater than \mathbf{n}^* , its growth is accompanied by a decrease in free energy and occurs spontaneously. A cluster of size \mathbf{n}^* has equal probability of both growth and decay, hence, such clusters are called critical and represent the nuclei of the new phase.

The final expression for the statistical-mechanical derivation of the nucleation rate encompassing classical nucleation theory,¹⁸ can be represented as:

$$\mathbf{J} = \mathbf{V}^* \cdot \mathbf{Z} \cdot \mathbf{n} \cdot \exp(-\mathbf{G}^*/k_B T),$$

Where \mathbf{V}^* is the rate of attachment of monomer units to the nucleus, \mathbf{Z} is the *Zeldovich factor*, which accounts for the width of the free energy profile $\Delta\mathbf{G}(\mathbf{n})$ in the vicinity of the maximum $\Delta\mathbf{G}^*$ and \mathbf{n} is the number density of molecules in solution.¹⁹ In this equation, it is assumed that the replacement partition function of the nucleus is equal to one. This factor accounts for the additional stabilisation of the nuclei due to their translational and rotational degrees of freedom.²⁰ The kinetic factor is associated with the rate of fusion of molecules to the critical nucleus, therefore is reliant on molecular mobility of the system.²¹ Molecular mobility alters quickly with temperature and so the temperature dependence of the pre-exponential factor can be very important.

As has been previously mentioned, the classical nucleation theory is an oversimplified model system based on the condensing of a vapour to a liquid drop. Therefore a number of assumptions have been made to generalise the theory, making it for the most part, incompatible with other applications and cases such as nucleation of crystals in solutions. Such assumptions are listed below:

1. Nuclei clusters are modelled upon spherical droplets, each having a uniform density and sharp surface interfaces. The droplet density is independent of its size and equal to the density of the bulk-condensed phase. In a solution, this assumption means that the molecular building blocks are

in some way ordered and that the interior of the crystal embryo has an identical structure to that of the crystal.²²

2. The curvature or size dependence of the surface tension is ignored. The surface energy is estimated to be independent of temperature. (Capillarity approximation).²³
3. A growing cluster will continue to increase in size by the attachment of one monomer at any single time.²⁴ Collisions of multiple particles as well as other clusters themselves colliding or fragmenting into smaller clusters are ignored. Clusters are stated to be at rest and do not undergo translational, vibrational or rotational motion.
4. The stationary distribution of sub-critical solute clusters is established as soon as super saturation has been achieved (see ref 8). The rate of nucleation is time-independent and the process is considered in steady-state kinetic terms.
5. The clusters are incompressible and the vapour-phase around them is considered to have classical thermodynamic properties of an ideal gas. Generation of clusters has no effect on the vapour state.

2.6 Inconsistency of Classical Nucleation theory

Although all input parameters for classical nucleation theory were known with a fine degree of accuracy for condensation experiments, there still remained a few orders of magnitude between the theoretical and experimentally measured nucleation rates for single-component fluids. This was an indication of the theories insufficiency. Experiments on homogeneous nucleation of water showed that the prediction of the nucleation rate at various degrees of supersaturation and varying temperatures by a classical theory approximation was reasonable, however the temperature dependency of the predicted rates was not correct.²⁵ Classical theory has practical success in single-component systems but is oversimplified for binary nucleation theory as composition is assumed to be uniform throughout the droplet.

The steady-state nucleation rate was calculated using the conditioning that the size distribution of clusters throughout the system does not alter over time. This results in an invariable nucleation rate with a linear increase of the number of nuclei with time.²⁶ The assumption fails at the start of the process of nucleation, as a certain time-period, called the transition time, is necessary to establish a steady-state distribution of pre-critical clusters.²⁷ In the case of some experiments, the relaxation path into steady-state takes a much longer time period than the characteristic lifetime of the supersaturated system. Hence, a steady-state nucleation does not exist.

In a paper by Yau and Vekilov, atomic force microscopy was used in-situ on crystallising apoferritin from solution, to capture images of newly arranged molecules in near-critical clusters ranging above and below the size of the critical crystal nucleus. By using a protein modelled system they overcame two problems concerning the size of the molecular species being visualised and the systems short lifetimes.^{28, 29}

As the critical clusters are relatively small they are free to move around the available bulk volume under Brownian diffusive control.

A further advantage of atomic force microscopy (AFM) is that it can monitor in-situ, real-time molecular environments at atmospheric temperature and pressures where protein crystallisation tends to occur. A limitation of AFM is that it can observe clusters, which exist in the solution bulk only if they adsorb onto an available surface site.³⁰

These experiments showed that the arrangement of the molecules of the nuclei in the new phase was similar to that in the crystal and that the nucleus shape can vary from the normally accepted shape for quasi-spherical molecules such as apoferritin.

This technique would not be as effective in discerning the structure of small organic molecules as their critical nuclei would appear less clear when imaged by AFM. The lifetimes of small organic molecular clusters are smaller than for proteins. As they are orders of magnitude smaller they diffuse more quickly into the bulk. As a surface characterisation technique, AFM would not be as useful in observing clustering species which were not adsorbed onto a surface. Yau and Vekilov concluded that for the protein apoferritin, the ordering of molecules in the nuclei is similar to that in the crystal and that the nucleus shape can vary from the generally accepted shape. This could lead to significant deviations of the thermodynamics and kinetics of nucleation of first-order phase transitions predicted from classical nucleation theory. If the critical nuclei forming are not spherical, CNT can no longer be valid.

Whilst the classical nucleation theory allows the estimation of the size of the critical nucleus and subsequently the nucleation rate, it does not afford any information about the structure of aggregated species or possible/favourable pathways leading from the solution to the crystal state.

2.7 Two-Step Nucleation

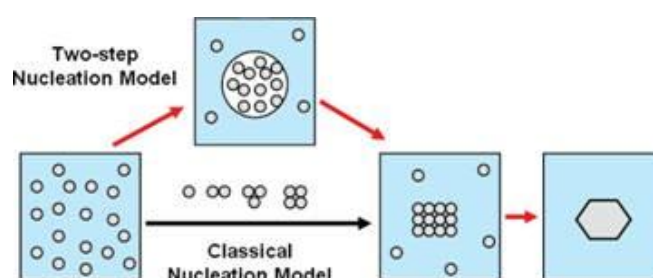


Fig. 5. Comparison of the growth steps of two crystal nucleation theories.³¹

Two-step or non-classical nucleation theory makes the assumption that large density fluctuations within the component system allow the formation of a new more-dense liquid phase within the mother solution. The generation of this dense phase is considered the first in the two-stage process of nucleation and results in

the decrease of free energy of the system. The liquid phase, formed in solution, is made up of building block components, which are able to re-arrange and configure to make more complex structures (Fig. 5). Such building blocks can be small liquid droplets, aggregated species or even amorphous regions. The dense phase contains a larger concentration of solute molecules compared to that found in the bulk solution. The formation of liquid droplets is considered to be due to the generation of this higher concentration of solute particles, possibly by some liquid-liquid separation.

The nucleation of crystals and their growth involves some rearranging in the randomised structure of the molecules making up the new phase and in the average molecular density, in the case of solution we refer to its solute concentration. There exist two order parameters that affect the nucleation process and they need not be intrinsically entwined. An order parameter is a quantity that is zero in one phase and non-zero in the other. This value characterises the extent of the order/disorder at a phase transition. For a solid/liquid system, the order parameter is concerned with density; this includes the proximity of molecules as well as their arrangement relative to one another.

Specifically, for small-molecule liquids, which tend to be largely incompressible, changes in density can be achieved only after the crystal structure has formed. Hence, the critical nucleus is dominated by changes in the structure order parameter.³² Lomakin *et al.* produced a paper in 2003 based on the two-step nucleation process of proteins. They found that a protein crystal should typically nucleate not as a small crystal but instead as a more stable aggregate. When this disordered aggregate reaches a critical size, only then, can it form a new crystal structure. The limiting step of the nucleation process is the ordering of a critical aggregate, not the subsequent unordered crystal growth, which follows.³³

Kaschiev *et al.* recorded a further study into the kinetics of nucleation processes in 2005. They proposed the mechanism of a two-step nucleation process, involving firstly, the generation of a droplet of dense liquid and secondly, crystallisation within the droplet upon ordering of a critical number of molecules. The conclusions made in this paper revealed that crystallisation of a supersaturated solution can be delayed by either a slow growth rate of the droplets or by the slow nucleation mechanism of the crystals within them or a combination of both. This showed that the formation rate of the intermediate metastable region determined the number of nucleated crystals.³⁴

A non-classical nucleation route has also been put forth for the crystallisation pathway of small molecules and due to the dense-liquid state being established as energetically favourable compared to the classical path, it was suggested that a liquid-liquid separation might be a common phenomenon.³⁵

The liquid-liquid separation as a mid-step preceding crystallisation was first observed in larger supersaturated solutions, containing proteins. Vekilov studied the nucleation rate of lysozyme crystals in concentrated solution.^{36, 37} The existence of a liquid phase at high concentration of protein was shown to significantly affect the crystal nucleation kinetics. Nucleation rates under conditions that are close to the liquid-liquid separation boundary in the phase diagram of the protein solution are smaller than predicted for a given protein concentration and temperature. In contrast, the nucleation kinetics for experimentation in the region slightly above this phase barrier is greater by up to 20 times the expected rate. Additional

research of metastable liquid protein clusters in supersaturated and undersaturated solutions was carried out using dynamic light scattering and atomic force microscopy. Results provided proof of the existence of clusters ranging from 10s to 1000s of nanometres in size. These dense regions were found to be metastable with respect to the solid crystal phase as well as the low-concentration protein solution. Within an undersaturated solution the clusters have a typical lifetime of only a few seconds whereby they re-disperse into the lower density bulk solution. Conversely in a supersaturated solution the clusters are metastable with respect to the crystalline phase and are the precursor to the formation of the ordered structures. The general size of the clusters remained independent of the protein concentration in the solution but the frequency with which they were detected increased with higher concentrations of protein. This would seem to indicate that a preferred cluster size exists through which nucleation is more likely to occur.^{38, 39}

One of the principle studies which first supported a two step mechanism for the process of nucleation was recorded by ten Wolde and Frenkel who studied homogeneous nucleation in a Lennard-Jones system of short range attraction by the Monte Carlo technique.⁴⁰ They confirmed that away from the fluid - fluid critical point ($T > T_c$ or $T < T_c$), fluctuations along density and structure order-parameters occur concurrently, in a similar manner as the classical standpoint. Large density fluctuations were monitored near the critical point, which caused a sudden change in the route for nucleation and crystal growth. The generation of a highly disordered liquid cluster was preceded by the generation of a crystalline nucleus within the dense liquid phase (Fig. 6). Moreover, proximity to the critical point reduces the free energy barrier for crystallisation and therefore increases the nucleation rate by many orders of magnitude. The presence of this intermediary dense liquid phase was shown to be a common feature for solutions, which interact through short-range interactions.⁴¹ Such interactions are characteristic of protein solutions.

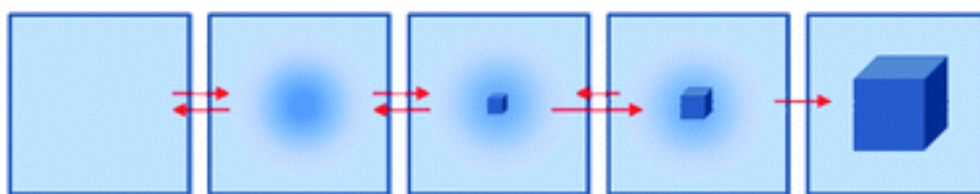


Fig. 6. Diagram of the two-step mechanism of nucleation.⁴² A clustered phase growing more ordered from left to right.

The lack of experimental evidence for two-step nucleation in simple fluids could be explained by the very short lifetime of the metastable phase in these systems. By careful calculation of the parameters, which govern the concentration fluctuations in solutions, pre-nucleation clusters for a number of salts were observed to have an amorphous structure with diffuse boundaries.⁴³ In light of these findings it was concluded that nucleation was at the very least, a two-step barrier pathway in respect to thermodynamics and chemical potentials, where the first step necessary for the formation of clusters requires a lower energy than the foremost barrier essential for the transformation of the pre-formed cluster into a stable crystal nucleus.

In addition, measurements of the concentration profile and Gibbs free energy of the interface between protein crystal and aqueous solution confirmed the two-step nucleation mechanism.⁴⁴ It would appear more likely that a mechanism with small activation energies for each individual step would be expected to be faster than a one-step mechanism with a single large activation barrier.

In a lysozyme solution, the formation of liquid droplets with high protein concentration, that is, the first step, was found to be the rate-determining step of the nucleation process. In more recent studies, a phenomenological system of protein crystallisation by way of an intermediate liquid state was developed and demonstrated that the rate-determining step in the nucleation mechanism was the formation of an ordered cluster within the dense liquid intermediate.⁴⁵

2.8 The Metastable zone

The discovery that liquids and solutions could be cooled to temperatures (sometimes significantly) below their thermodynamic freezing temperatures indicates that there has to be a kinetic boundary for the crystallising phase transition (Fig. 7). This could result from the slowness of the nucleation process. In the absence of heterogeneous impurities to catalyse the nucleation process, the fluctuation required to access the crystal phase can be many times the magnitude of the free energies, which are obtained thermally.⁴⁶ The barrier for crystal formation can be sufficiently lowered by supercooling or super-saturation to observe nucleation in a real timescale. However, kinetic factors related to a decrease in the rate of diffusion can prevent nucleation or the crystal growth step regardless of the large thermodynamic driving force.

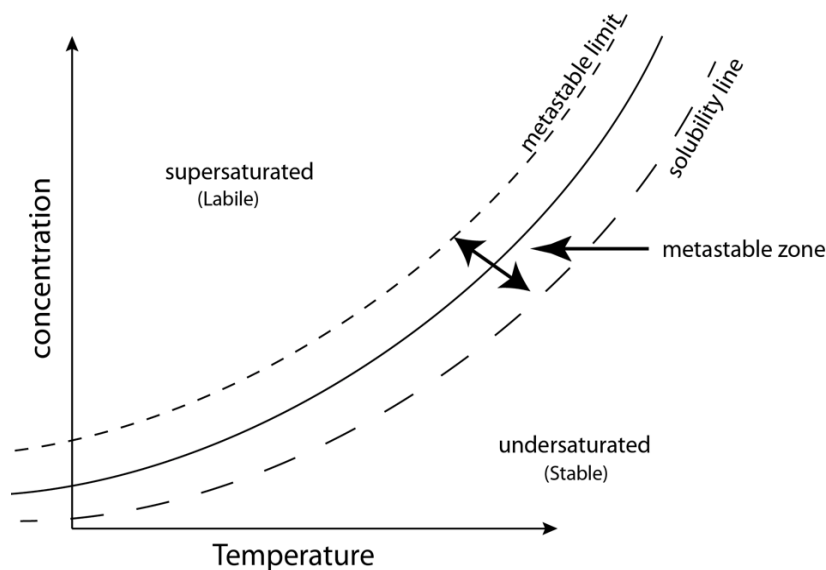


Fig. 7. Super-solubility curve diagram

Studies carried out by Oxtoby had been concerned with the tendency of small organic molecules to be predominantly affected by the structural order parameter, only allowing changes in density once the crystalline structure had appeared (ref 26). For colloids and proteins, the presence of a metastable critical point beneath the liquid-crystal phase coexistence line means that fluctuations in density can become very large. This would tend to suggest the possibility that the generation of critical nuclei might be an aggregation process, which would involve clusters of disordered particles. Were the periodic arrangement of the crystalline structure takes a smaller role later in the nucleation process lifetime. Talanquer *et al.* intended to investigate this theory by applying the density functional theory methodology to the same problem that had fascinated ten Wolde and Frenkel (ref 36). They had suggested that the conditions of optimal crystal growth, containing the smallest nucleation barrier possible, corresponded to the non-classical critical nucleus. They linked the presence of a metastable fluid-fluid critical point to the observed enhancement of crystal nucleation in solutions of globular proteins under certain conditions (Fig. 8). Talanquer *et al.* concluded that the nature of crystal nucleation changed qualitatively close to an underlying metastable critical point and that the barrier to nucleation is decreased significantly there and so increases nucleation rates by approximately 10 orders of magnitude.

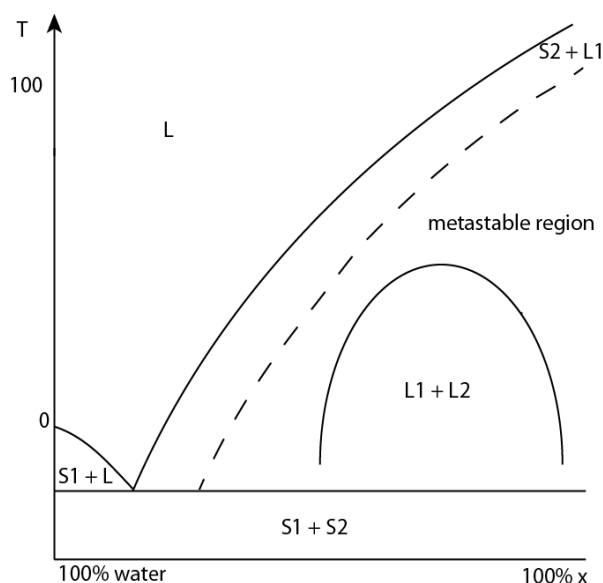


Fig. 8. Composition diagram of a liquid-liquid separation region within the metastable zone.

The metastable zone width is defined as an extent of the degree of supersaturation. It is uniquely characteristic of a supersaturated system and can be influenced by a number of factors, including temperature of saturation, rate of supersaturation generation (also known as cooling profile), impurity level, degree of solution mixing and the solutions state history in general.⁴⁷

Investigation into the metastable zone width has been well documented and a number of techniques have been utilised to carry out the research. The polythermal technique is one of the most abundantly used techniques for MSZW determination.⁴⁸ The process involves cooling a saturated solution at a constant rate

until nucleation is triggered. The experiment is repeated for numerous cooling profiles and saturation temperatures with the noted nucleation temperature allowing the calculation of the metastable zone width for a given rate – this in turn gives some information about the nucleation kinetics. The techniques used to detect the physical onset of nucleation include visualisation⁴⁹, electro-zone sensing⁵⁰ and optical turbidity.⁵¹ The choice of detection method is not trivial as often there is a time delay following nucleation when the particles grow to the detectable size range. This often has a sway over the success of the kinetics estimation.⁵²

2.9 Liquid-liquid Separation

The liquid-liquid separation phenomena was first observed to be an intermediate step within the crystallisation process by Vekilov *et al.* while experimenting on the nucleation rates of large proteins within supersaturated environments (see ref. 36 and 37). Hass and Drenth looked at the protein-water phase diagram; the phase diagram revealed a metastable liquid-liquid expanse where nucleation advances by way of two steps. This first being generation of small liquid droplets and the second being the formation of small crystalline nuclei inside the densely populated, high concentration region.⁵³

The crystallisation process has been studied to a greater extent with respect to small molecular solutions and numerous papers have recorded some evidence of some supersaturated systems that generate phases, which retain liquid-like attributes.^{54, 55}

Many of these studies agree that solutes tend to associate to form clusters involving a number of solute units.

A nucleation study was carried out by Davey *et al.*, to observe molecular crystal nucleation of supersaturated solutions of aqueous urea, sucrose and citric acid using small angle X-ray scattering (SAXS) and wide angle X-ray diffraction (WAXD) to find evidence of any in-situ structural rearrangement preceding crystallisation. No pre-rearranging structures were detected within the supersaturated aqueous solutions of urea, sucrose or citric acid and it was theorised by the authors that the lack of evidence could stem from such solutions having very short lifetimes or even suggesting that the aqueous solutions could follow an alternative nucleation mechanism⁵⁶

Implementing both thermodynamic and structural modelling methodologies, the dependence of solvent in nucleation of saccharin from acetone and ethanol was observed. The study maintained that nucleation of saccharin arose from the monomer species when solvated in acetone as opposed to an association of dimers when carried out in ethanol. It was shown that the specific kind of solute-solvent interactions could significantly alter a preliminary association of solute molecules supplying evidence of a direct relation between molecular structural association in solution and within the solid crystal phase.⁵⁷

Small Angle Neutron Scattering (SANS) exposed colloidal structures or metastable clusters of the amino acid vanillin formed when dissolved in solutions of aqueous alcohol. It was theorised that there existed two diverse phenomena linked with phase separation, one region undergoing a liquid-liquid phase separation by way of spinodal decomposition and the other undertaking crystallisation.⁵⁸

There still remains much uncertainty about concerning the role of solvent-solute interactions in influencing polymorph nucleation processes. Georgalis *et al.* considered both supersaturated and undersaturated solutions of sodium chloride, ammonium sulphate and sodium citrate using dynamic light scattering. The study showed that both solutions contain two pre-dominant constituents, molecular species with a radius less than 1nanometre (suggesting solvated ions) and larger particles with radii between 50-500nanometres (suggesting ion clusters).⁵⁹

Veesler *et al.* began investigation into the phase diagram of a pharmaceutical compound called irbesartan ($C_{35}H_{42}N_3O_2$) within a solvent mixture of ethanol and water. Irbesartan has two structural polymorphs, the solubility of which is high in ethanol and low in water. For an in-depth investigation into the liquid-liquid phase separation phenomena within the phase diagram, Static light scattering, HPLC measurements and video microscopy were utilised. The data compiled concluded that the mechanism of crystallisation and the process kinetics would alter depending on the initial position on the phase diagram. Due to these findings, the final product can have a different solid phase, crystal habit, morphology and size. Furthermore, it was observed that the liquid-liquid phase separation modifies the medium as well as the conditions of crystallisation and hinders its nucleation for several hours.^{60, 61, 62, 63}

The nucleation mechanisms of a simple amino acid, glycine, have been studied extensively due to its molecular simplicity and three existing polymorphic arrangements: alpha, beta and gamma. Their thermodynamic stability under normal temperature and pressure is $\gamma > \alpha > \beta$. Each can be attained via different methods, alpha glycine is crystallised out from aqueous solution, gamma glycine is established from a solution with $pH > 8.9$ or $pH < 3.8$ or from deuterated aqueous solution with $pH = 7$. The labile/metastable beta polymorph crystallises from water-ethanol aqueous mixtures or via freezing of aqueous solutions.^{64, 65, 66, 67, 68}

The polymorph formation process is more complex than previously believed and the three polymorphs of glycine have been discovered in the same solution defined as a concomitant mixture.^{69, 70}

Myerson looked into the diffusion coefficients of supersaturated solutions of glycine and concluded that the clusters, which formed were largely dimers and trimers, though a few clusters were found that contained hundreds of molecules.⁷¹

Further SAXS studies of the nucleation process of glycine proposed that the first step of glycine crystallisation involved the formation of liquid-like clusters of solute molecules, while the second step involved the rearrangement of these clusters into a more ordered crystalline structure.^{72, 73}

The SAXS results presented in a paper by Gidalevitz demonstrates data which may indicate larger structures present in crystallising aqueous solutions of glycine, with sizes of a few hundred nanometers. These large clusters could be considered dense glycine- rich liquid clusters which incite the first step in the

crystallisation route and could be compared to the dense liquid-protein clusters reported by Vekilov.^{74, 75, 76} Additional research into supersaturated aqueous glycine (by Davey *et al*) indicated that solute molecules in solution also existed as clusters resembling each of the known polymorphs. (See ref. 56).

Huang *et al* utilised freezing point depression and diffusion measurements on supersaturated solutions of glycine to confirm in what binding state glycine largely consisted of. It was discovered that glycine, in supersaturated solution, is made up of 70% monomer units with the remainder estimated to be dimers.⁷⁷ This was agreed upon by Hamad *et al.* who used Molecular Dynamic simulation to study the nucleation of glycine from aqueous solution. He did however also observe evidence that the remainder existed as dimers, trimers and few of an even larger size, *i.e.*, tetramers and pentamers⁷⁸

To glean the most accurate set of interpretable data to give an accurate depiction of cluster and molecular sizes under supersaturated conditions, a number of techniques should be applied. Light scattering techniques such as DLS and SLS are more sensitive to larger particles than smaller species even when very few exist. It should also be compromised due to the existence of even larger dense-liquid clusters.

Advanced experimental techniques have allowed the monitoring of molecular interaction in under-saturated, saturated and supersaturated solutions of large protein and small organic and ionic molecules. The results show that a commonly proposed mechanism of nucleation involves a two-step mechanism: dense liquid precursor formation (liquid-liquid separation) followed subsequently by the appearance of solid crystalline nuclei. However, the liquid-liquid separation is still poorly understood and is often considered to be undesirable within the context of crystallisation processes as it leads to slow crystal growth and unpredictable crystal morphologies. It will become necessary, in future research, to improve our understanding of the liquid-liquid phase separation phenomena as well as the conditions under which a liquid-liquid partition occurs. This will grant us a better chance of controlling these processes that lead to formation of desirable crystal products.

Chapter 3 - Experimental Methods

3.1 Chemicals and solvents

All chemicals and solvents used were of laboratory reagent grade and did not require further purification.

They were supplied by:

- Urea – analytical agent – purity $\geq 99.5\%$ (Analar)
- Glycine – Assay spec: $\geq 99.0\%$ (Sigma Aldrich)
- Sodium Chloride – purity $\geq 99.0\%$ (Fisher Scientific)
- Potassium Chloride – purity $\geq 99.5\%$ (Analar)
- Sodium Nitrate – purity $\geq 99.0\%$ (Sigma Aldrich)
- D-(+)-Glucose – assay $\geq 99.5\%$ (GC) – (Sigma Aldrich)
- Deionised water was supplied from an in-lab milipore water system

3.2 Concentrated aqueous solutions

For preparation of each aqueous solution all glassware was washed with acetone, ethanol and distilled water. Glass cuvettes were wrapped in aluminium foil and left to dry in a drying-oven. All 2ml syringes were sealed and sterilised.

Each solution was prepared by adding weighed amounts of each compound to sample vials containing 10ml of distilled-deionised water. Each solution was mixed vigorously at room temperature to encourage dissolution. Once all solute was dissolved successfully, 2ml of solution was then removed via a Terumo syringe and injected slowly through a 0.2 μm pore size PTFE filter into a dried cuvette. Each cuvette was then sealed and left to equilibrate for a period of 24 hours at laboratory temperature. Prior to each cuvette sample being inserted into the DLS sample holder ethanol was used to remove any dirt or fingerprint marks on the glass.

The following solutions were prepared by the methods outlined above:

- Urea concentrations - 0.083, 2.059, 6.185 and 8.234 molL⁻¹
- D-(+)-glucose - 0.5, 2.5 and 4.5 molL⁻¹
- Glycine - 0.5, 1.5 and 2.5 molL⁻¹
- Sodium nitrate - 3, 6 and 9 molL⁻¹
- Sodium chloride - 2 and 4 molL⁻¹
- Potassium chloride - 2 and 4 molL⁻¹

For any solutions where solute was not completely dissolved by vigorous mixing, samples were then sonicated for between 30 minutes and 1 hour.

3.3 Solubility measurements

All chemicals and solvents used were of laboratory reagent grade and did not require further purification (see 5.1). In order to carry out experimentation on supersaturated solutions at specific temperatures, the solubility data was required for those temperatures. Therefore a number of solubility measurements were carried out and compared with data found in literature.

3.3.1 Filtration

An excess quantity of each compound was weighed out and added to a pre-weighed sample vial then agitated with a small volume of distilled water and heated to a steady temperature of 40 degrees Celsius. The solution was then left for a period of 24 hours. After heating, the remaining undissolved material was removed by filtration using a pre-weighed 0.45µm pore size filter (Anotop). The filter and the sample vial with any remaining solute were left to completely dry at laboratory temperature for 7 days. They were then both weighed and the mass of dissolved solute was calculated from the overall change in weight.

3.3.2 Dissolution of crystals

Data acquired from the filtration solubility measurements was used in order to make the dissolution experiment more efficient with relation to time of experiment and allow for a more accurate approach to the measurement by adding smaller quantities of solvent at each interval.

For each substance, a 0.5g quantity was measured out and placed in a clean and sterile sample vial. Each vial was placed in an incubator heated to around 40°C. An acetone-washed and oven-dried beaker filled with deionised water was placed in the incubator along with a glass pipette. Once the equipment had been given an hour to reach temperature equilibrium with the incubator chamber, the solubility experiment was begun.

A quantity of deionised water equal to 90% of that calculated in the filtration solubility measurement (for each specific solute) was measured out with a pipette (at 40°C) and added to the sample vials. The vials were then sealed and left in the chamber for 24 hours to settle and warm back to incubator temperature. Next, a small volume of solvent (approx. 10 micro-litres) was added. After every new addition of solvent

the solution was mixed and left for an hour before being observed for existence of crystals. This process was repeated until all solute was fully dissolved. Based on this observation, the solubility was calculated.

This measurement was carried out for samples of Urea, NaCl, KCl, NaNO₃, glucose and glycine.

3.4 Preparation of Supersaturated Solutions

All chemicals and solvents used were of laboratory reagent grade and did not require further purification (see Section 5.1). All equipment was cleaned with acetone/ethanol and rinsed with the solvent liquid, in this case deionised water then oven-dried in the case of glassware. All sample vials and syringes were sterilised before use.

The supersaturated solution of urea was prepared by dissolution of a predetermined mass of Urea in 10 ml of deionised water in a sealed sample vial. The vial was then placed in an incubator, preheated to 60 degrees Celsius and allowed to warm. After an hour the solution is shaken vigorously to encourage dissolution of the solute. This is repeated until no solute is visible. The solution is then filtered by a 0.2µm PTFE syringe-filter (using a sterilised syringe) into a glass cuvette. The cuvette is sealed and kept in the incubator for 24 hours. The filter, syringe and cuvette are all preheated to 60°C to prevent spontaneous crystallisation taking place. The cuvette is positioned in a small beaker of preheated water in order to prevent any formation of crystals during or preceding filtration.

The same method for the preparation of the supersaturated urea solution was repeated for preparation of D-(+)-glucose, glycine, sodium nitrate, sodium chloride and potassium chloride supersaturated solutions. New sterile vials, syringes and PTFE filters were used and new cuvettes were washed carefully and oven dried.

3.5 Cooling Crystallisation

All chemicals and solvents used were of laboratory reagent grade and did not require further purification (see Section 5.1). The supersaturated solutions of urea, KCl, NaCl, NaNO₃, glucose and glycine were prepared as described in 5.4.1. The cuvettes were placed into a small beaker full of incubator heated water and the samples were moved to the DLS sample holders which were preheated to 45°C beforehand to prevent significant reduction in temperature causing spontaneous crystal nucleation, when the sample cuvette was inserted. The cuvette was left to equilibrate with the sample holder temperature for an hour to stop temperature convection currents from affecting the diffusion of the solute particles in the solution. After an hour had passed the DLS measurement was taken at a range of angles and then the temperature of the sample holder was lowered by 5°C. This process was repeated until a temperature of 20°C was reached.

Chapter 4 - Light scattering Theory

Light scattering is a mechanism, which involves the absorption and re-emission of electromagnetic radiation. When light impinges on matter, the electric field of the light induces an oscillating polarisation of electrons within the molecules.⁷⁹ The polarised molecules then emit a secondary source of light and so, subsequently scatter light.

In a perfectly homogeneous and isotropic material the radiation scattered by individual particles interferes destructively, meaning that no scattered radiation will be observed. Hence, scattered radiation is only captured when the solution being investigated is in some way heterogeneous. For a multi-component system, the main scattering signal is due to the difference in optical properties, which is the difference in refractive indexes.⁸⁰

In a typical experimental set-up, a monochromatic laser beam illuminates a dispersion of particles within a solution. The directional magnitude of this beam is defined by an incident wave vector k_i with magnitude equal to:

$$k_i = 2\pi m_1 / \lambda_0 = m_1 n_0 / c,$$

where λ_0 , n_0 , m_1 and c are the wavelength, circular frequency in vacuum, the medium refractive index and the speed of light in vacuum, respectively. The radiation scattered under an angle θ with respect to the incident beam is characterised by a scattering wave vector k_s in the direction of propagation of this beam. The scattering vector \mathbf{q} is an important indicator of the properties of the scattered light. It is defined as the difference between the incident and scattered wave vector:

$$\mathbf{q} = k_i - k_s,$$

In dynamic light scattering the magnitude of \mathbf{q} is given by:

$$q = (4\pi n_0 / \lambda_0) \sin(\theta/2)$$

Dynamic light scattering, also known as photon correlation spectroscopy and quasi-elastic light scattering, is able to determine the size-distribution profile of small particles in suspension or within solution. Light is scattered by the interaction of the electrons with the incident radiation. The oscillation electric field causes a vibration on the electrons turning them into oscillation dipoles. These dipoles emit radiation and as the electrons are constantly moving sources of radiation (due to Brownian motion), the frequency of the radiation is shifted to higher or lower frequencies, depending on its velocity and direction relative to the detector (Doppler effect).⁸¹

When light hits small particles the light is scattered in all directions (Rayleigh scattering) as long as the particles are small in comparison to the wavelength of the incident light. If the incident light source is a laser and thus is monochromatic and coherent, then a time-dependent fluctuation is observed in the scattering intensity. These fluctuations are caused by small particles in the solution undergoing Brownian motion – the random movement of particles due to bombardment of the solvent molecules surrounding them - and hence the distance between the scattering particles in the solution are ever changing with time. The scattered light then undergoes either constructive or destructive interference by the surrounding particles and within this intensity fluctuation, information is contained about the time scale of movement of the scattering particles.

3.1 Dynamic Light Scattering

In dynamic light scattering the dynamic information of the particles are derived from an autocorrelation of the intensity trace recorded during the experiment. The auto-correlator acts as a signal comparator, measuring the degree of similarity between two signals, or one signal with itself at varying time intervals. If the intensity of a signal is compared with itself at a particular point much later in time, then for a randomly fluctuating signal it is can be surmised that the intensities are not going to relate in any way, *i.e.*, there will be very little or no correlation between them. However if the intensity of the signal at time t is compared to the intensity a very small time later ($t + dt$), there will be a strong relationship or correlation between the intensities of the two signals. At short time delays, the correlation is high because the particles do not have a chance to move any great distance from their initial state. As the time delays become longer, the correlation starts to exponentially decay to zero. Via an auto-correlator, these functions are monitored and a time-dependent intensity correlation function is calculated.

In systems where the solutions are of higher concentration, *i.e.*, have a larger density and consequently involve more inter-particle forces, diffusion becomes highly dependent on interactions which makes interpretation of data more complex and the scattering function no longer decays as a single exponential.

Once the autocorrelation data has been generated, mathematical approaches are employed to analyse it. The signals collected by the detector are transferred to the correlator which then takes the varying intensity measurements and converts them to the intensity autocorrelation function: $G_2(\tau)$,

$$G_2(\tau) = \langle I(t) \cdot I(t + \tau) \rangle$$

The autocorrelation function of scattering intensity $g_2(\tau)$ is defined as the average intensity value registered at a specific time $I(t)$ multiplied by the intensity taken at a later time $I(t + \tau)$. The autocorrelation function $G_1(\tau)$ can then be used to calculate the distribution of particles of different sizes throughout the sample.

For a mono-dispersion of particles in solution, the autocorrelation function $g_2(\tau)$ decays exponentially due to Brownian motion with equation:

$$g_1(\tau) = B \exp(-\Gamma \tau)$$

with a decay rate of $\Gamma = \mathbf{D} \cdot \mathbf{q}^2$ where B is the intercept equal to $g_1(0)$, D is the particle diffusion coefficient and \mathbf{q} is the scattering wave vector:

$$q = (4\pi n / \lambda) \cdot \sin(\theta/2)$$

where n is the refractive index of the solvent, λ is the wavelength of the laser in vacuum conditions and θ is the scattering angle.

From the Stokes-Einstein equation:

$$D_t = k_B T / 6\pi\eta R_H$$

We can calculate the average hydrodynamic radius of the particles R_H , where k_B is Boltzmann's constant, T is the absolute temperature and η is viscosity of the bulk liquid at a specific temperature.

The analysis is slightly more complex in the case of a poly-dispersed sample, the autocorrelation function $g_1(\tau)$ decays such that:

$$g_1(\tau) = \Sigma \langle I_i(t) \rangle \exp(-\Gamma_i \tau) ; \Gamma_i = D_i \cdot q_i^2$$

i.e., $g_1(\tau)$, is the intensity weighted sum of all exponential decays due to the diffusion of varying sized particles within the sample.

As the scattering intensity of micron and submicron sized particles is significantly dependent on the scattering angle and particle size, the situation may occur whereby a certain fraction of particles within a polydispersed solution become difficult to detect at certain angles while it may dominate the signal at others. Due to this phenomenon a survey of correlation functions over several angles could give more information concerning the solutions size distribution than any one single-angle analysis. A primary concern when using multiple scattering methods is that the size distribution data gathered is purely mathematical calculation from correlation data and not the actual separation of particles. Therefore, the data has only limited value without supporting data via other experimentation methods.

Analysis of the autocorrelation data can be carried out using numerous methods of fitting such as Cumulant or Contin. These methods are of primary use when estimating particle size and size distribution. 82, 83, 84

The use of dynamic light scattering has been prevalent throughout the observance of pre-crystalline species and metastable liquid clusters. Onuma and Kanzaki used the technique to monitor molecular clustering of proteins through the aggregation process.⁸⁵ Moreno *et al* continued with the approach in looking at proteins in pre-crystalline environments.⁸⁶ As previously mentioned, Vekilov and co detected dense liquid clusters in undersaturated and supersaturated protein solutions (see ref. 74-76).

Chapter 5 - Data Acquisition and Analysis

Dynamic light scattering measurements carried out to ascertain particle hydrodynamic radii during cooling crystallisation were performed using a class 3b He-Ne laser with a wavelength of 633nm from the JDSU laser company. The laser is connected to an ALV compact goniometer system and an ALV light scattering electronics and multiple tau digital correlator. In addition the laser is equipped with water heated temperature control.

The cumulant analysis of autocorrelation function data is widely used for determination of particles hydrodynamic radius. When analysing data for a mono-disperse sample (Fig. 8), the analysis consists of fitting the initial decay of the autocorrelation function, by use of a polynomial up to the third order, to the function $\ln(g_1(\tau))$, where:

$$g_1(\tau) = (g_2(\tau)-1)^{1/2}, g^1(\tau) = (e^{-\Gamma\tau})$$

so,

$$\ln(g_1(\tau)) \approx -\Gamma \cdot \tau,$$

where the graph of $\ln(g_1(\tau))$ vs. τ is a straight line with a gradient proportional to the decay rate and the decay rate is inversely proportional to the particle size (Fig 10). The average diffusion coefficient D and the average hydrodynamic radius R_H are related via the Stokes- Einstein equation:

$$D = k_B T / 6\pi\eta R_H$$

Where the diffusion coefficient D can be found via the equation:

$$\Gamma = D.q^2$$

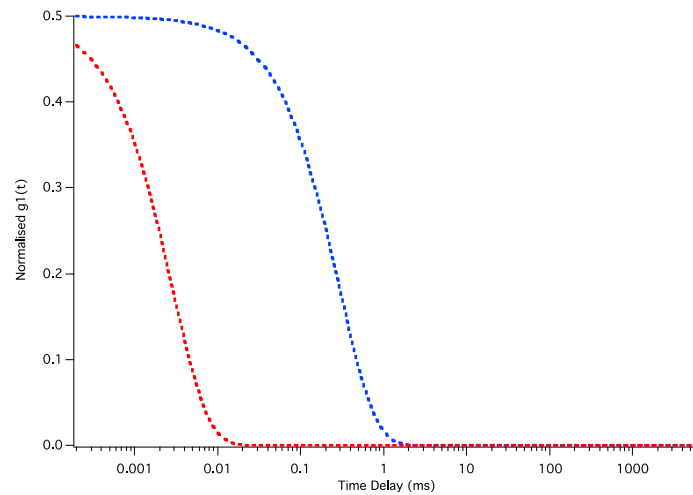


Fig. 9. Monomodal autocorrelation function of small particles (red) and large particles (blue).

In a polydispersed or greater solution, we can add the sum of the autocorrelation functions to replicate a double decay (Fig. 10), which provides information on the radius of two or more species diffusing within the solution.

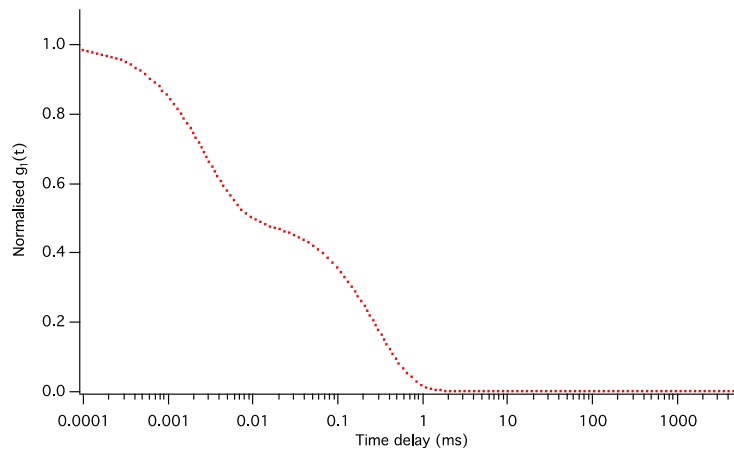


Fig. 10. Bimodal decay autocorrelation function.

For any poly-dispersed samples the graph $g_1(\tau)$ is a sum of the exponential decays and as a consequence the graph of $g_1(\tau)$ vs τ is no longer linear and so can be fitted by a polynomial of up the third order (Fig. 11 and Fig. 12) with the initial decay rate being calculated from the linear term coefficient B and $\ln(g_1(\tau))$ becomes non-linear. (Linder *et al* 2002).

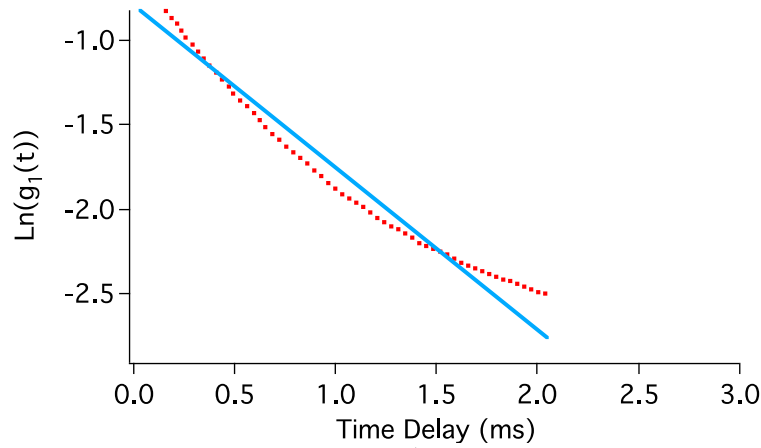


Fig. 11. Polynomial fit of the function $\ln(g_1(\tau))$ vs t , using 1st order fit with polynomial $ax+b$

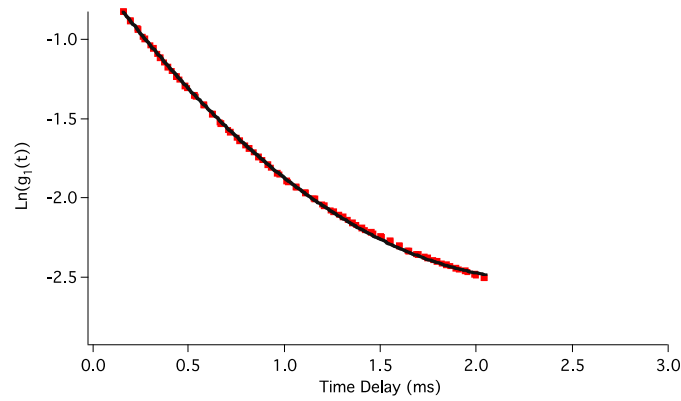


Fig. 12. Polynomial fit of the function $\ln(g_1(\tau))$ vs t using second order fit with polynomial ax^2+bx+c .

When considering the analysis of multi-angle measurements, the initial approach is to account for the angular dependence of the particle scattering intensities.⁸⁷ This results in an angular dependence of the intensity weights, c_i and of the decay rates, Γ_i .

$$g_1(q, t) = \sum_{i=1}^N c_i(q) \exp\{-\Gamma_i(q) t\}$$

The intensity weights, c_i , can be related to the number of particles, n_i , in each particle size class, i on a relative scale by

$$c_i(q) = n_i S_i(q)$$

where $S_i(\theta)$ is the intensity scattered at an angle θ by a single particle with diameter d_i .

5.1 Latex sphere analysis

Latex spheres of known diameter – (0.105 ± 0.003 micrometers) - were diluted in aqueous solution and used to obtain an autocorrelation function (Fig. 12), which could be used as a standard with which to calibrate an autocorrelation function analysis program template. The solutions were diluted in deionised water until solution was no longer opaque and was then sonicated to assist dispersion of any agglomerated latex units within the sample.

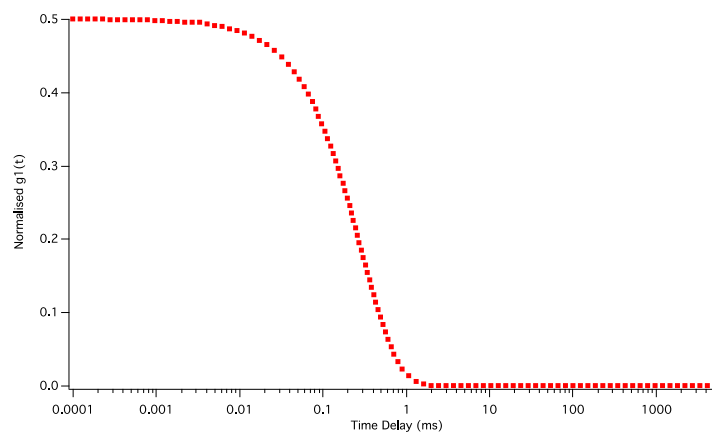


Fig. 13. Autocorrelation function of mono-disperse aqueous diluted latex sphere solution.

By fitting a polynomial to the graph of $\ln(g_1(\tau))$ vs lag time, the average particle size of a molecular species can be determined using cumulant analysis. An example of an autocorrelation data fit from **Fig. 12** can be seen in **Fig. 13**. The average radius calculated by using the 1st and 2nd order polynomials is approximately 55.5 nm and 51.9 nm, respectively.

Because the experimental data can be quite noisy, especially when referring to the first decay, the higher orders of the fitted polynomial are less accurate and therefore less useful.

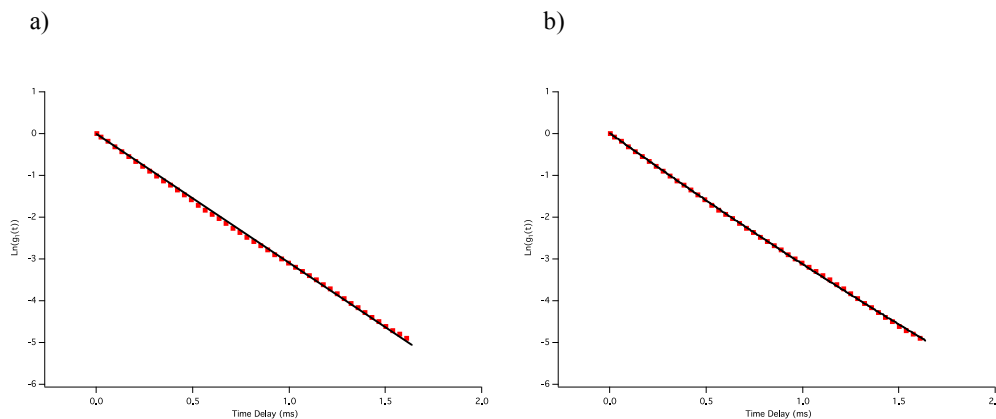


Fig. 14. Polynomial fit of the mono-dispersed latex sphere autocorrelation function $\ln(g_1(\tau))$ vs t , a) 1st order fit with polynomial $ax+b$ and b) second order fit with polynomial ax^2+bx+c .

Concentration (mol/ml)	Hydrodynamic Droplet Radius (nm) -1 st order	Hydrodynamic Droplet Radius (nm) -2 nd order	Hydrodynamic Cluster Radius (nm) -1 st order	Hydrodynamic Cluster Radius (nm) -2 nd order
Dilute Latex Sphere	52.95(±0.524)	52.56(±0.490)	-	-

Table 1. Average hydrodynamic radii of mono-disperse latex sphere in aqueous solution.

In order to account for an accurate error approximation of the average hydrodynamic radius a common estimator for variance is an adjusted version of standard deviation; what is known as Bessel's correction.⁸⁸ For this correction of the sample standard deviation, where N is the total number of sample observations, N-1 is used in place of N; this helps correct the bias in the estimation.

$$S_N = \sqrt{\frac{1}{N} \sum_{i=1}^N (x_i - \bar{x})^2} \qquad S_N = \sqrt{\frac{1}{N-1} \sum_{i=1}^N (x_i - \bar{x})^2}$$

Where x_1, \dots, x_N are the observed values of the sample and \bar{x} is the mean of these observations.

The bias is created during estimation of a sample when the complete population mean is unknown; the sample variance becomes a biased estimator of the population variance and hence underestimates its value. While the sample variance (using Bessel's correction) is an unbiased estimate of the population variance, its square root, the sample standard deviation, is a biased estimate of the population standard deviation.

Chapter 6 - Dynamic Light Scattering Experimental

Chapter 6 Summary:

1. Deionised water – sample background analysis

2. Undersaturated solutions analysis

- Urea, Glucose, Glycine, Sodium Chloride, Potassium Chloride, Sodium Nitrate

3. Supersaturated solutions analysis

- Urea, Glucose, Glycine, Sodium Chloride, Potassium Chloride, Sodium Nitrate

4. Multi-angle scattering solution analysis

- Urea, Glucose, Glycine, Sodium Chloride, Potassium Chloride

6.1 Deionised water background signal

Control background experiments were performed to show that no scattering species were present within the filtered deionised water solutions prior to mixing (Fig. 15). The results produced can, therefore, not be ascribed to the formation of impurities or bubbles, but must arise due to the solute-solute and solute-solvent interactions in the undersaturated solutions.

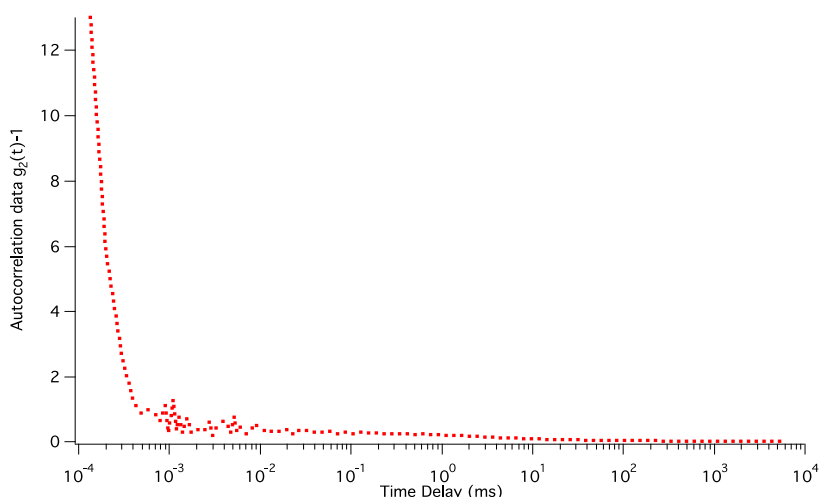


Fig. 15. Autocorrelation function, $g_2(t)-1$, of water filtered through $0.2\mu\text{m}$ PTFE filter.

6.2 Undersaturated Solutions

Dynamic light scattering provides characterisation of nano-sized particles within solution. Diffusion coefficients of molecules under Brownian diffusive control can be determined along with their mean particle size with use of time-dependent fluctuations of light intensity.

The following data was collected from various aqueous solutions of known concentrations.

6.2.1 Urea

Dynamic light scattering analysis was executed on a number of undersaturated solutions over a range of concentrations. The resulting autocorrelation functions revealed the existence of both molecular clusters as well as larger nano-droplet species within some undersaturated solutions.

Even solutions well below the measured solubility limit at room temperature show evidence for larger aggregated moieties. Although nano-droplets were observed for each sample solution, their average size does not appear to be influenced by the extent of the concentration. The following figures (14-19) represent the data analysis of each molecular solution of specified concentrations.

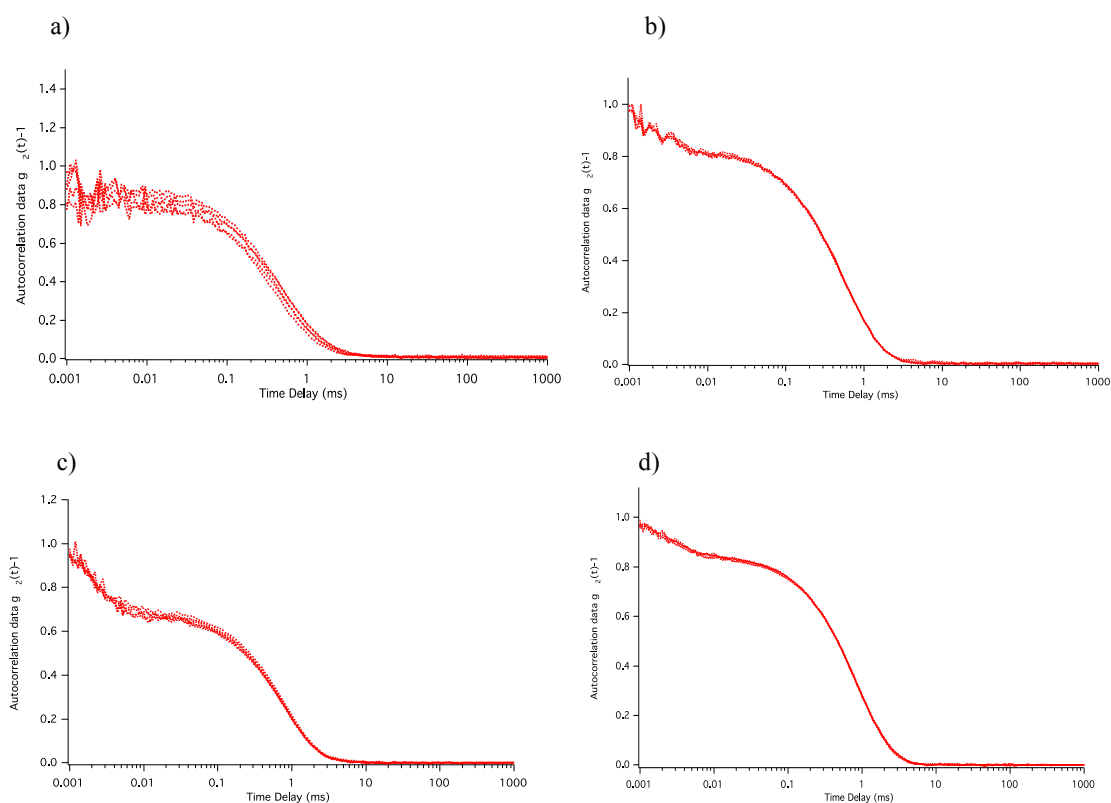


Fig. 16. Graphs of autocorrelation functions ($g_2(t)-1$) against time (t) of undersaturated aqueous urea at specific concentrations: a) 0.842 molar, b) 2.059 molar, c) 6.185 molar and d) 8.234 molar.

For each sample, a number of data sets were collected and plotted against one another to give some indication of the average time fluctuating signal. From the resulting analysis of the scattering species, the average radii was calculated from the autocorrelation function ($g_2(t)-1$).

Samples of undersaturated urea solutions were created when urea was added to deionised water and dissolved before being filtered through a 0.2 micrometre PTFE filter. From each autocorrelation function collected over the range of urea concentrations, the hydrodynamic radii were calculated from the rates of decay of the particles present in solution. These radii values were used to calculate an average value for each solution molarity and then calculate a standard error.

All graph plots of undersaturated urea (Fig. 15) agree that there exists some presence of nano-metre sized aggregate for all concentrations. The data for graphs of Fig. 15 a) shows no sign of the existence of any sub-nano sized particles i.e. small clusters of single or few monomer units of urea. This could suggest that under low concentrations the solution dynamics allow almost all urea-water molecules to interact, likely via hydrogen bonding.

Concentration (mol/ml)	Hydrodynamic Droplet Radius (nm) -1 st order	Hydrodynamic Droplet Radius (nm) -2 nd order	Hydrodynamic Cluster Radius (nm) -1 st order	Hydrodynamic Cluster Radius (nm) -2 nd order
0.083	78.7 (\pm 19.3)	97.7 (\pm 9.03)	-	-
2.059	106.5 (\pm 0.84)	99.5 (\pm 4.1)	0.482(\pm 0.081)	0.506(\pm 0.033)
6.185	151.8 (\pm 1.7)	142.3 (\pm 2.9)	0.454(\pm 0.102)	0.408(\pm 0.043)
8.234	169.2 (\pm 2.0)	169.5 (\pm 2.07)	0.465(\pm 0.090)	0.374(\pm 0.012)

Table 2. Average hydrodynamic radii of concentrated aqueous urea solutions – measured using polynomial line fits of each autocorrelation function ($g_2(t)-1$).

According to the literature, we would expect to see molecular clusters. Possibly of varying size ranges, from monomers to tetramers etc. This would be due to a polar solute dissolved in a polar solvent with the chance of partial association. Immediately we can see the existence of some larger particles throughout all data sets and the appearance of some smaller cluster as urea concentration is increased - two scattering signals forming a binomial decay. Calculated droplet radii magnitudes of the first and second decays show an increase in size as the concentration of solute increases (Table 2). This increase in size could be indicative of a concentration dependent agglomeration of associative polar solutes, within an undersaturated bulk solution

6.2.2 Glucose

Much like the urea solutions, the glucose solutions were prepared using an equivalent methodology using 0.2 micrometre filters. The autocorrelation functions ($g_2(t)-1$) of Fig a), and b) demonstrate decays of molecular species with varying sizes. Each of the curves, measured from aqueous glucose at specific concentrations, both display strong binomial decay signals (Fig. 16).

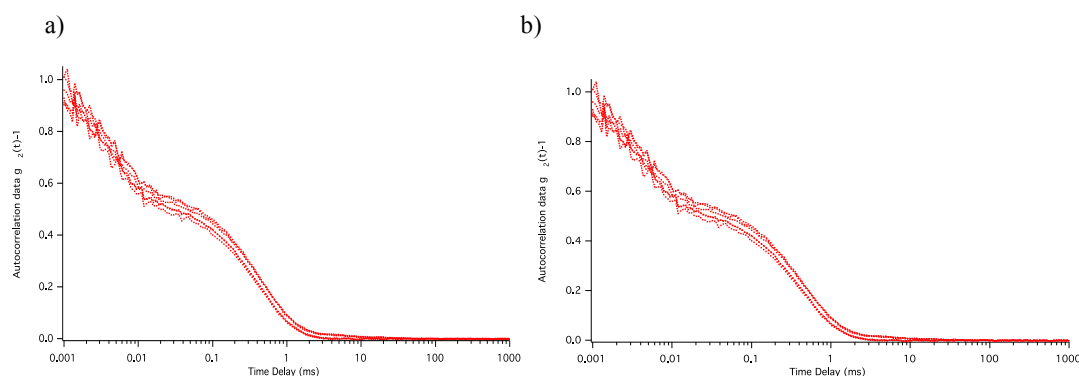


Fig. 17. Graphs of autocorrelation functions ($g_2(t)-1$) against time (t) of aqueous glucose solutions at specific concentrations: a) 0.5 molar, b) 4.5 molar.

For both glucose solution concentrations there exists a two-part decay curve indicating the existence of two differently sized aggregates. The first, at the microsecond timescale, is of a single molecule size range approximately 1 nm in size and could be made up of monomers or possibly dimer units; this depends on the clustering scheme of the glucose and water molecules. The second decay shows an average droplet size of around 90 nm. The dynamics of undersaturated glucose solutions show similar behaviour to that of the previous urea solutions. Each show that in stable and even weakly concentrated solutions, agglomerate particles readily exist within the bulk solution. The data recorded in Table 3 shows a good agreement in hydrodynamic radii calculations of both the small cluster species and of the larger droplet species.

Concentration (mol/ml)	Hydrodynamic Droplet Radius (nm) -1 st order	Hydrodynamic Droplet Radius (nm) -2 nd order	Hydrodynamic Cluster Radius (nm) -1 st order	Hydrodynamic Cluster Radius (nm) -2 nd order
0.5	82.2 (± 0.7)	82.9 (± 2.7)	0.875 (± 0.4)	0.963 (± 0.06)
4.5	97.3 (± 5.4)	95.2 (± 4.6)	0.984 (± 0.06)	1.21 (± 0.9)

Table 3. Average hydrodynamic radii of concentrated aqueous glucose solutions - measured using polynomial line fits of each autocorrelation function ($g_2(t)-1$).

6.2.3 Glycine

Three solutions of aqueous glycine, again prepared in a standardised fashion, as previously described, provide signals suggestive of large droplet nano-particles approximately 70 nm in size (Fig. 17). These concentrated solutions show weak to no evidence for the existence of molecular clusters, or at least any consistent validation of stable sub-nano species. This could suggest that glycine, in an aqueous solution, is almost incapable of existing as a single monomer unit or even as a small oligomer group within an undersaturated solution.

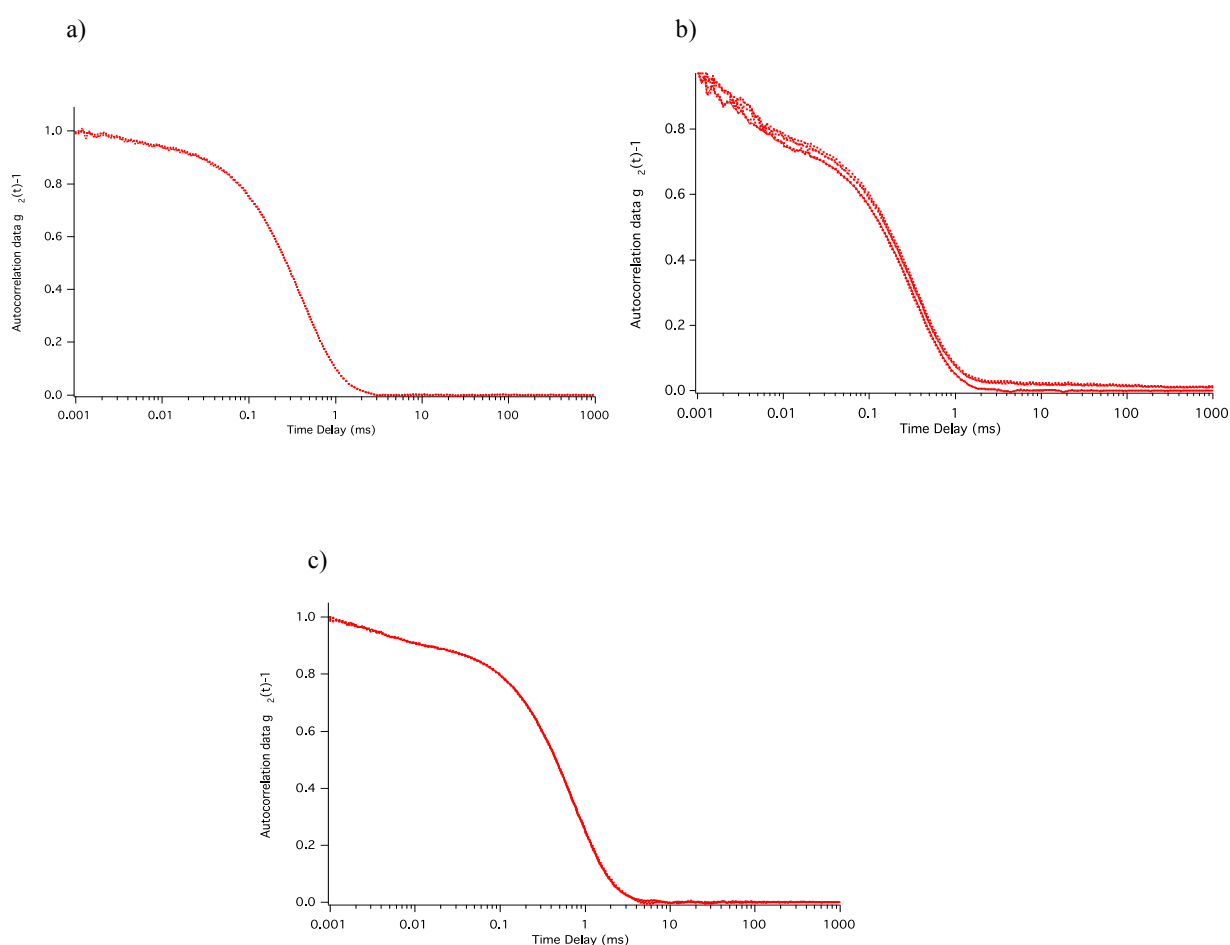


Fig. 18. Graph of autocorrelation functions ($g_2(t)-1$) against time (t) of aqueous glycine solutions at specific concentrations: a) 0.5 molar, b) 1.5 molar, c) 2.5 molar.

Concentration (mol/ml)	Hydrodynamic Droplet Radius (nm) -1 st order	Hydrodynamic Droplet Radius (nm) -2 nd order	Hydrodynamic Cluster Radius (nm) -1 st order	Hydrodynamic Cluster Radius (nm) -2 nd order
0.5	73.3 (±0.06)	73.3 (±1.7)	-	-
1.5	63.5 (±3.4)	55.6 (±3.4)	0.67 (±0.067)	0.87 (±0.4)
2.5	129.3 (±0.5)	121.2 (±17.9)	-	-

Table 4. Average hydrodynamic radii of concentrated aqueous glycine solutions - measured using polynomial line fits of each autocorrelation function ($g_2(t)-1$).

The selected glycine solutions indicate that there does exist a dual decay of exponential functions within concentrated solutions, though for some of these the molecular sized species are difficult to determine (Table 4). This is perhaps due to the larger species dominating the signal in some cases.

Publications from sources such as Gidalevitz, Vekilov and Davey have demonstrated that, within solutions of crystallising glycine, there is proof of the generation of larger pre-crystalline structures. These structures, however, have only been presented within solutions in a super saturated state. The suggestion that these larger species may also exist within undersaturated solutions is unexpected.

6.2.4 Sodium Chloride

Solutions of sodium chloride salts were prepared by dissolution of pre-weighed salt in deionised water followed by filtration through 0.2 micrometre PTFE filters. Autocorrelation function data indicates the presence of one or more constituents in the undersaturated solution (Fig. 18).

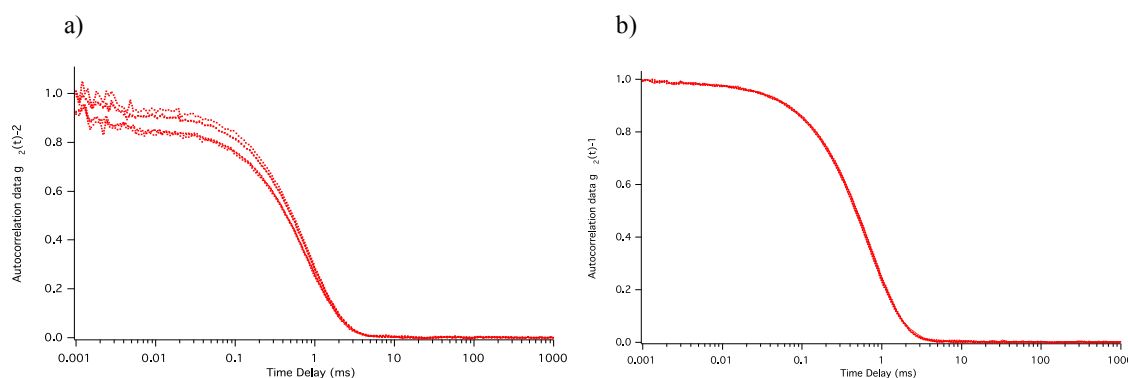


Fig. 19. Graphs of autocorrelation functions ($g_2(t)-1$) against time (t) of undersaturated aqueous sodium chloride solutions at specific concentrations: a) 2 molar, b) 4 molar.

Georgalis *et al.* recorded findings of both small solvated ions and larger ion droplet structures.⁸⁹ Some of the data is not sufficiently strong as to allow accurate fitting of the smaller species, but we can presume that these decays are most likely due to solvated ions in the solution. The larger constituent of the exponential decays can only be estimated as being caused by the aggregation of ionic clusters within solution.

Concentrated aqueous solutions of undersaturated sodium chloride appear to have such weak small cluster signals that they appear invisible due to the domination of the decay curve by the larger molecular species within solution. The dynamic light scattering analysis gives only an insight into the generation of larger nanodroplets. These precursors to critical nuclei are within the range of 100 - 150 nm (Table 5) and could possibly increase in size as more solute is added to solution, though more thorough experimentation would be required to verify this. Research carried out by Alexandre and Hansen commented that clustering and nucleation of ions in aqueous solutions supposedly results from a competition between ion hydration and association.⁹⁰

Concentration (mol/ml)	Hydrodynamic Droplet Radius (nm) -1 st order	Hydrodynamic Droplet Radius (nm) -2 nd order	Hydrodynamic Cluster Radius (nm) -1 st order	Hydrodynamic Cluster Radius (nm) -2 nd order
2	123.3(±8.5)	111.7(±4.8)	-	-
4	145.8(±8.4)	139.3(±6.8)	-	-

Table 5. Average hydrodynamic radii of concentrated aqueous Sodium Chloride solutions – measured using a polynomial line fit of each autocorrelation function ($g_2(t)-1$).

6.2.5 Potassium Chloride

Potassium chloride solutions were prepared in a similar method to the sodium chloride solutions. The autocorrelation functions indicate reveal the presence of molecular droplets of size range 100-120 nm (Fig. 19). These large molecular droplets can be assumed to be the result of the agglomeration of ionic clusters within solution. As with the sodium chloride previously, there appears to be weak (or no) small cluster species shown, but as before we can assume that these signals are simply too small to plot effectively or accurately.

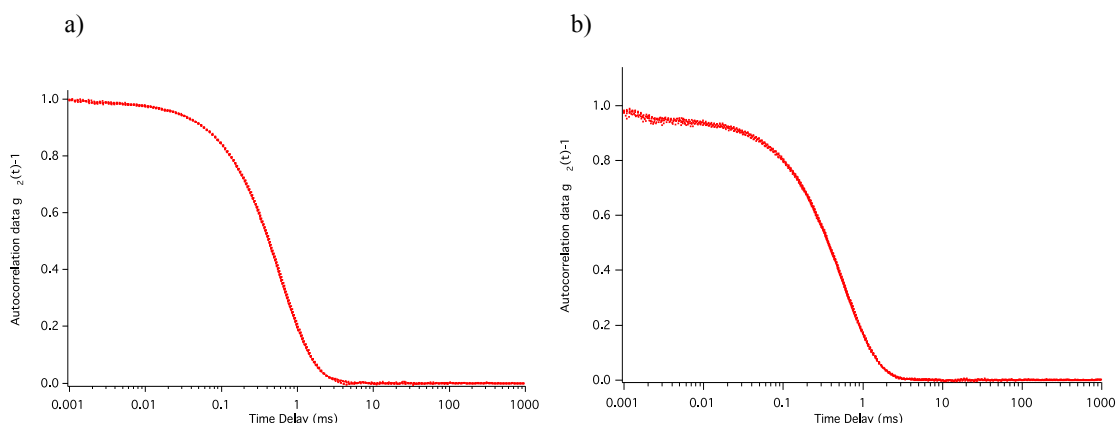


Fig. 20. Graphs of autocorrelation functions ($g_2(t)-1$) against time (t) of undersaturated aqueous potassium chloride solutions at specific concentrations: a) 2 molar, b) 4 molar.

Potassium chloride solutions of low concentrations show only monomial exponential decays, indicating the existence of 100 nm sized ionic clusters (Table 6). The lack of any binomial signal, indicating the existence of small clusters, may be due to charged ionic particles dispersed throughout the solution. These charged species; potassium and chlorine ions, do not appear to form small partial clusters, either consisting of ions of opposing charge or water molecules.

Concentration (mol/ml)	Hydrodynamic Droplet Radius (nm) - 1 st order	Hydrodynamic Droplet Radius (nm) - 2 nd order	Hydrodynamic Cluster Radius (nm) - 1 st order	Hydrodynamic Cluster Radius (nm) - 2 nd order
2	120.5(±6.6)	100.8(±8.9)	-	-
4	101.6(±3.1)	95.4(±7.1)	-	-

Table 6. Average hydrodynamic radii of concentrated aqueous Potassium Chloride solutions – measured using polynomial line fits of each autocorrelation functions ($g_2(t)-1$).

6.2.6 Sodium Nitrate

Sodium nitrate solution provides clearer evidence for the existence of both entities manifestation within the bulk. The plot of $g_2(t)-1$ vs t becomes steadily noisier in signal at the beginning of the decay, this noise takes the shape of the first decay of a binomial which appears increasingly more characterised as the concentration increases (Fig. 20). This allows us to distinguish between single ion and ionic cluster decays more easily than in the sodium chloride and potassium chloride solutions. This clarity could be due to the size and polarisation difference between the free nitrate ion and the single chlorine ions of the other two salt solutions.

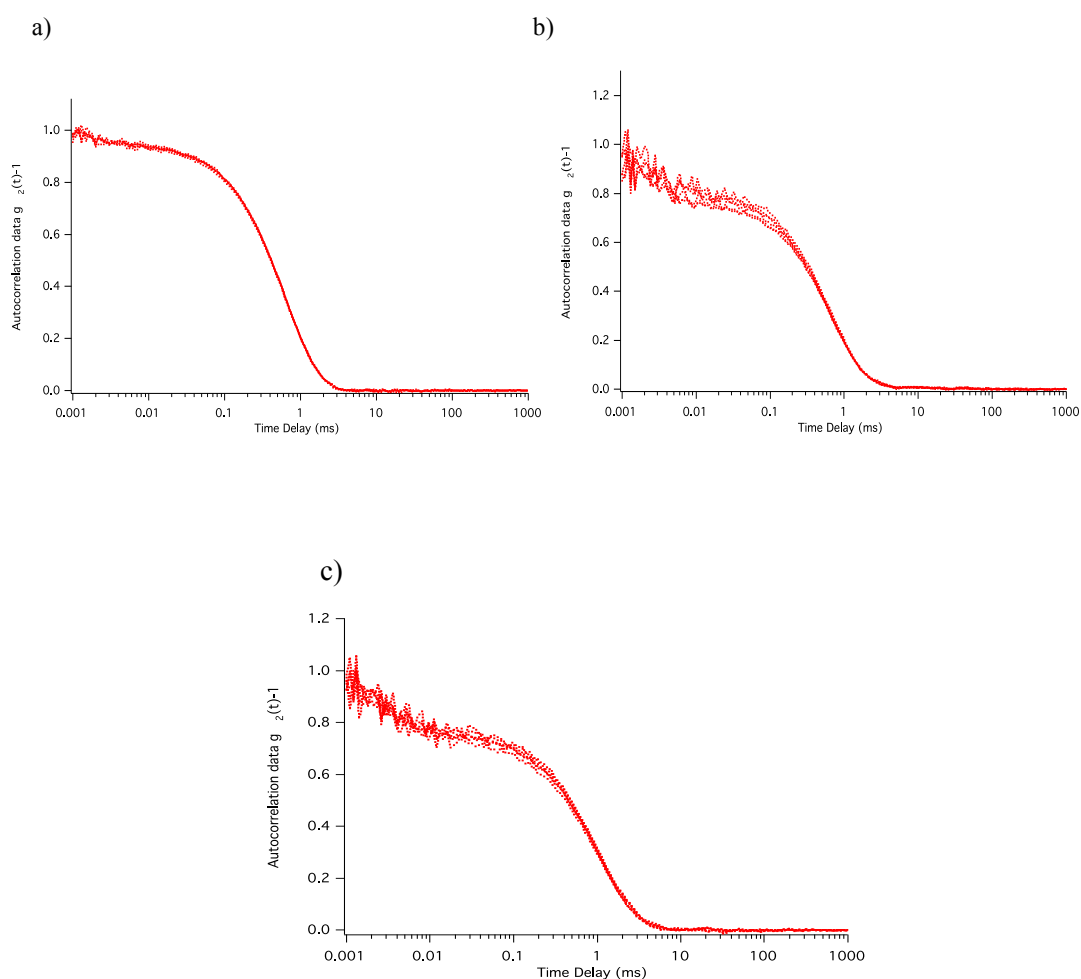


Fig. 21. Graphs of autocorrelation functions ($g_2(t)-1$) against time (t) of undersaturated aqueous sodium nitrate solutions at specific concentrations: a) 3 molar, b) 6 molar and c) 9 molar.

Large clusters alluded to by the autocorrelation data has a size range of between 100 and 200 nm. Whether this is an accurate depiction of a growing cluster or an arbitrary cluster without yet a definite size ordering, is unclear. The data presented below (Table 7) indicates that although the cluster radii fluctuate around 0.6 nm, the hydrodynamic droplet radii increases rapidly upon increase of solute.

Concentration (mol/ml)	Hydrodynamic Droplet Radius (nm) -1 st order	Hydrodynamic Droplet Radius (nm) -2 nd order	Hydrodynamic Cluster Radius (nm) -1 st order	Hydrodynamic Cluster Radius (nm) -2 nd order
3	98.5(±4.1)	95.2(±2.5)	-	-
6	130.6(±13.6)	94.3(±2.4)	0.628(±0.077)	0.617(±0.053)
9	200.7(±7.7)	180.8(±3.2)	0.682(±0.094)	0.563(±0.032)

Table 7. Average hydrodynamic radii of concentrated aqueous Sodium Nitrate solutions

6.3 Supersaturated Solutions

To ensure that the solvent itself, *i.e.*, water, did not produce any scattering species during cooling crystallisation, deionised water samples were analysed by DLS using the same method as the supersaturated solutions. The water samples were filtered using 0.02 μ m PTFE filters and then heated to 45 °C. Samples were cooled in 5 °C steps were data was collected (Fig. 21, Fig. 22). The results showed no scattering from solvent either by introduction of impurities or formation of micro bubbles.

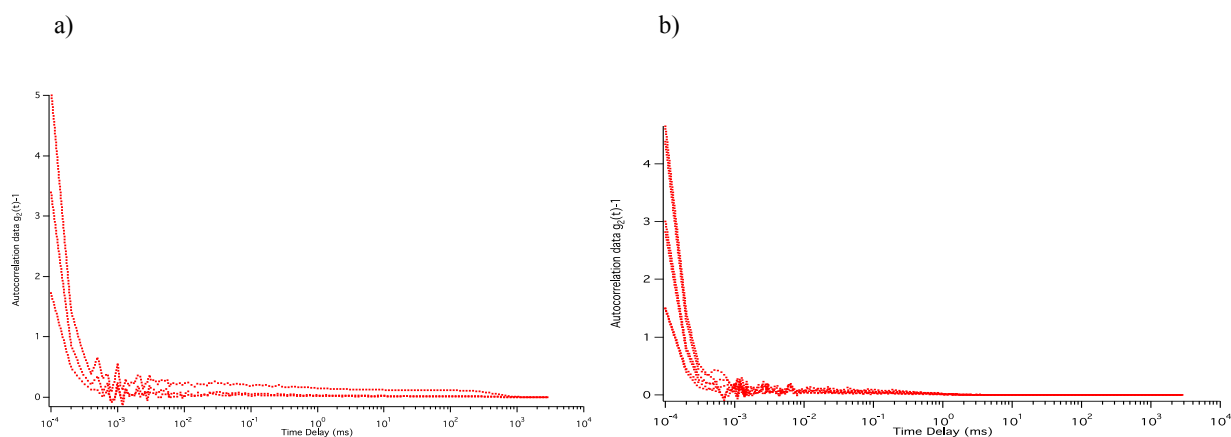


Fig. 22. Autocorrelation function $g_2(t)-1$ of deionised water filtered through a 0.02 μ m PTFE filter, a) 45 °C and b) 25 °C.

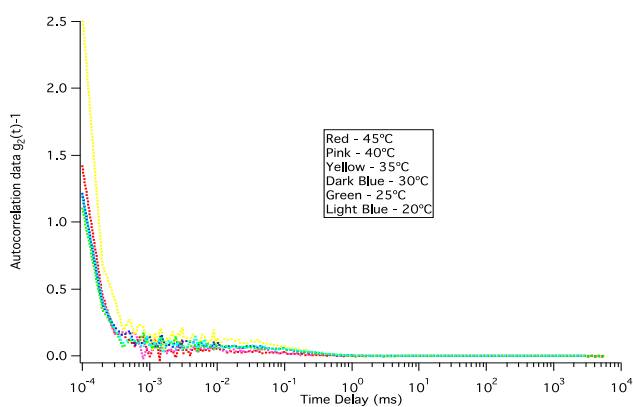


Fig. 23. Average light scattering autocorrelation function $g_2(t)-1$ of deionised water via cooling crystallisation at varying temperature measurements.

6.3.1 Urea

Solutions of aqueous urea were prepared and saturated at a temperature of 45°C. At the point where all solute has been visibly dissolved the solution is carefully cooled to 40°C and then to 35°C, etc. A saturated solution, which is then cooled, becomes a supersaturated solution: a chemical state that is not stable in its present form and eventually solidifies through crystallisation. Once each temperature was reached the solutions were allowed to settle until equilibrium had been restored and then DLS analysis could take place.

Upon analysis of each autocorrelation function of supersaturated urea, first through polynomial fits of the graphs of $g_2(t)-1$ and then through appropriate use of the Stokes-Einstein equation, the radii of species present within each solution can be discovered and examined (Fig. 23).

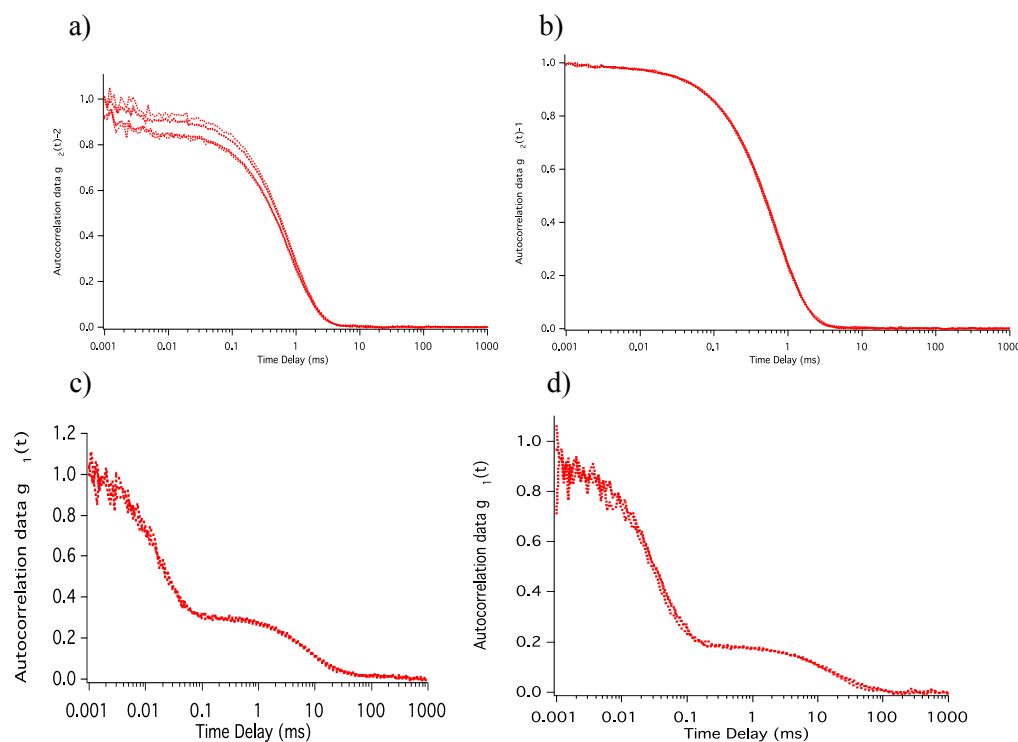


Fig. 24. Autocorrelation functions of supersaturated aqueous urea solutions cooling crystallised from 45 °C to 25 °C: : a) 45 °C, b) 40 °C, c) 35 °C, d) 30 °C.

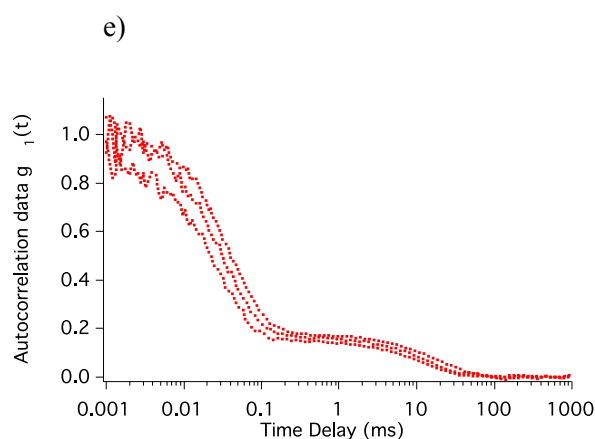


Fig. 24. B Autocorrelation functions of supersaturated aqueous urea solutions cooling crystallised from 45 °C to 25 °C: e) 25°C.

Hydrodynamic radii determination of each of the autocorrelation functions provide us with ample evidence to the existence of some critically bound aggregate size within the confines of nucleation theory. With a calculated radius range of between 0.5 – 0.7 nm for molecular clusters and 120 – 190 nm for pre-crystalline nanodroplets, it can be observed that some upper bound magnitude appears to exist in the form of a possible precursor to crystal nucleation. In this analysis, the small molecular clusters present themselves uniformly alongside the rich droplets.

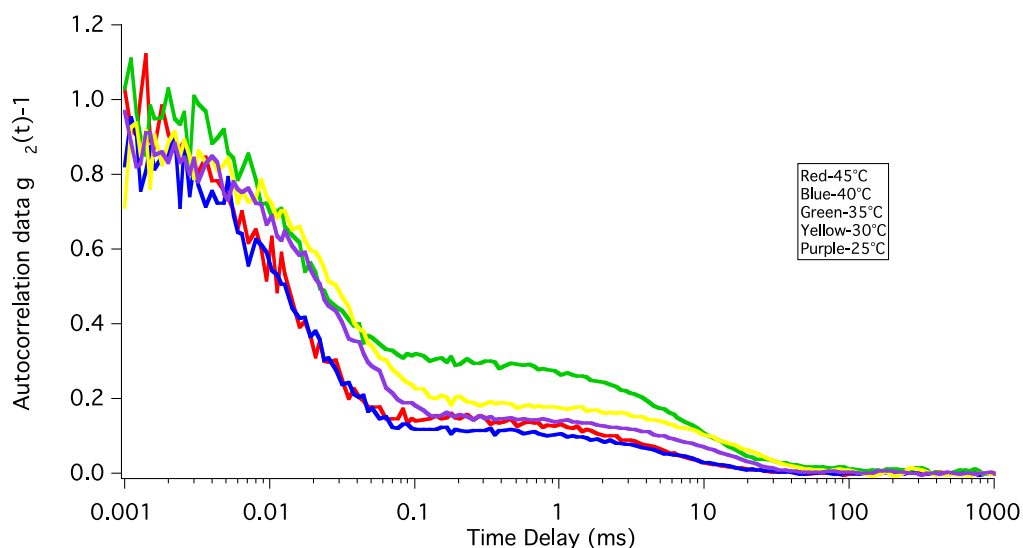


Fig. 25. Graph of overlaying autocorrelation function's ($g_2(t)-1$) against (t) of Supersaturated solutions of aqueous urea – concentration: 1.67g/ml at 40 °C. Cooling crystallisation carried out at 45 °C to 25 °C.

Comparing the autocorrelation functions ($g_2(t)-1$) of undersaturated and supersaturated urea solutions we can see a large increase in intensity of the small molecular component of the signal (Fig. 24). This would

indicate that as the solution becomes further concentrated, a greater quantity of single molecules are left disassociated in the bulk solution. The larger structured species seems to approach an average radius size of approximately 150 nm (Table 8). Whether or not this is evidence for the existence of a critical nucleus as a precursor to crystal nucleation is not certain.

Temperature (K)	Hydrodynamic Droplet Radius (nm) – 1 st order	Hydrodynamic Droplet Radius (nm) – 2 nd order	Hydrodynamic Cluster Radius (nm) – 1 st order	Hydrodynamic Cluster Radius (nm) – 2 nd order
318	168.3(±23.9)	146.8(±29.7)	0.635(±0.054)	0.600(±0.065)
313	135.8(±34.9)	121.6(±27.4)	0.530(±0.067)	0.510(±0.035)
308	190.3(±47.7)	161.8(±40.1)	0.690(±0.214)	0.610(±0.134)
303	181.5(±69.1)	158.4(±62.0)	0.580(±0.086)	0.540(±0.043)
298	173.8(±26.4)	155.8(±25.3)	0.519(±0.058)	0.467(±0.032)

Table 8. Average hydrodynamic radii of cooling crystallised aqueous urea solutions and approximate error. Calculated from autocorrelation decay and appropriate use of the Stokes-Einstein equation.

6.3.2 Glucose

Aqueous glucose solutions, saturated at 45 °C, were prepared and then cooled systematically in 5 °C increments. At each cooling step the solutions were allowed to equilibrate with the ambient lab temperature over a period of time before analysis took place. At every temperature decrease the degree of supersaturation of a system is increased and so a solution becomes more and more labile and therefore more likely to fulfil spontaneous nucleation. It is within these ranges of supersaturation that critical nuclei are most likely to develop.

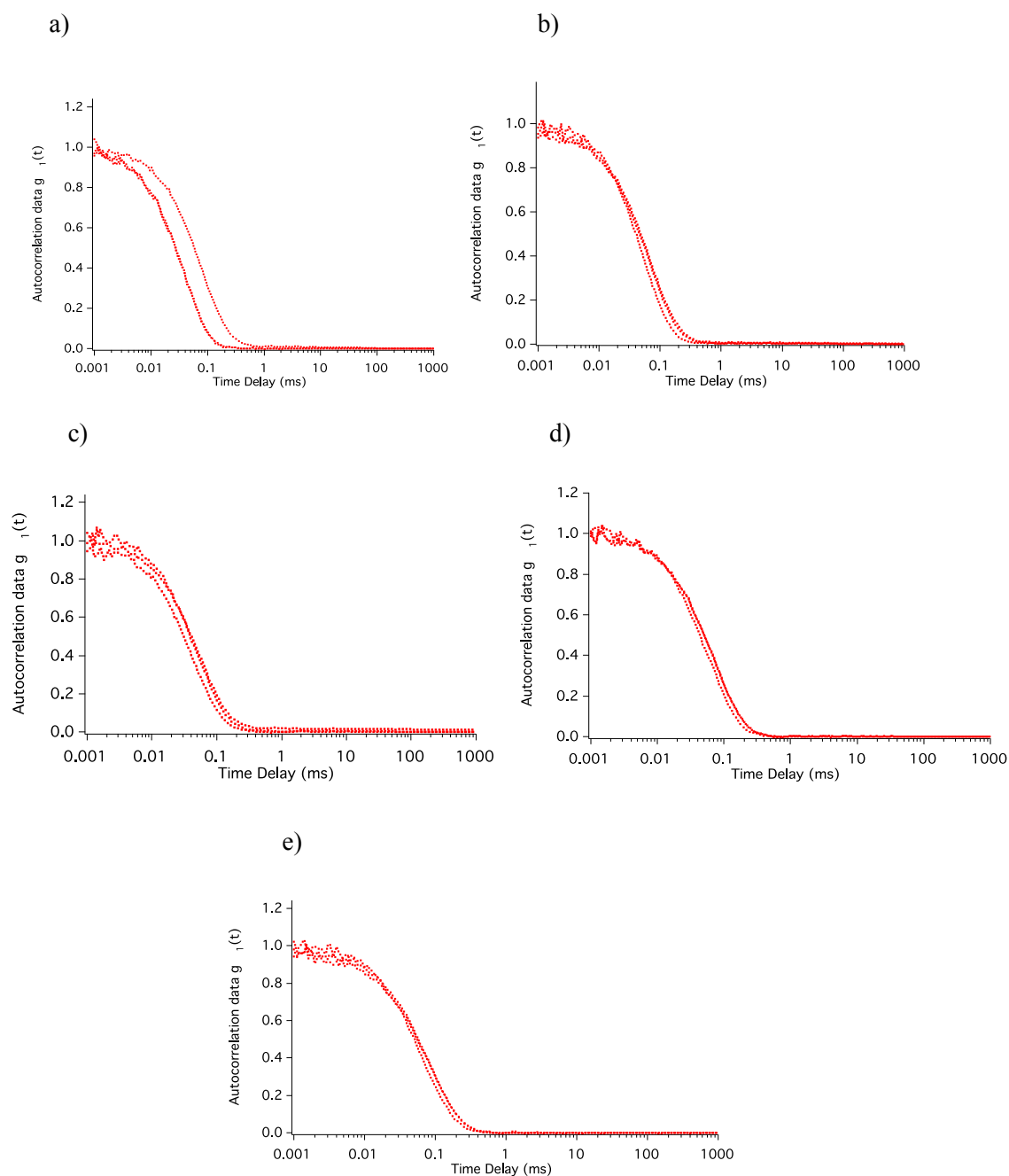


Fig. 26. Autocorrelation functions of supersaturated aqueous glucose solutions cooling crystallised from 45 to 25 °C: a) 45 °C, b) 40 °C, c) 35 °C, d) 30 °C and e) 25 °C.

Each autocorrelation function presented in Fig. 25 illustrates that aqueous glucose, at any extent of its supersaturation, contains no large nano-droplet species. Instead, a consistent sub-nano cluster, approaching 1 nm radius (Table 9) is evident in all cases.

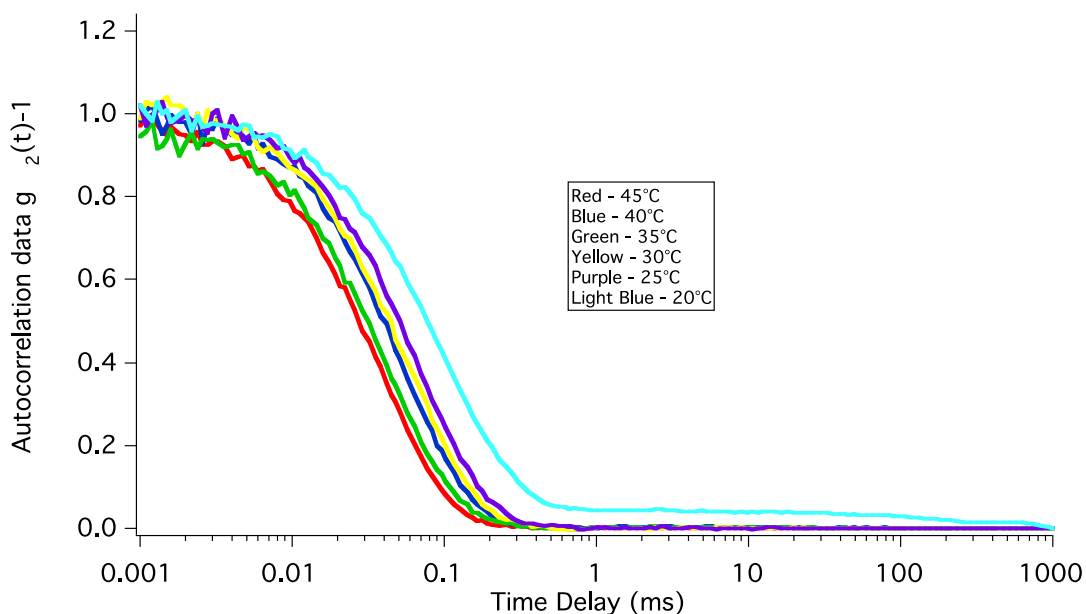


Fig. 27. Graph of overlaying autocorrelation function's ($g_2(t)-1$) against time (t) of Supersaturated solutions of aqueous glucose – concentration: 0.617g/ml at 40 °C. Cooling crystallisation from 45 to 20 °C.

Once the concentration of glucose has surpassed its solubility limit, it can be observed from Fig. 26 that the autocorrelation function of the supersaturated solution exhibits no evidence for the presence of large molecular structures within solution.

Temperature (K)	Hydrodynamic Droplet Radius (nm) – 1 st order	Hydrodynamic Droplet Radius (nm) – 2 nd order	Hydrodynamic Cluster Radius (nm) – 1 st order	Hydrodynamic Cluster Radius (nm) – 2 nd order
318	-	-	0.835(±0.052)	0.780(±0.175)
313	-	-	0.909(±0.029)	0.836(±0.112)
308	-	-	0.941(±0.043)	0.861(±0.078)
303	-	-	0.905(±0.088)	0.856(±0.093)
298	-	-	0.955(±0.075)	0.875(±0.109)
293	-	-	1.060(±0.112)	1.007(±0.115)

Table 9. Average hydrodynamic radii of cooling crystallised aqueous glucose solutions and approximate error. Calculated from autocorrelation decay and appropriate use of the Stokes-Einstein equation.

The strength of the signal pertaining to, approximately 1 nm sized species, appears to be absolute (Table 9). This suggests that as the concentration is increased, the stability of the larger structures collapses and the formation of such species become unfavourable. This scenario could be related to the large growth in the solution viscosity of glucose as solute concentration is increased. Further data would be required to support any theory.

6.3.3 Glycine

Supersaturated solutions of aqueous glycine were prepared using similar methodology to that of urea and glucose. Dissolution of solute particles was carried out at 45 °C and mixed readily until all solute was fully dissolved. Solutions were then cooled in 5 °C stages, then given appropriate time to equilibrate with the local laboratory temperature to decrease the effect of thermal fluctuations within the sample from corrupting the analysed data.

Data collected was plotted and used to calculate average hydrodynamic radii from their autocorrelation functions. The autocorrelation decay curves plotted show good consistency in their appearance (Fig. 27) and only show slight changes with respect to minor movement along the x-axis but no immediately obvious pattern emerges as to why this would be.

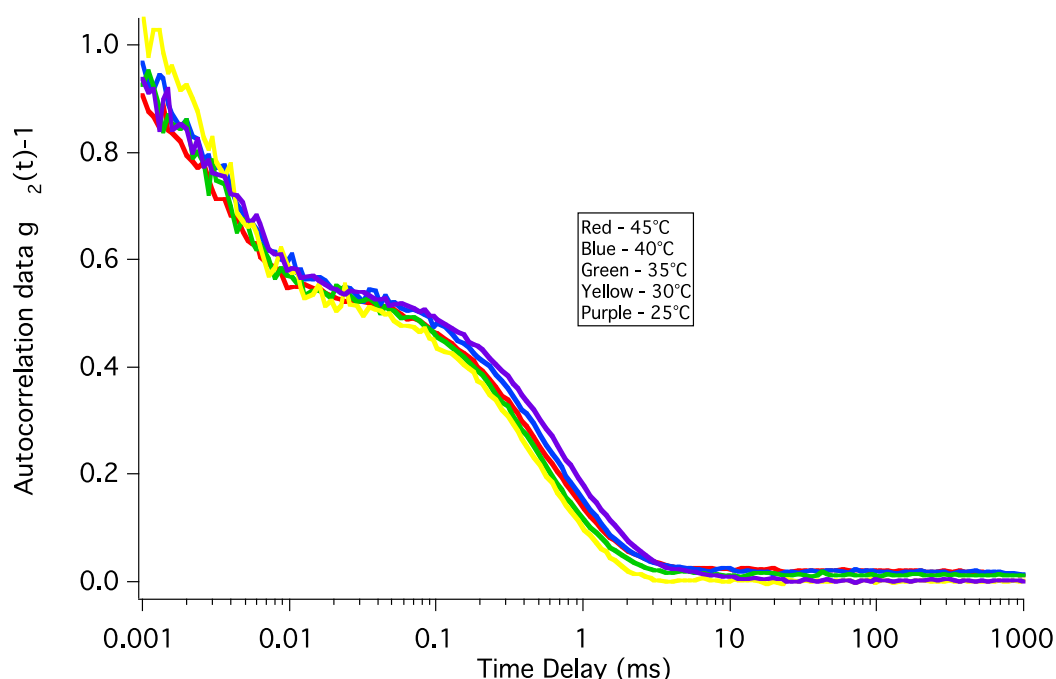


Fig. 28. Graph of overlaying autocorrelation function's ($g_2(t)-1$) against time (t) of Supersaturated aqueous solution of glycine – concentration: 0.317g/ml at 40 °C. Cooling crystallisation from 45 to 25 °C.

Much like the supersaturated urea solutions, glycine appears to tend to some possible limit with regards to an average radius size (Table 10). As well as producing a binomial signal with an increased intensity for the first decay component indicating that a larger quantity of the glycine solution exist as single monomer units in supersaturated conditions than that of undersaturated.

Temperature (K)	Hydrodynamic Droplet Radius (nm) – 1 st order	Hydrodynamic Droplet Radius (nm) – 2 nd order	Hydrodynamic Cluster Radius (nm) – 1 st order	Hydrodynamic Cluster Radius (nm) – 2 nd order
318	175.4(±60.9)	153.6(±41.8)	0.675(±0.060)	0.667(±0.088)
313	142.8(±31.3)	116.7(±12.0)	0.635(±0.032)	0.700(±0.035)
308	153.7(±48.9)	131.8(±27.1)	0.667(±0.187)	0.516(±0.054)
303	148.8(±39.8)	133.3(±32.3)	0.671(±0.061)	0.549(±0.043)
298	155.8(±46.9)	138.7(46.3)	0.698(±0.062)	0.552(±0.048)

Table 10. Average hydrodynamic radii of cooling crystallised aqueous glycine solutions and approximate error. Calculated from autocorrelation decay and appropriate use of the Stokes-Einstein equation.

Huang *et al.* had previously carried out experiments using diffusion calculations and freezing point depression to establish the binding state of glycine molecules within supersaturated glycine solutions (see ref. 76). Gidalevitz also presented data, which indicated larger structures present within crystallising solutions of glycine reported as a few hundred nanometre sizes.⁹¹

6.3.4 Sodium Chloride

The supersaturated solutions of sodium chloride show a very consistent exponential decay as we lower the temperature of the sample. Solutions for the ionic salt show a weaker baseline than that of the previous organic solutions. This could have an effect in reducing accuracy of calculated hydrodynamic radii, but as the slope of the autocorrelation function tends to some like-zero point we can more-or-less neglect its implication to calculations.

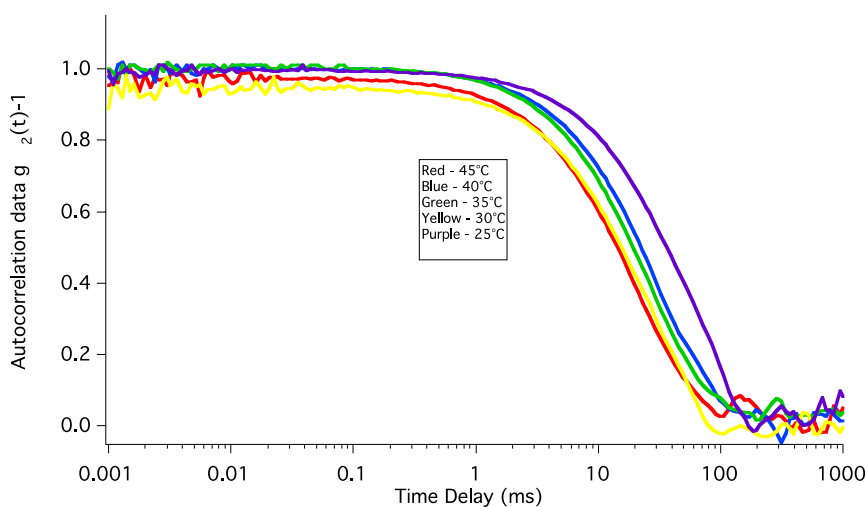


Fig. 29. Graphs of overlaying autocorrelation function's ($g_2(t)-1$) against time (t) of supersaturated aqueous solution of sodium chloride - concentration: 0.364g/ml at 40 °C. Cooling crystallisation from 45 to 25 °C.

The analysis of sodium chloride provides us with only a monomial decay (Fig. 28), which is indicative of large, solute-dense pre-crystalline clusters. There is no evidence provided through cooling crystallisation of the supersaturated sodium chloride solutions that any sub-nano sized clusters appear in conjunction with the nuclei sized species.

Temperature (K)	Hydrodynamic Droplet Radius (nm) – 1 st order	Hydrodynamic Droplet Radius (nm) – 2 nd order	Hydrodynamic Cluster Radius (nm) – 1 st order	Hydrodynamic Cluster Radius (nm) – 2 nd order
318	759.4(±154.2)	831(±149.9)	-	-
313	736.0(±183.3)	731.0(±151.8)	-	-
308	593.8(±135.5)	571(±147.4)	-	-
303	573.8(±148.9)	560.5(148.1)	-	-
298	666.0(±116.3)	651(±124.7)	-	-

Table 11. Average hydrodynamic radii of cooling crystallised aqueous sodium chloride solutions and approximate error. Calculated from autocorrelation decay and appropriate use of the Stokes-Einstein equation.

There is a noticeable size difference between the hydrodynamic radii calculated from sodium chloride solutions and that of all previous organic aqueous solutions. Radii measured for sodium chloride tend to be in the range of hundreds of nano-metres (between 550nm and 850 (Table 11)) compared to almost a micron in some cases. This is likely due to the ease of clustering for ionically charged species within water.

6.3.5 Potassium Chloride

Solutions of supersaturated potassium chloride analysed through dynamic light scattering over a range of temperatures are shown below (Fig. 29). The well-defined exponential decay of each autocorrelation function provides us with very useful data to analyse. With the exception of the baseline, a problem shared by sodium chloride, we can calculate with a good degree of accuracy the hydrodynamic radius of each autocorrelation function given.

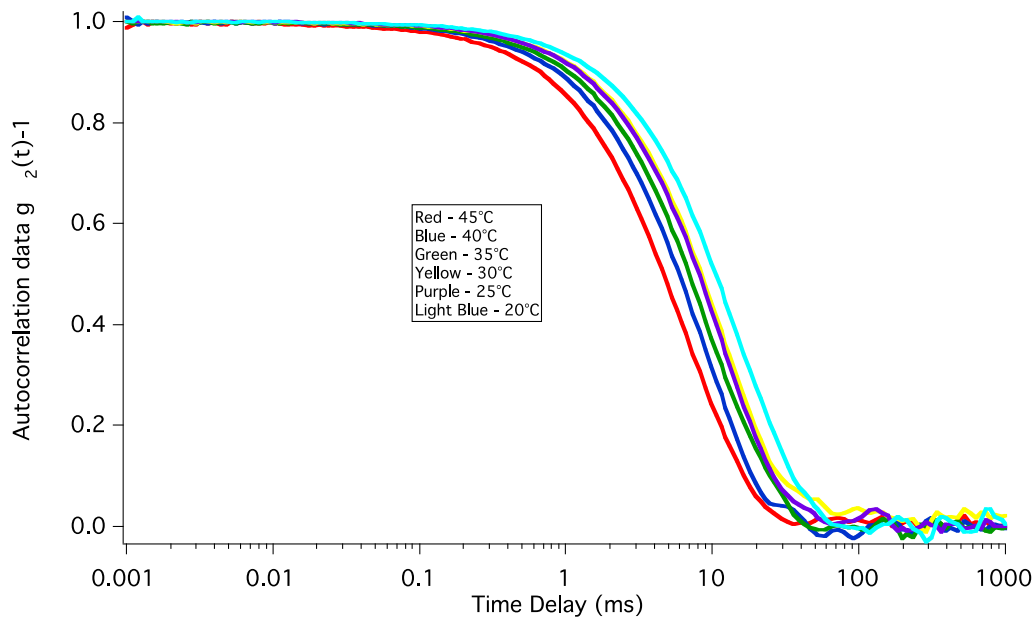


Fig. 30. Graph of overlaying autocorrelation function's ($g_2(t)-1$) against time (t) of Supersaturated aqueous solution of potassium chloride- concentration: 0.390g/ml at 40°C. Cooling crystallisation from 45 to 20°C.

For potassium chloride, as with sodium chloride, we are given no information from the monomial exponential decay of any smaller sized clusters. Only data on the larger critically sized molecular species can be found. These species of around 200-230 nm in size (Table 12) allow us to visualise more easily theory behind the generation of a critical nucleus. The extracted data gives us a strong insight into the non-classical nucleation model whereby a dense mass of solute clusters together within a supersaturated solution and reaches a size limit that causes the droplet to either nucleate and in essence reorder itself into a solid structure, or collapse again into the diffuse solution.

Temperature (K)	Hydrodynamic Droplet Radius (nm) – 1 st order	Hydrodynamic Droplet Radius (nm) – 2 nd order	Hydrodynamic Cluster Radius (nm) – 1 st order	Hydrodynamic Cluster Radius (nm) – 2 nd order
318	186.6(±6.7)	184.4(±11.4)	-	-
313	204.5(±4.4)	202.3(±8.3)	-	-
308	227.2(±20.8)	225.5(±21.7)	-	-
303	224.3(±26.6)	223.8(±21.4)	-	-
298	222.0(±17.8)	221(±17.7)	-	-

Table 12. Average hydrodynamic radii of cooling crystallised aqueous potassium chloride solutions and approximate error. Calculated from autocorrelation decay and appropriate use of the Stokes-Einstein equation.

6.3.6 Sodium Nitrate

Sodium nitrate supersaturated solutions were prepared as described above for aqueous solutions of potassium chloride and sodium chloride. Sodium nitrate shows a significant amount of noise in each of the measured exponential decays along with a poor baseline. These two discrepancies coupled together call into question the accuracy of the calculated hydrodynamic radii provided (Table 13). There are no allusions to the existence of any small-scale ionic clusters – analogous to previous salt solutions.

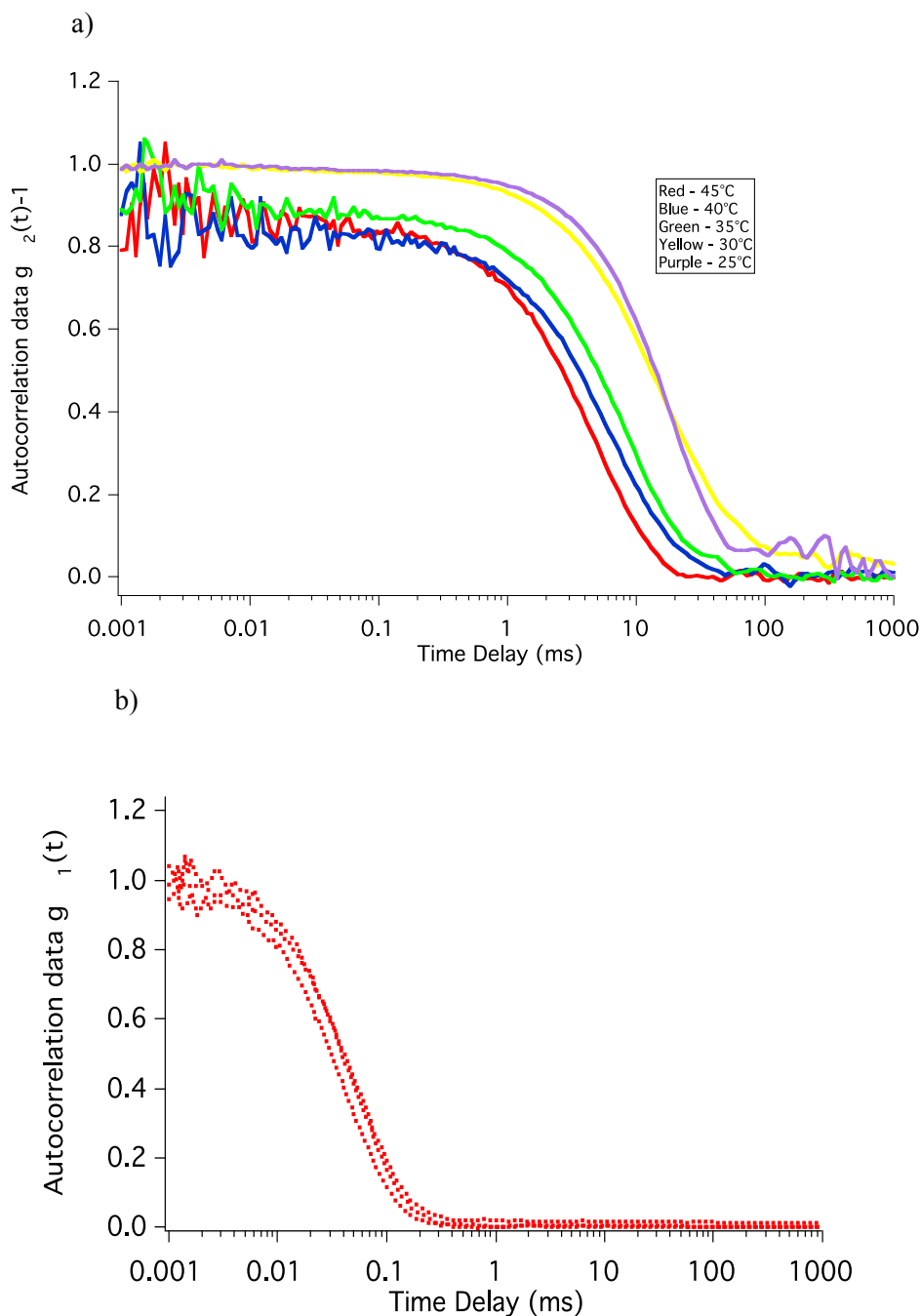


Fig. 31. Graph of overlaying autocorrelation function's ($g_2(t)-1$) against time (t) of Supersaturated aqueous solution of sodium nitrate - concentration: 1.040g/ml at 40 °C. a) Cooling crystallisation from 45 to 25 °C b) Cooling crystallisation from 45 to 35 °C.

Considering Fig. 30, if we were to ignore autocorrelation functions of 30°C and 25°C (yellow and purple lines respectively) and observe only those decays with moderate baselines we can see a dramatic noticeable change in the average species radii. The radii acquired from the first three measurements present us with an overall average particle radius of approximately 560 nm as opposed to 644 nm with the inclusion of the 30°C and 25°C decays (Table 13). Although at this juncture we have no way of knowing which one is, in practice, more accurate, it is reasonable to suggest that the large jump in size of over 200nm for radii calculations could be attributed to incongruities of the exponential decays.

Temperature (K)	Hydrodynamic Droplet Radius (nm) – 1 st order	Hydrodynamic Droplet Radius (nm) – 2 nd order	Hydrodynamic Cluster Radius (nm) – 1 st order	Hydrodynamic Cluster Radius (nm) – 2 nd order
318	516.5(±38.5)	471.7(±14.4)	-	-
313	581.5(±88.7)	572.5(±82.0)	-	-
308	585.5(±141.9)	579.0(±147.3)	-	-
303	745.2(±271.7)	712.6(±279.8)	-	-
298	793.4(±301.7)	836.4(±358.5)	-	-

Table 13. Average hydrodynamic radii of cooling crystallised aqueous sodium nitrate solutions and approximate error. Calculated from autocorrelation decay and appropriate use of the Stokes-Einstein equation.

All supersaturated salt solutions exhibit only a large particle scattering and therefore demonstrate no scattering decay from any solvated free ions. Unlike the small organic molecular solutions of urea and glycine, the salt solutions of NaCl and NaNO₃ contain aggregates of much larger average radii. Some of these species approach 1 micron in size. The exponential decay's recorded from analysis of supersaturated salt solutions are not as consistent as that of the organic solutions, as we increase the extent of the supersaturation. This may be due to a more erratic change in the solution as temperature is lowered.

The potassium chloride solution shows a more dependable array of autocorrelation functions as the extent of the supersaturation is increased. There appears to be a critical limit with respect to the hydrodynamic radii measured from the KCl solution, indicating that not all salts behave in an erratic nature and, similarly to some organic molecules, may obey a standard pathway to nucleation.

6.4 Multi-Angle Scattering

This experimentation is concerned with discerning whether or not supersaturated solutions display a polydispersity of particle sizes or if all solutions tend to a uniform size as the degree of supersaturation is increased. The method of measurement is to observe each solutions autocorrelation decay and subsequent

particle radius at consecutive angles ranging from 20° to 90°. According to theory each particle can be distinguished by its size depending on the angle of detection used. At small angles, the large particles will dominate the signal and inversely, small particles scatter more at large angles.

6.4.1 Urea

Supersaturated solutions of urea were prepared at 50°C at a concentration of 1.67g/ml. The first sample was slowly cooled to 45°C and then measured at angles ranging from 20° to 90° in 10° steps. The second sample was cooled to room temperature (approx. 25°C) and allowed to equilibrate to lower effect of thermal currents within solutions. Autocorrelation functions were compared over the detection angles (Fig. 31).

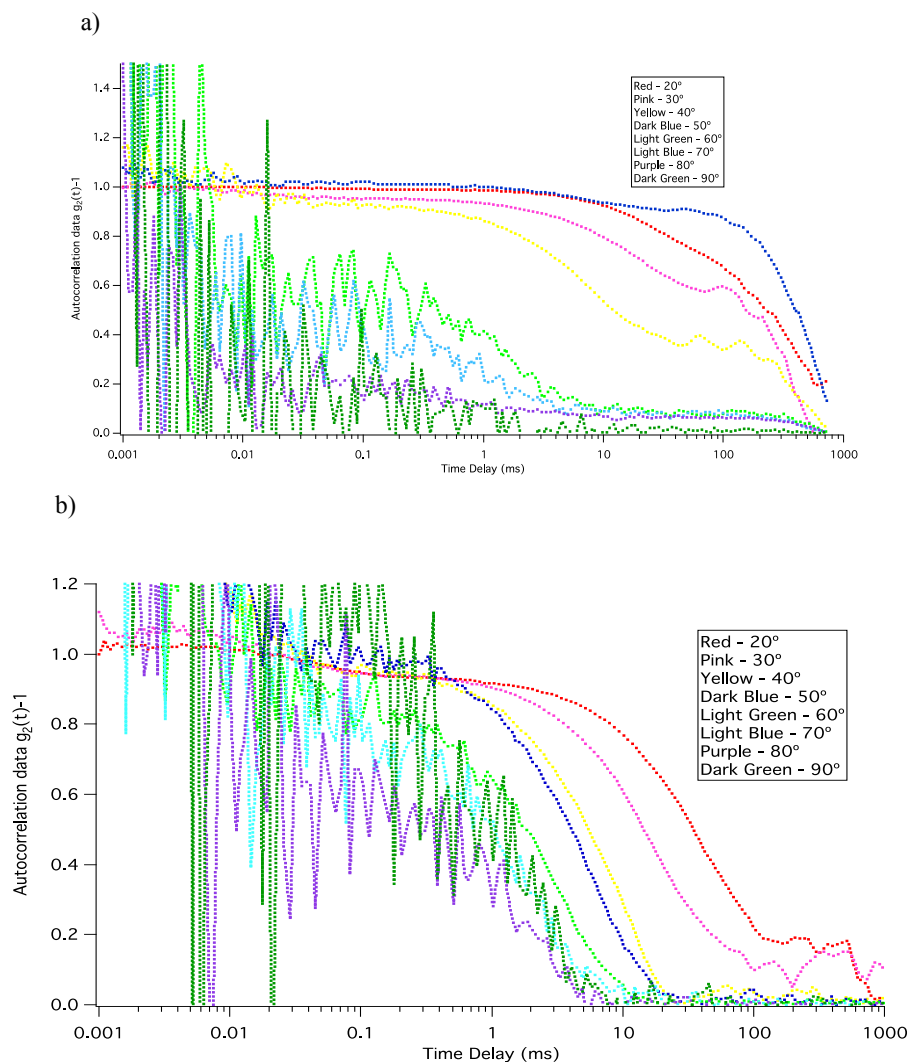


Fig. 32. Multi-angle detection of urea solution, concentration 1.67g/ml. Autocorrelation function $g_2(t)-1$ at a) 45 °C and b) room temperature. Autocorrelation functions measured at angles 20, 30, 40 and 50 within graph “a)” are too distorted to give any appreciably accurate data.

The autocorrelation data collected over a wide scope of angles show a poor decay at smaller angles. These decays are largely unplottable and as they have no baseline and could provide no relevant data for analysis. Much of the data used for investigation of the solutions are very noisy with respect to the decays but can still provide reasonably accurate information on the average size of cluster detected at specific angles within the supersaturated solutions.

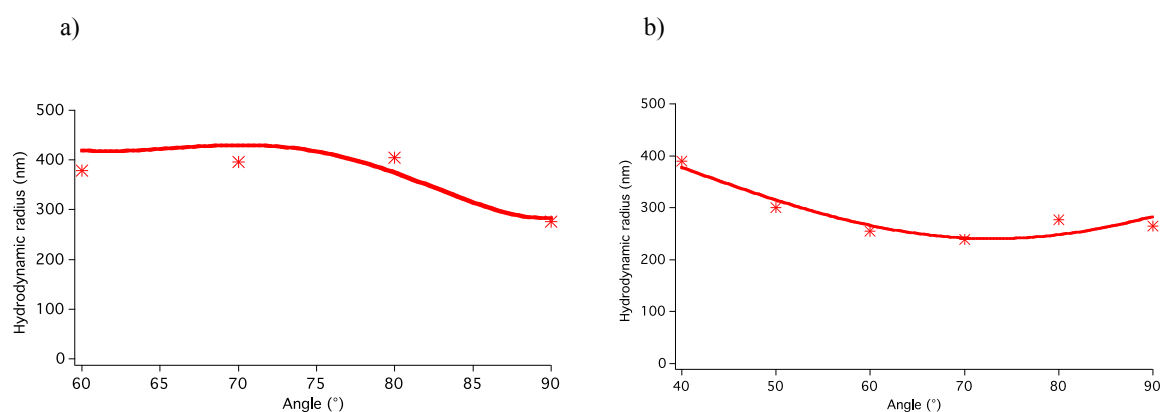


Fig. 33. Graphs of measured radii magnitude for supersaturated urea solution at varying angles of detection, a) 45 °C b) Room temperature. For graph a): Angles in the range of 20° to 50° are not reliable points due to signal distortion and lack of baseline in autocorrelation data. For graph b): Angles 20° and 30° have no baseline and so can be discarded also. Disregarding these points has the effect of altering the hydrodynamic size range to a 400nm maximum.

Not all the autocorrelation functions can be relied upon for accurate radii size calculations due to significant noise and signal distortion; lines of best fit were used only to calculate an estimated size range and general trend for each angle measured and allow us to observe and compare correlation intensity changes with each alteration in angle.

The data of radii against angle in Fig. 32 illustrates the presence of varying sized particle radii throughout the range of angle detection. Although there appears to be a size variance over the angle measurements there is a tendency towards some maximum. At larger angles the size of particle we observe decreases, as we would expect of a polydisperse sample.

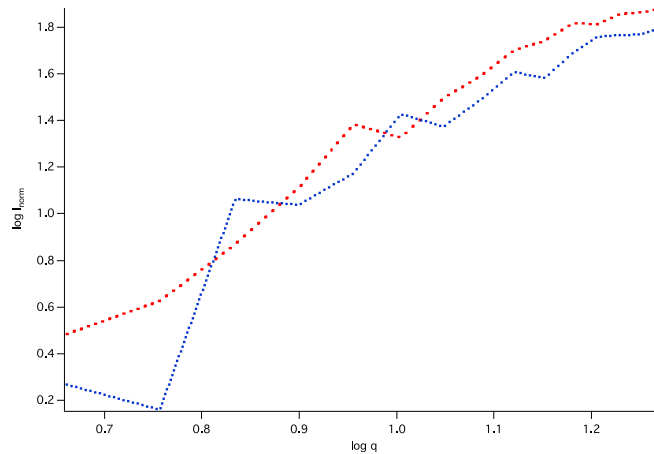


Fig. 34. Log-Log plot of the absolute scattering intensity, measured at 45 °C (red) and at room temperature (blue), versus the wave vector, q . Urea supersaturated solution concentration: 1.67g/ml.

Fig. 33 shows the correlation between the normalised incident intensity upon the sample and the calculated wave vector. The total normalised intensity from the laser increases as the scattering intensity from the sample decreases, *i.e.*, the signal becomes weaker due to the scattering of smaller radii. It can be assessed that the incident intensity tends to increase for both samples as the wave vector increases. The supersaturated and undersaturated urea both contain a polydispersed collection of randomly sized nano-clusters. Whether these randomly sized particles tend to a maximum or critical size is unclear. More work would be needed to make any such claim.

6.4.2 Glucose

Supersaturated glucose samples were prepared in the same manner as urea and analysed over the same range of angles. One sample was cooled to 45°C and the other to room temperature. The autocorrelation functions taken at all angles are plotted together and shown in Fig. 34 below.

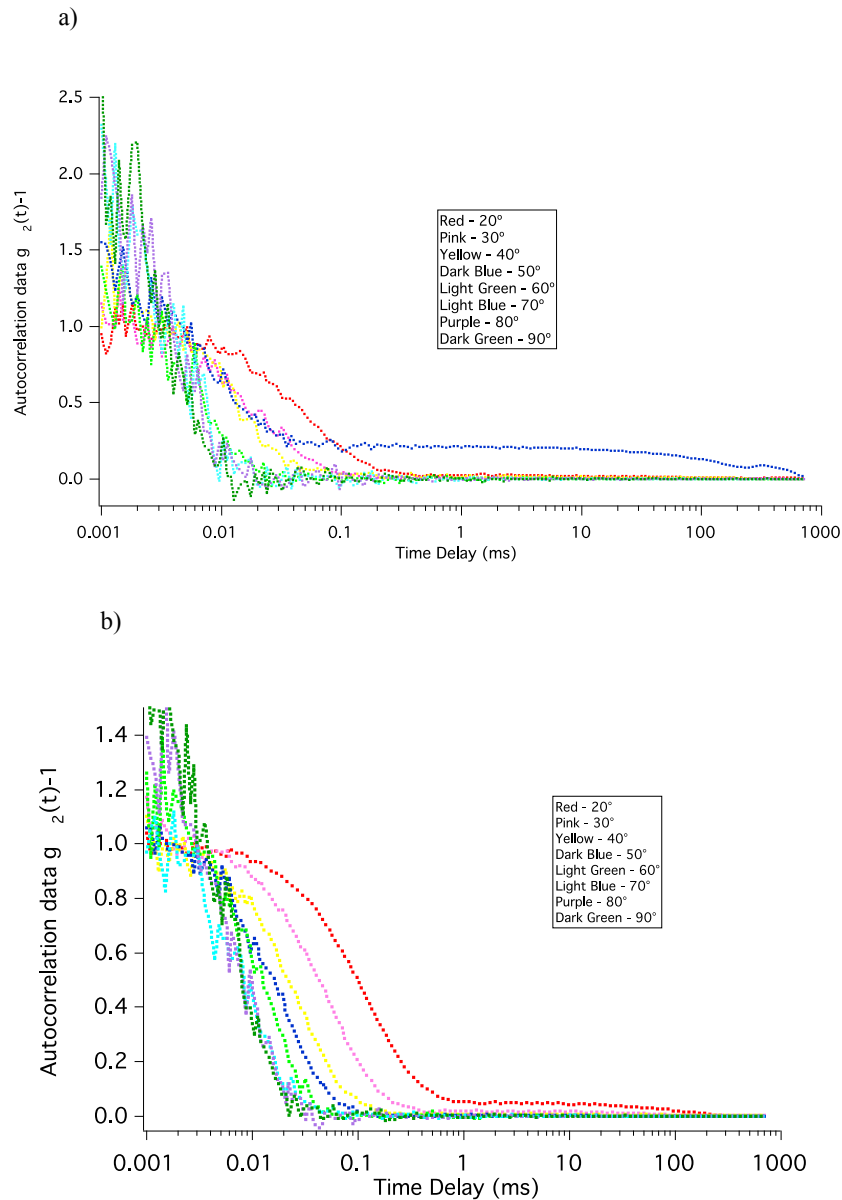


Fig. 35. Multi-angle detection of glucose solution, concentration 0.617g/ml. Autocorrelation function $g_2(t)-1$ at a) 45°C and b) room temperature.

Exponential decays of supersaturated glucose solutions altogether provide seemingly consistent data. Each function aligned with its neighbour appears to agree that any species that exists within these solutions is of some uniform size. This impression is supplemented when we observe the gradient of each decay slope to be unchanging at all angles measured. The small exception being with regards to the

autocorrelation function at 50 degrees in graph a). The data calculated from this exponential decay was not omitted when hydrodynamic radii were considered however, as the data point refrained from obscuring the overall graph.

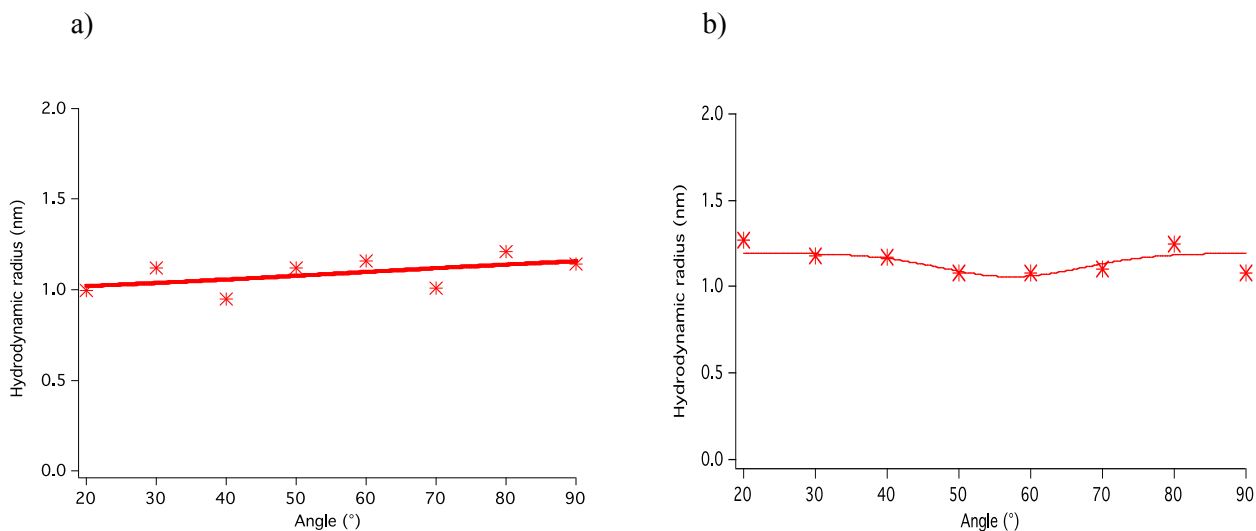


Fig. 36. Graphs of measured radii magnitude for supersaturated glucose solution at varying angles of detection, a) 45 °C b) Room temperature.

The average radii calculated from each angle measurement show little fluctuation on size over all angles. Little difference is observable between the hydrodynamic radius measurements of either sample. At sample supersaturated at 45°C the average approximate particle radius is of/around 1 nm. The sample solution supersaturated to room temperature has an estimated average radius of around 1.2 nm (Fig. 35).

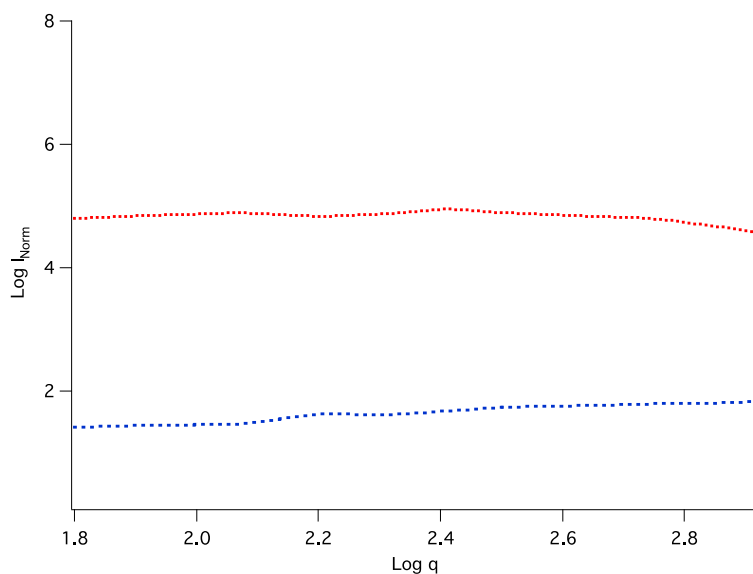


Fig. 37. Log-Log plot of the absolute scattering intensity, measured at 45 °C (red) and at room temperature (blue), versus the wave vector, q . Glucose solution, and concentration: 0.617g/ml.

Unlike the urea samples, discussed previously, the glucose $g_2(t)-1$ plot doesn't appear to vary intensity as the angle of detection rises from 20 to 90 degrees (Fig. 36). This would indicate that the glucose solutions are made up predominantly of small particle species. These species seem to remain uniform in size at all angles as observed from Fig. 35 where one can see no appreciable change in particle radius. This is again agreed upon when looking at the graph of incident intensity versus wave vector.

These data collections all congruently imply that glucose solution is monodisperse throughout solution. The fact that glucose solutions appears to remain monodisperse at any degree of saturation could be evidence for the generation of some critically sized nucleus as a precursor to crystal nucleation.

6.4.3 Glycine

As with previous solutions of urea and glucose, supersaturated solutions were prepared at 50°C. One sample was then cooled to 45°C and the other to room temperature (approx. 25°C). Each sample was allowed to equilibrate to lower possible data corruption due to thermal currents within solution. The exponential decay of each autocorrelation function was plotted together so that direct comparisons of decay curves could be drawn up (Fig. 37).

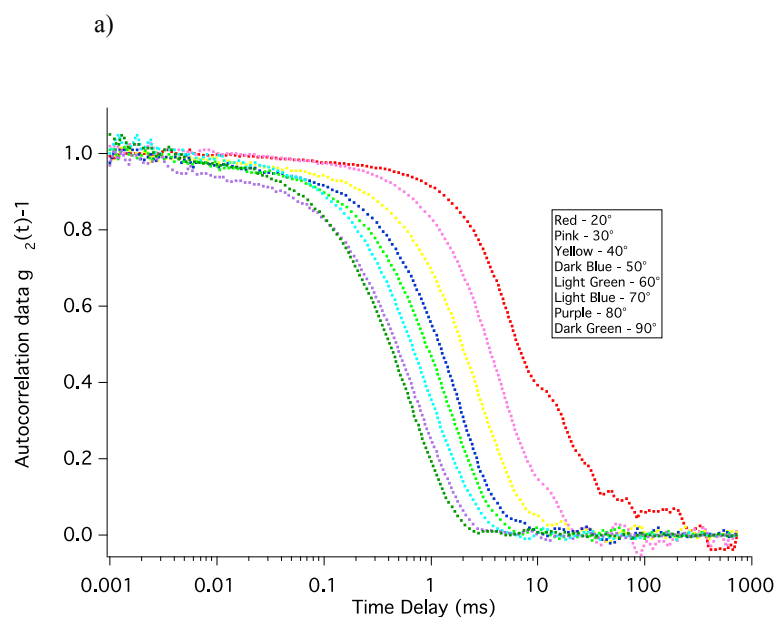


Fig. 38. A Multi-angle detection of glycine solution, concentration 0.317g/ml. Autocorrelation function $g_2(t)-1$ at a) 45 °C.

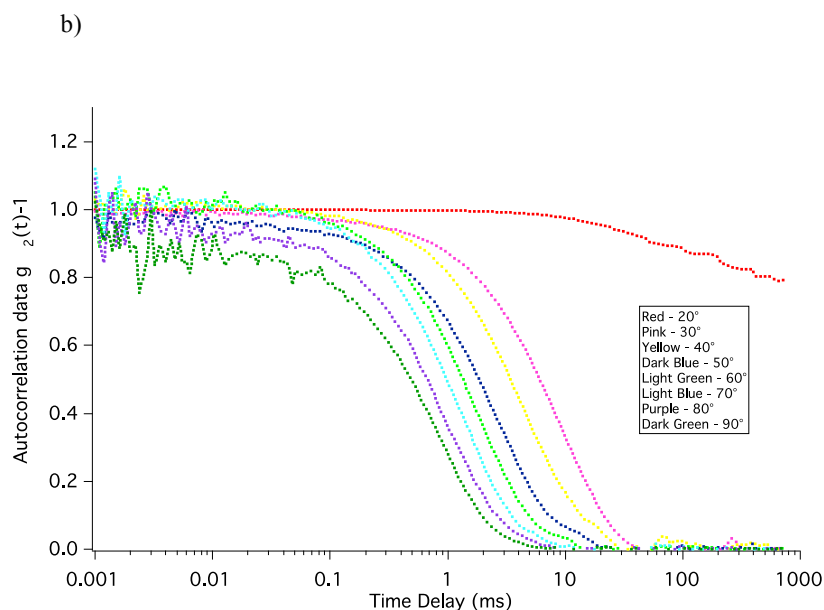


Fig. 38. B Multi-angle detection of glycine solution, concentration 0.317g/ml. Autocorrelation function $g_2(t)-1$ at b) room temperature. The autocorrelation function for 20°, due to distortion of decay curve and lack of baseline, will not be used to calculate hydrodynamic radii.

The exponential decays plotted against one another show little in the way of variation in terms of size or gradient. This holds true for both the 45°C and room temperature sample. The autocorrelation functions were analysed using fitted polynomial curves and use of the Stokes-Einstein equation to calculate appropriate hydrodynamic radii, which were then plotted in tables against change in angle (Fig. 38).

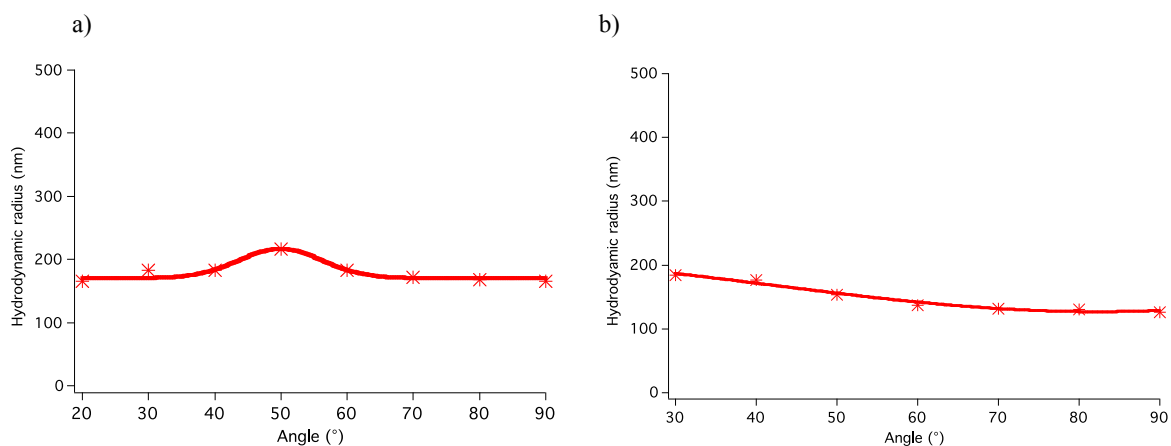


Fig. 39. Graphs of measured radii magnitude for supersaturated glycine solution at varying angles of detection, a) 45 °C b) Room temperature. The point at 20° was left unplotted in graph b) as the exponential decay was too distorted to allow proper analysis.

Fig. 38 shows very little deterioration with respect to average particle size as we sweep over a range of angles. A size maximum is defined at approximately 200 nm for both graphs. This evidence points to a mono-dispersion of molecular species within the solution. As seen before in the glucose solution this could again be a steady approach towards a critically sized nuclei whereby each particle extends its surface and volume magnitudes until a certain energy boundary is crossed and spontaneous nucleation can occur or the energy falls short and the whole molecular cluster collapses into dispersion.

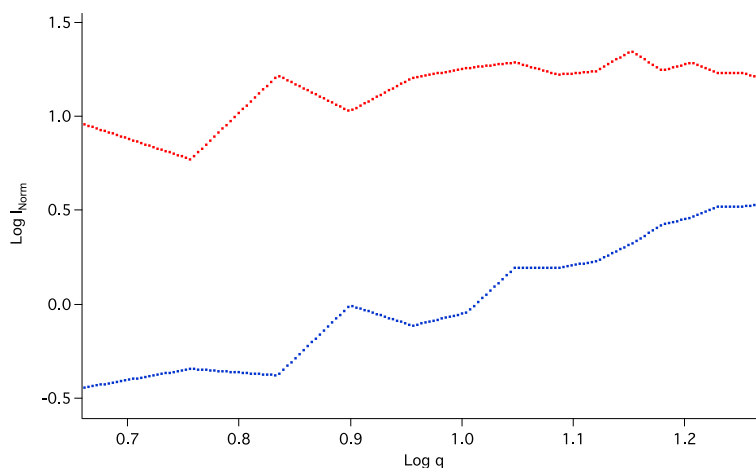


Fig. 40. Log-Log plot of the absolute scattering intensity, measured at 45 °C (red) and at room temperature (blue), versus the wave vector, q . Glycine solution, concentration: 0.317g/ml.

Similarly to the glucose solutions, glycine solutions show no appreciable change in their scattering intensity as the angles of detection increase (Fig. 39). The multi-angle detection of the glycine solution run at room temperature conditions show a slight decrease in their scattering intensity than that of the solution run at 45 °C. This may indicate a greater polydispersity in the 45°C sample, possibly due to the solution being so close to its saturation point that the room temperature sample or perhaps an effect of thermal currents within the supersaturated solution as temperature equilibrium had not been fully achieved.

6.4.4 Sodium Chloride

Two supersaturated solutions of sodium chloride samples were prepared at 50°C and then cooled to 45°C and 25°C (respectively). Solution concentrations were both 0.364g/ml. Once prepared, each solution was analysed across a range of angles with intent to probe the labile solutions and inspect the series of particle sizes existing within the solutions.

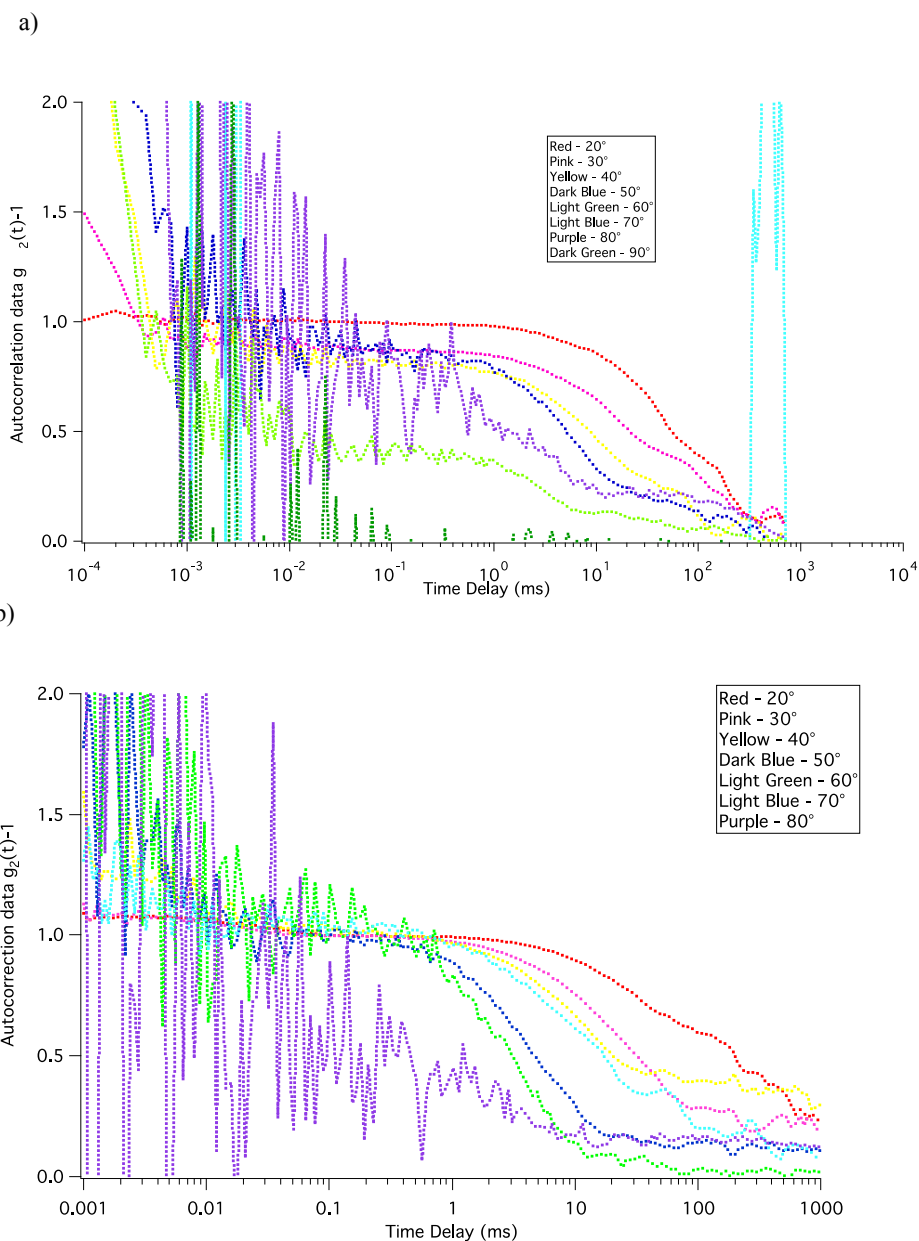


Fig. 41. Multi-angle detection of sodium chloride solution, concentration 0.364g/ml. Autocorrelation function $g_2(t)-1$ at a) 45 °C and b) room temperature.

The data collected over a wide-angle range of supersaturated sodium chloride was not sufficiently good and contained neither satisfactory exponential decay nor an acceptable baseline (Fig 40). Noise within the signals persisted to the point of causing certain decays to appear off the graph altogether. As a result of these poor decay curves, accurate hydrodynamic radii could not be calculated and subsequent conclusions on whether or not sodium chloride solutions within a supersaturated medium pertained to mono- or poly-dispersity. At this juncture we can only describe the dynamics of sodium chloride solution as erratic and analysable to any useful degree.

6.4.5 Potassium Chloride

Solutions of potassium chloride, prepared similarly to that of sodium chloride (see section above), were analysed using dynamic light scattering at angles of detection 20° to 90° .

The data gathered from the 45°C sample (Fig. 41 a) contains too much noise throughout the signal and causing distortion and corruption in any calculations made on interpretation of corresponding hydrodynamic radii. These exponential decays lack consistency along with a suitable baseline and hence provide us with no truthful insight into the dispersity of the ionic supersaturated solution.

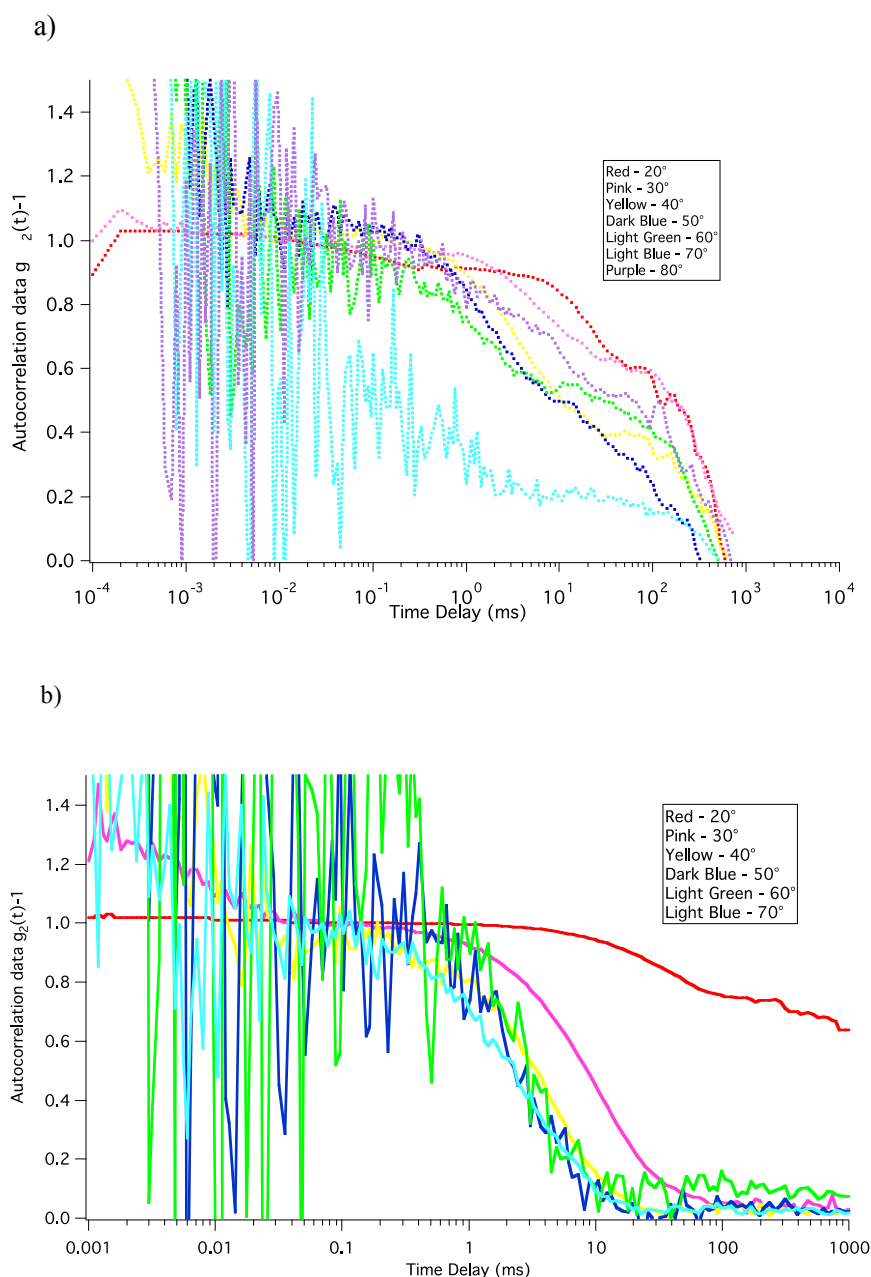


Fig. 42. Multi-angle detection of potassium chloride solution, concentration 0.390g/ml . Autocorrelation function $g_2(t)-1$ at a) 45°C and b) room temperature.

The autocorrelation functions captured from analysis of supersaturated potassium chloride cooled to room temperature (Fig. 41 b) were significantly better than those of the 45°C sample. All decays, with the exception of that measured at 20°, could be used for computing an average particle hydrodynamic radius found at each angle. Although much noise still exists within the exponential decays there is enough of a curve and baseline to observe the overall trend and plot a polynomial line fit.

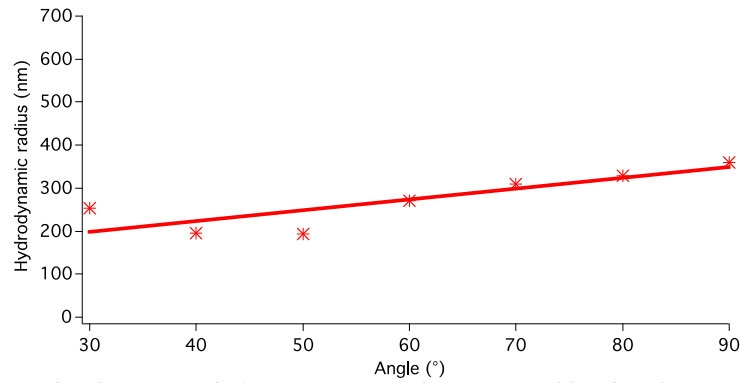


Fig. 43. Graphs of measured radii magnitude for supersaturated potassium chloride solution at room temperature and over varying angles of detection.

Average hydrodynamic radius measurements were calculated from gathered autocorrelation data points. Data from point 20° was omitted from Fig. 42 in order to clarify the natural trend of solution. The hydrodynamic radii measured are of magnitude 200 to 400nm. This size gap seems a little vague and ultimately too large to resolve the question of mono- or poly-dispersion within the sample.

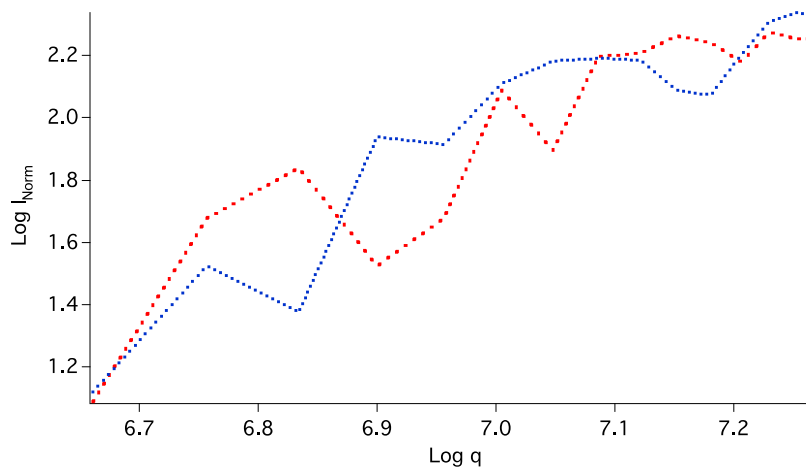


Fig. 44. Log-Log plot of the absolute scattering intensity, measured at 45 °C (red) and at room temperature (blue), versus the wave vector, q . Potassium Chloride solution, concentration: 0.390g/ml.

Solutions of potassium chloride behave much like sodium chloride with respect to the robustness of the data and what can be speculated from it. The autocorrelation data is, again, far too noisy and for any dependable radius calculations a certain amount of guesswork is required.

Though, we can again see that the incident intensity versus wave vector forms a curve for both sets of sample solution data (Fig. 43). This could very well be a durable development for salt solutions but more work would be required to provide solid evidence for this.

Chapter 7 – Conclusions

After analysing the small organic solutions in undersaturated conditions and at low concentrations, we can observe that aggregates begin to form even at the lowest concentrations. These molecular droplet particles tend to be in the region of 100 - 150 nanometres in radius and are in a constant state of flux; generating, growing and then, just as quickly, collapsing and dispersing into the bulk solution. The same behaviour is also visible within undersaturated ionic salt solutions with a similarity in particle size (100-150nm). These solution dynamics coincide with the Gibbs model and a growing nuclei's Gibbs free energy requirement. If a nucleus incurs rapid growth through the acquisition of solute within the bulk, but does not attain sufficient size to cross an energy barrier (governing state change favourability) then nucleation will occur and the system will remain in its liquid state.

Secondary decay signals were observed for some autocorrelation functions of particular solutions. These functions gave rise to the existence of minor molecular droplets. Small clusters were visible only for certain samples; urea and sodium nitrate solutions, species of approximately 0.5 nm radius were detected at various concentrations - often these were observed at higher levels of concentration. Glucose solutions also revealed a secondary decay with size of approximately 1 nm in radius. Glycine displays inconsistent data in the undersaturated state for the verification of sub-nano clusters. Neither NaCl nor KCl gave any indication of small moieties. The generation of these minor clusters could be linked with the specific size of the individual solute molecule. This theory gains some support when we compare the sizes of both the urea and nitrate molecules, which appear to share a similarity in size of small aggregations compared to that of glucose, whose molecular size is larger than urea and nitrate. The concentration also appears to affect the existence of smaller hydrodynamic species.

When we next analyse each system's behaviour under supersaturated conditions, we can observe substantial disparities with regards to their dynamics, and it becomes more difficult to generalise the dynamics of each solution. Supersaturated solutions of urea and glycine show mimicked data in a number of respects. Both demonstrate a consistent binomial exponential decay throughout all temperature measurements. For urea, the molecular droplet is within the range of 120 and 190 nm in radius and the small cluster tends between 0.5 – 0.6 nm radius. This is remarkably close to that of data taken from measurements of glycine with droplet size in the region of 115 – 170 nm and a molecular cluster size of between 0.5 and 0.7 nm. It had already been recorded in certain papers by Chattopadhyay *et al.*(2005)⁹² and Erdemir *et al.* (2007) that glycine was reported to have molecular clusters in both under- and supersaturated aqueous solutions. The authors concluded that glycine mainly existed in small molecular clusters such as dimer or trimer formations. It would appear, according to data, that urea behaves in a similar way to glycine, perhaps also forming small molecular clusters of urea dimers.

Supersaturated solutions of ionic salts provide only monomial decays within the range of few to many hundred nanometres. There is no evidence to suggest the existence of any smaller clusters within the ionic solutions at any point during cooling crystallisation. For sodium chloride and sodium nitrate, hydrodynamic radius measurements are between 500 and 800 nm, though their signal contains some random noise and for sodium nitrate in particular the baseline is less than satisfactory. For these reasons, one would estimate that in reality the hydrodynamic radii may be smaller, however this is merely guess work and would require more experimentation to confirm.

Potassium chloride delivers perfectly consistent and valuable data with particle radii in the region of 180 and 220 nm. Again, there is no suggestion of smaller sized clusters of 1 nm radii or less. The reason for such differences between data sets of ionic solutions is uncertain, but may simply be attributed to atomic size and the charge of the atomic ions involved.

Solutions of supersaturated glucose contradict any pattern so far occurring within the small organic solutions. The glucose samples show no large droplet species at all. Instead there is only a coherent monomial exponential decay referring to particles of 0.8 – 1.0 nanometre radius. This is very curious, as it is the only supersaturated solution specified here to behave in this manner. The fact that, within undersaturated conditions, glucose contains binomial signals containing information of 100 nm droplets and 1 nm molecular clusters makes the change in solution dynamics very interesting when we care them to that of the supersaturated state.

This finding was consistent with the theory of nucleation, which implies that solute molecules will congregate together to form a denser region of solute molecules within the bulk solution. No evidence was gathered that linked together the process of nucleation involving these nano-sized droplets, however, it would seem likely that any ensuing nucleation process would be more likely to initiate from a richly populated dense solute phase. If we are to assume that the precautions taken to prevent foreign impurities finding their way into these solutions were sufficiently effective, then it could be plausible to assess that the route of nano-droplet adsorption onto the surface of the sample cuvette could be a likely alternate pathway to the formation of crystals. This would be a slower pathway than that of spontaneous nucleation from the conjoining of solute molecules to a rapidly growing crystal nucleus. Most crystals formed in the sample cuvettes are done via contact with the cuvette wall surface. This process of crystallisation normally takes days and so would be consistent with the surface adsorption theory.

Observing multiple-angle scattering of each solution contributes a broader view of the solution dynamics. For solutions such as glucose and glycine the wide angle approach confirms previous data, but for urea and ionic solutions the exponential decays are too corrupted to be sufficiently accurate. The multi-angle data of sodium nitrate was far too degraded to analyse at all.

The structural composition of the dense solute regions are yet unknown and therefore it is not clear why an aggregate would be required to reach some critical size before the commencement of spontaneous nucleation into crystal growth. According to classical nucleation theory, smaller clusters of solute molecules do not contain an ample quantity of solute molecules and so are not sufficiently sized to act as critical

nuclei. This is more plausible if we consider that each nano-sized particle contained only enough solvent to encourage the growth of crystals up to tens of nanometres. The observed critical nucleus would then resemble the volume of solvent, which contained sufficient solute to form a stable crystal. Using this system we can speculate that solute abundant nano-droplets of varying size sporadically sample the crystalline region but more often than not simply revert back to their liquid phase. A contrasting argument would be that the prospect of spontaneous nucleation occurring within smaller nano-droplets would be negligible. It is only when a critical volume has been attained that nucleation becomes possible. It is likely that both arguments are self-supporting and in fact reinforce one another.

In the selection of supersaturated solutions investigated here, stable nano-droplets appeared to form over a broad concentration range and thus were able to provide a strong DLS signal. With the exception of glucose, all solutions generated large droplet structures up to hundreds of nanometres in radius. The size of these droplets, in all cases, appeared to be independent of the concentration of the solute molecules.

Direct comparison of small organic solutions with ionic salt solutions grants us recognition of their immediate differences. While organic molecular solutions appear, in general, to be more ordered or at least less erratic than that of ionic solutions there are still questions to be answered concerning the changes in solution dynamics when traversing from under- to supersaturated states. The exponential decays of urea solution in both states of saturation maintain a binomial trend, signifying the preservation of both types of molecular species - droplets and smaller sub-nano clusters. For solutions of glycine, a binomial signal indicating both large and small-scale clusters exists to some degree in both saturation conditions, but more prominently in the supersaturated solution than the undersaturated. This is reason to think that concentration of solute does indeed play a role in forming sub-nano sized clusters but not until the saturation boundary is crossed do they gain stability.

Glucose is unique to all solutions studied here and follows no obvious trend. The undersaturated solutions contain evidence of both agglomerate sizes but unlike supersaturated solutions of urea and glycine the supersaturated solution of glucose contains only confirmation of small clusters (approximately 1 nm in radius) and no further indication of the existence of larger aggregates on the hundred-nanometre scale. Comparison of small organic molecular solutions with ionic salt solutions gives us sufficient data to recognise that there are fundamental differences related to the dynamics of each solutions nucleation pathway. Understanding these crystallisation pathways more fully could be the key to understanding nucleation theory more fully and allow us to investigate further into the subject and explore new methods of drug design, production and delivery.

The increasing degree of polydispersity in supersaturated solutions of urea and glycine could be indicators of a fluctuation in particle size near and about a critical cluster size, which must be attained and exceeded to permit rapid crystallisation. Further research investigating these metastable components and their composition and function within these phenomena are still on going.

Chapter 8 – Appendix

8.1 Solubility

The solubility of a substance concerns the largest quantity of solute that can be dissolved in a given solvent. This concentration is known as the saturation point of the solute in a solvent at a specific temperature and pressure. The crystallisation process is dependent on solubility data, which can be used to predict theoretical yields and determine the most suitable crystallisation technique, *e.g.*, cooling crystallisation, evaporation or anti-solvent crystallisation.

In all experiments the solvent used was distilled and deionised water. Gravimetric methods of solubility determination were used to measure the solubility of each component solute.

Solubilities were taken of solutions saturated at 40 °C and kept at 40 °C within a sealed incubator.

	Mass Fraction of Urea	Mass Fraction of Water	Solubility (mg/ml)
Crystal dissolution	0.107	0.893	124.583
Filtration	0.101	0.899	118.400
Literature*	0.105	0.895	117.600

Table 14. Solubility data of Urea ^{*93}

	Mass Fraction of Glucose	Mass Fraction of Water	Solubility (mg/ml)
Crystal dissolution	0.383	0.617	620.100
Filtration	0.381	0.619	617.200
Literature*	0.376	0.624	603.000

Table 15. Solubility data of Glucose *

	Mass Fraction of Glycine	Mass Fraction of Water	Solubility (mg/ml)
Crystal dissolution	0.240	0.759	317.500
Filtration	0.229	0.770	298.000
Literature*	0.249	0.751	331.600

Table 16. Solubility data of Glycine*

	Mass Fraction of NaCl	Mass Fraction of Water	Solubility (mg/ml)
Crystal dissolution	0.246	0.733	363.600
Filtration	0.271	0.728	371.900
Literature*	0.267	0.733	364.200

Table 17. Solubility data of NaCl*

	Mass Fraction of KCl	Mass Fraction of Water	Solubility (mg/ml)
Crystal dissolution	0.279	0.720	388.200
Filtration	0.280	0.719	390.100
Literature*	0.287	0.713	403.100

Table 18. Solubility data of KCl *

	Mass Fraction of NaNO ₃	Mass Fraction of Water	Solubility (mg/ml)
Crystal dissolution	0.511	0.488	1048.000
Filtration	0.506	0.493	1027.500
Literature*	0.509	0.490	1040.000

Table 19. Solubility data of NaNO₃*

8.2 Viscosity

Temperature (K)	Viscosity ($\mu\text{Pa}\cdot\text{s}$)
318	559.0
313	652.7
308	719.1
303	797.3
298	890.2
293	1002.0
288	1138.3

Table 20. Viscosity of deionised water at specific temperatures.

8.3 Background signal

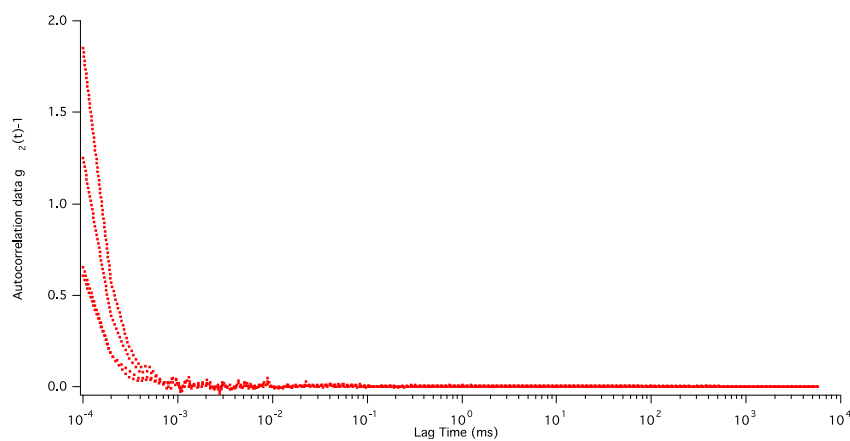


Fig. 44 Autocorrelation function of ethanol (reagent grade).

8.4 Collected data

Temperature (K)	Detected Angle (°)	Scattered Intensity (KHz)	Normalised Intensity	Hydrodynamic Radius (nm)	Diode
318.180	28	70.918	33.629	160	2384949
313.428	24	78.308	30.624	202	2398099
311.026	24	75.277	31.466	157	2368670
308.617	30	83.731	28.562	235	2391539
306.215	20	208.885	11.462	366	2394250
303.807	24	78.684	30.389	211	2391155
301.395	22	80.404	29.833	205	2398714
298.982	24	86.123	27.737	180	2388803

Table 21. Measured and calculated data from Urea solution of composition 16.7 g/ml of water.

Temperature (K)	Detected Angle (°)	Scattered Intensity (KHz)	Normalised Intensity	Hydrodynamic Radius (nm)	Diode
318.202	16	140.398	0.059	0.883	2362368
313.383	18	123.042	0.051	0.859	2386068
308.587	22	100.783	0.042	0.888	2377906
303.807	20	107.262	0.045	0.905	2370289
298.983	20	109.717	0.046	1.14	2358307
294.215	20	114.244	0.048	0.829	2353817

Table 22. Measured and calculated data from Glucose solution of composition 8.333 g/ml of water.

Temperature (K)	Detected Angle (°)	Scattered Intensity (KHz)	Normalised Intensity	Hydrodynamic Radius (nm)	Diode
318.147	75	82.1	0.035	117	2372037
313.376	50	72.302	0.031	104	2362777
308.571	50	115.732	0.048	114	2402835
303.783	60	102.903	0.043	113	2401905
298.954	70	75.765	0.032	98.4	2388105

Table 23. Measured and calculated data from Glycine solution of composition 2.85 g/ml of water.

Temperature (K)	Detected Angle (°)	Scattered Intensity (KHz)	Normalised Intensity	Hydrodynamic Radius (nm)	Diode
318.177	30	58.905	0.524	793	30890.69
313.404	26	89.194	0.347	732	30966.53
308.607	24	93.361	0.332	760	30998.55
303.803	30	59.689	0.518	619	30911.06
298.973	30	74.917	0.412	682	30896.03
294.183	31	56.786	0.542	564	30770.23

Table 24. Measured and calculated data from NaCl solution with composition 3.636 g/ml of water.

Temperature (K)	Detected Angle (°)	Scattered Intensity (KHz)	Normalised Intensity	Hydrodynamic Radius (nm)	Diode
318.154	40	120.642	0.564	200	213802.7
313.399	40	136.886	0.641	212	213409.7
308.603	40	200.999	0.939	215	214010.7
303.799	40	215.891	1.012	219	213233.3
299.001	40	227.456	1.051	217	216446.8
294.219	40	232.167	1.079	181	215071.3

Table 25. Measured and calculated data from KCl solution with composition 3.528 g/ml of water.

Temperature (K)	Detected Angle (°)	Scattered Intensity (KHz)	Normalised Intensity	Hydrodynamic Radius (nm)	Diode
318.212	50	14.204	0.147	479	96231.41
313.397	46	14.644	0.152	656	96090.07
308.587	50	12.429	0.129	686	95895.18
303.820	46	238.102	0.358	982	664607
298.978	42	136.255	0.203	756	670828.6

Table 26. Measured and calculated data from NaNO₃ solution with composition 10.5 g/ml of water.

Temperature (K)	Detected Angle (°)	Scattered Intensity (KHz)	Normalised Intensity	Hydrodynamic Radius (nm)	Diode
318.177	90.1	7.878	0.003	--	2379274
313.409	90	8.822	0.003	--	2364142
308.602	90	8.038	0.003	--	2368601
303.823	90	17.052	0.007	--	2394126
298.985	90	10.429	0.004	--	2365046

Table 27. *Measured and calculated data from pure deionised water.*

1 Chapter 9 - References

1. A. G. Jones, *Crystallization Process Systems*, Butterworth-Heinmann, (2002), **61**
2. A. Mersmann, *Trans. I Chem. E.* (1996), **74**, A812-A820
3. M. Giuliotti, M. M. Seckler, S. Derenzo, M. I. Re, E. Cekinski. *Braz. J. Chem. Eng.*, **18**
4. A. G. Jones, *Crystallization Process Systems*, Butterworth-Heinmann, (2002), 59-60
5. J. W. Mullin, *Crystallization*, (2001), **5**, 182 - 195
6. P. G. Vekilov, *Crystal Growth & Design*, (2010), **10**, 5007-5019
7. http://www.geog.ucsb.edu/~joel/g110_w08/lecture_notes/pressure/pressure.html - 02/05/2011
8. <http://missbakersbiologyclasswiki.wikispaces.com/glossary> - 02/05/2011
9. K. L. Moazed, J. P. Hirth, *Surfave Sci.*(1964), **3**
10. K. L. Moazed, J. P. Hirth, *Physics of Thin Films*, (1967), **4**
11. J. Prausnitz, L. Foose, *Pure and Applied Chemistry*, (2007), **79**, 1435
12. J. W. Gibbs, *Trans. Connect. Acad. Sci.*(1876), **3**, 108
13. I. Ya. Frenkel, *Kinetic Theory of Liquids*, (1955)
14. D. Erdemir, A. Y. Lee, A. S. Myerson, *Acc. Chem. Res.*,(2009), **42**, 621-629
15. R. J. Davey, J. Garside, *From Molecules to Crystallisers*, (2000),
16. J. W. Mullin, *Crystallisation*, (1993), **3**
17. M. Volmer, *Kinetik der Phasenbildung*, Steinkopff, Dresden, (1939)
18. B. Mutaftschiev, *Handbook of crystal growth*, (1993), **I**, 189
19. P. G. Vekilov, L. A. Monaco, B. R. Thomas, *et al.*, *Acta Crystallogr.*(1996), **52**, 785
20. J. Lothe, G. M. Pound, *The Journal of Chemical Physics*, (1966), **45**, 630
21. D. W. Oxtoby, D. A. Kaschiev, *J. Chem. Phys.*, (1994), **100**, 7665-7771
22. B. J. Mokross, *Mater. Phys. Mech.*, (2003), **6**, 13-20
23. A. Laaksonen, I. Napari, *J. Phys. Chem. B.* (2001), **105**, 11678-11682
24. D. Kashchiev, *Nucleation: Basic Theory with Applications*, Butterworth-Heinemann, Oxford, (2000)
25. J. Wolk, R. Strey, *J. Chem. Phys.*, (2001), **105**, 11683
26. J. Drenth, C. Haas, *Acta Crystallogr.* (1998), **54**, 867-872
27. D. Knezic, J. Zaccaro, S. A. Myserson, *J. Phys. Chem.*, (2004), **108**, 10672-10677
28. T. E. Creighton, *Proteins: structure and molecular properties*, (1993)
29. S. T. Yau, B. R. Thomas, P. G. Vekilov, *Phys. Rev. Lett.*,(2000), **85**, 353-356
30. S. T. Yau, P. G. Vekilov, *J. Am. Chem. Soc.*, (2001), **123**, 1080-1089
31. <http://web.mit.edu/myersongroup/research/> - 02/05/2011
32. Y. C. Shen, D. W. Oxtoby, *J. Chem. Phys.*, (1996), **104**, 4233
33. A. Lomakin, N. Asherie, G. B. Benedek, *PNAS*, (2003), **100**, 10254 - 10257
34. D. Kaschiev, P. G. Vekilov, A. B. Kolmeisky, *J. Chem. Phys.*, (2005), **122**, 244706
35. J. K. Lutsko, G. Nicolis, *Physical Rev. Letts.*, (2006), **96**, 244706/1 – 244706/6
36. O. Galkin, P. G. Vekilov, *J. Am. Chem. Soc.*, (2000), **122**, 156-163
37. O. Galkin, P. G. Vekilov, *J. Crystal Growth*, (2001), **232**, 63-76

-
38. G. Gliko, N. Neumaier, W. Pan, I. Hasse, M. Fisher, A. Bacher, W. Weinkauff, P. G. Vekilov, *J. Am. Chem. Soc.*, (2005), **127**, 3433-3438
 39. G. Gliko, W. Pan, P. Katsonic, N. Neumaier, O. Galein, S. Weinkauff, P. G. Vekilov, *J. Phys. Chem. B.*, (2007), **11**, 3106 - 3114
 40. P. R. ten Wolde, D. Frenkel, *Science*, (1997), **277**, 1975-1978
 41. G. Nicolis, C. Nicolis, *Physica A*, (2003), **323**, 139-154
 42. P. G. Vekilov, *Nanoscale*, (2010), **2**, 2346
 43. E. B. Treivus, *Kristallografiya*, (2001), **46**, 1125-1131
 44. C. Haas, J. Drenth, *J. Phys. Chem. B*, (2000), **104**, 368-377
 45. W. Pan, A. B. Kolomeisky, P. G. Vekilov, *J. Chem. Phys.* (2006), **122**, 174905
 46. V. Talanquer, D. W. Oxtoby, *J. Chem. Phys.*, (1998), **109**, 223-227
 47. J. Nyvlt, O. Sohnle, M. Matuchova, M. Broul. *The Kinetics of Industrial Crystallization*, (1985)
 48. J. Nyvlt, *J. Crystal Growth*, (1968), **3,4**, 377-383
 49. O. Sohnle, J. W. Mullin, *Chem. Eng. Res. Des.*, (1998), **66**, 537-540
 50. J. W. Mullin, S. J. Jancic, *Trans. I. Chem. E.*, (1997), **57**, 188-193
 51. A. R. Gerson, K. J. Roberts, J. N. Sherwood, *Powder Technol*, (1991), **65**, 243-249
 52. J. Nyvlt, R. Rychly, J. Gottfried, J. Wurzelova, *J. Crystal Growth*, (1970), **56**, 187-193
 53. C. Haas, J. Drenth, *Journal of Crystal Growth*, (1999), **196**, 388-394
 54. H. L. Chen, J. C. Hwang, J. M. Yang, R.C. Wang, *Polymer*, (1998), **39**, 26, 6983-6989
 55. Y. S. Soh, J. H. Kim, C. C. Gryte, *Polymer*, (1995), **36**, 19, 3711-3717
 56. R. J. Davey, W. Liu, M. J. Quayle, G. J. T. Tiddy, *Crystal Growth & Design*, (2002b), **2**, 4, 269-272
 57. R. J. Davey, K. Allen, N. Blagden, W. I. Cross, H. F. Lieberman, M. J. Quayle, R. Righini, L. Seton, G. J.T. Tiddy, *Cryst. Eng. Comm.*, (2002a), 257-264
 58. T. J. Sorensen, P. C. Sontum, J. Samseth, G. Thorsen, D. Malthe-Sorensen, *Chem. Eng. & Tech.*, (2003), **26**, 3, 307-312
 59. Y. Georgalis, A. M. Kierzak, W. Saenger, *J. Phys. Chem.*, (2000), **104**, 15, 3405-3406
 60. L. Lafferrere, C. Hoff, S. Veessler, *Crystal Growth & Design*, (2004a), **4**, 6, 1175-1180
 61. L. Lafferrere, C. Hoff, S. Veessler, *J. Cryst. Growth*, (2004b), **269**, 550-557
 62. S. Veessler, L. Lafferrere, E. Garcia, C. Hoff, *Organic Process Research & Development*, (2003), **7**, 6, 983-989
 63. S. Veessler, E. Revalor, O. Bottini, C. Hoff, *Organic Process Research & Development* (2006), **10**, 841-845
 64. M. J. Akers, N. Milton, S. R. Byrn, S. L. Nail, *Pharmaceutical Research*, (1995), **12**, 1457-1461
 65. C. E. Hughes, S. Hamad, K. D. M. Harris, C. R. A. Catlow, P. C. Griffiths, *Faraday Discussions*, (2007), **136**, 71-89.
 66. C. E. Hughes, K. D. M. Harris, *New Journal of Chemistry*, (2009), **33**, 713-716
 67. Y. Itaka, *Acta Cryst.*, (1961), **14**, 1-10.
 68. I. Weissbuch, V. Y. Torbeev, L. Leiserowitz, M. Lahav, *Angew. Chem. Int. Ed.*, (2005), **44**(21), 3226-3229.
 69. J. Bernstein, R. J. Davey, J. O. Henck. *Angew. Chem. Int. Ed.*, (1999), **38**(23), 3440-3461
 70. E. V. Boldyreva, V. A. Drebuschak, T. N. Drebuschak, I. E. Paukov, Y. A. Kovalevskaya, E. S. Shuova, *Journal of Thermal Analysis and Calorimetry*, (2003), **73**(2), 409-418.

-
71. A. S. Myerson, P. Y. Lo, *Journal of Crystal Growth*, (1990), **99**, 1048-1052
 72. S. Chattopadhyay, D. Erdemir, J. M. B. Evans, J. Ilavsky, H. Amenitsch, C. U. Segre, A. S. Myerson, *Crystal Growth & Design*, (2005), **5**(2), 523-527
 73. D. Erdemir, S. Chattopadhyay, L. Guo, J. Ilavsky, H. Amenitsch, C. U. Segre, A. S. Myerson, *Physical Review Letters*, (2007), **99**(11), 115702/1-115702/4
 74. G. Gliko, N. Neumaier, W. Pan, I. Haase, M. Fisher, A. Bacher, W. Weinkauff, P. G. Vekilov, *Journal of American Chemical Society*, (2005), **127**(10), 3433-3438
 75. G. Gliko, W. Pan, P. Katsonis, N. Neumaier, O. Galkin, S. Weinkauff, P. G. Vekilov, *Journal of Physical Chemistry B*, (2007), **111**(12), 3106-3114
 76. P. G. Vekilov, *Interdisciplinary Transport Phenomena*, (2009), **1161**, 377-386
 77. J. Huang, T. C. Stringfellow, L. Yu, *Journal of American Chemical Society*, (2008), **130**(42), 13973-13980.
 78. S. Hamad, C. E. Hughes, C. R. A. Catlow, K. D. M. Harris, *J. Phys. Chem. B*, (2008), **112**(24), 7280-7288
 79. B. J. Berne, R. Pecora, *Dynamic Light Scattering; With Applications to Chemistry, Biology and Physics*, (1976), Dover Publications, Inc.
 80. R. Finsy, *Advances in Colloid and Interface Science*, (1994), **52**, 79 - 143
 81. N. C. Santos, M. A. R. B. Castanho, *Biophysical Journal*, (1996), **71**, 1641 - 1650
 82. Brown W. (1993). *Dynamic Light Scattering. The method and some applications.*: Oxford Science Publications.
 83. Finsy R. (1994). *Advances in Colloid and Interface Science* 52:79-143.
 84. Linder P, Zember T, Pusey PN. (2002a). Neutron, X-rays and light scattering methods to soft condensed matter. *Dynamic Light Scattering.*: Elsevier Science B.V.
 85. Onuma K, Kanzaki N., *Journal of Crystal Growth*, (2007), 304(2):452-459.
 86. Moreno A, Mas-Oliva J, Soriano-Garcia M, Salvador CO, Bolanos-Garcia VM. (2000). *Journal of Molecular Structure* 519:243-256.
 87. R. Finsy, *Advances in Colloid and Interface Science*, (1994), **52**, 79-143
 88. W. J. Reichmann, *Use and abuse of statistics*, (1961), Oxford University Press, New York
 89. Y. Georgalis, A.M. Kierzek, W. Saenger, *J. Phys. Chem. B.*, (2000), **104**, 3405-3406
 90. J. Alejandro, J Hansen, *Phys. Rev. E.* (2007), **76**, 061505
 91. D. Gidalevitz, R. Feidenhans'l, S. Matlis, D. M. Smilgies, M. J. Christensen, L. Leiserowitz, *Angew. Chem. Int. Ed. Engl.*, (1997), **24**, 4476 - 4481
 92. S. Chattopadhyay, D. Erdemir, J. M. B. Evans, J. Ilavsky, H. Amemitsch, C. U. Segre, A. S. Myerson, *Crystal Growth & Design*, (2005), **5**(2), 523-527